9 Flow over Immersed Bodies

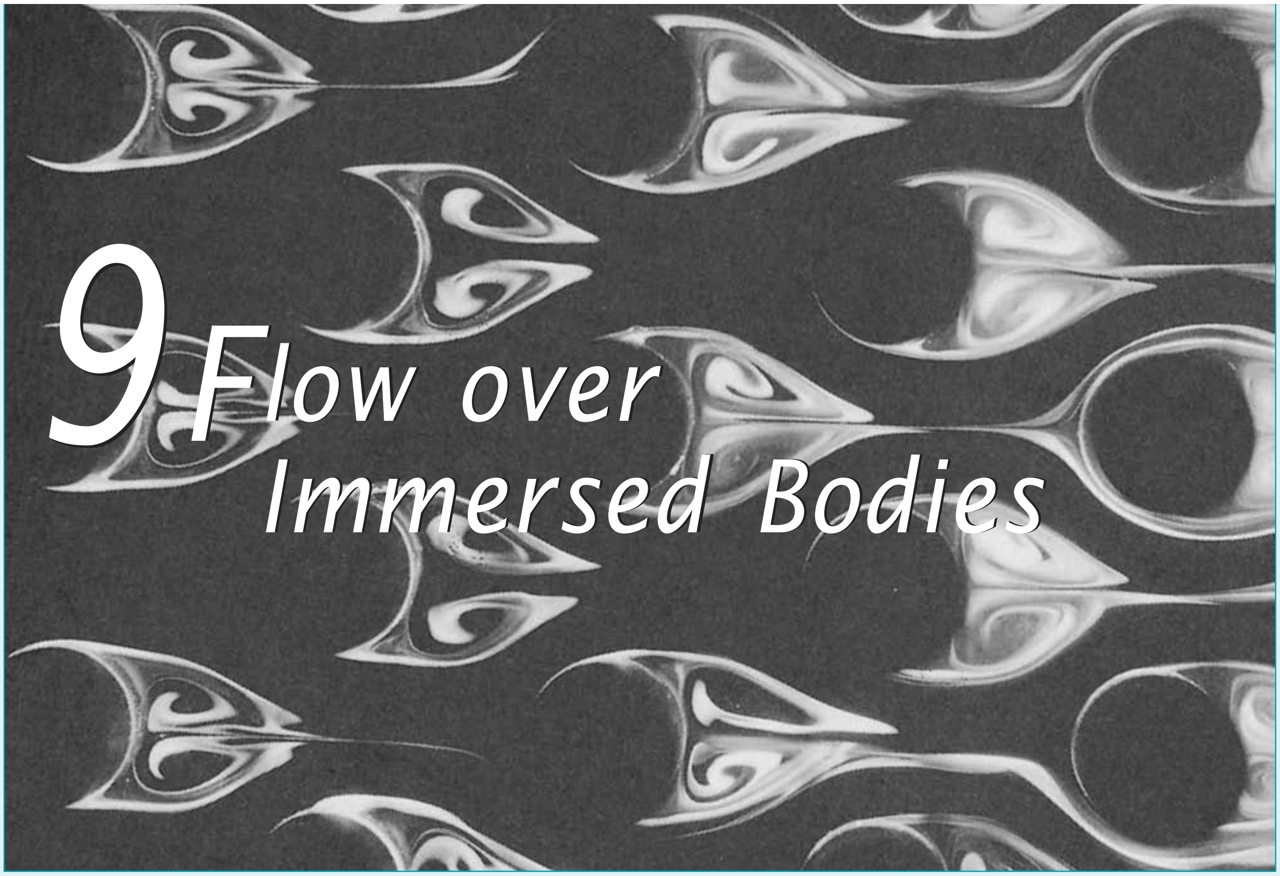

CHAPTER OPENING PHOTO: Impulsive start of flow past an array of cylinders: The complex structure of laminar flow past a relatively simple geometric structure illustrates why it is often difficult to obtain exact analytical results for external flows. (Dye in water.) *(Photograph courtesy of ONERA, France.)*

Learning Objectives

After completing this chapter, you should be able to:

- identify and discuss the features of external flow.
- explain the fundamental characteristics of a boundary layer, including laminar, transitional, and turbulent regimes.
- calculate boundary layer paremeters for flow past a flat plate.
- provide a description of boundary layer separation.
- calculate the lift and drag forces for various objects.

In this chapter we consider various aspects of the flow over bodies that are immersed in a fluid. Examples include the flow of air around airplanes, automobiles, and falling snowflakes, or the flow of water around submarines and fish. In these situations the object is completely surrounded by the fluid and the flows are termed *external flows.*

External flows involving air are often termed aerodynamics in response to the important external flows produced when an object such as an airplane flies through the atmosphere. Although this field of external flows is extremely important, there are many other examples that are of equal importance. The fluid force (lift and drag) on surface vehicles (cars, trucks, bicycles) has become a very important topic. By correctly designing cars and trucks, it has become possible to greatly decrease the fuel consumption and improve the handling characteristics of the vehicle. Similar efforts have resulted in improved ships, whether they are surface vessels (surrounded by two fluids, air and water) or submersible vessels (surrounded completely by water).

Many practical situations involve flow past objects.

Other applications of external flows involve objects that are not completely surrounded by fluid, although they are placed in some external-type flow. For example, the proper design of a

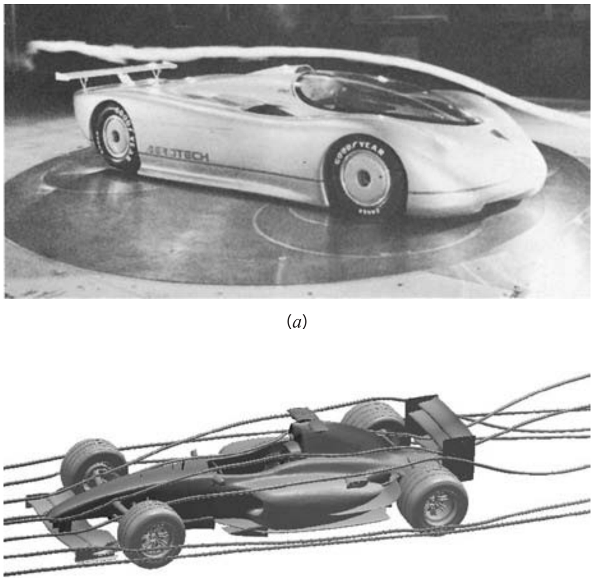

(*a*)

(*b*)

■ FIGURE 9.1 **(*a*) Flow past a full-sized streamlined vehicle in the GM aerodynamics laboratory wind tunnel, an 18-ft by 34-ft test section facility driven by a 4000-hp, 43-ft-diameter fan. (Photograph courtesy of General Motors Corporation.) (*b*) Predicted streamlines for flow past a Formula 1 race car as obtained by using computational fluid dynamics techniques. (Courtesy of Ansys, Inc.)**

building (whether it is your house or a tall skyscraper) must include consideration of the various wind effects involved.

As with other areas of fluid mechanics, various approaches (theoretical, numerical and experimental) are used to obtain information on the fluid forces developed by external flows. Theoretical (i.e., analytical) techniques can provide some of the needed information about such flows. However, because of the complexities of the governing equations and the complexities of the geometry of the objects involved, the amount of information obtained from purely theoretical methods is limited.

Much of the information about external flows comes from experiments carried out, for the most part, on scale models of the actual objects. Such testing includes the obvious wind tunnel testing of model airplanes, buildings, and even entire cities. In some instances the actual device, not a model, is tested in wind tunnels. Figure 9.1*a* shows a test of a vehicle in a wind tunnel. Better performance of cars, bikes, skiers, and numerous other objects has resulted from testing in wind tunnels. The use of water tunnels and towing tanks also provides useful information about the flow around ships and other objects. With advancement in computational fluid dynamics, or CFD, numerical methods are also capable of predicting external flows past objects. Figure 9.1*b* shows streamlines around a Formula 1 car as predicted by CFD. Appendix A provides an introduction to CFD.

In this chapter we consider characteristics of external flow past a variety of objects. We investigate the qualitative aspects of such flows and learn how to determine the various forces on objects surrounded by a moving liquid.

9.1 General External Flow Characteristics

For external flows it is usually easiest to use a coordinate system fixed to the object.

A body immersed in a moving fluid experiences a resultant force due to the interaction between the body and the fluid surrounding it. In some instances (such as an airplane flying through still air) the fluid far from the body is stationary and the body moves through the fluid with velocity U. In other instances (such as the wind blowing past a building) the body is stationary and the fluid flows past the body with velocity U. In any case, we can fix the coordinate system in the body and treat the situation as fluid flowing past a stationary body with velocity U, the *upstream velocity*. For the purposes of this book, we will assume that the upstream velocity is constant in both time and location. That is, there is a uniform, constant velocity fluid flowing past the object. In actual situations this is often not true. For example, the wind blowing past a smokestack is nearly always turbulent and gusty (unsteady) and probably not of uniform velocity from the top to the bottom of the stack. Usually the unsteadiness and nonuniformity are of minor importance.

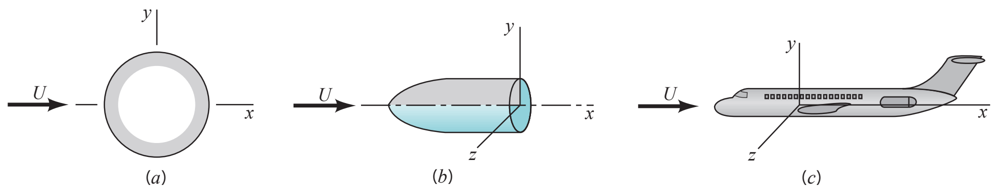

■ FIGURE 9.2 **Flow classification: (*a*) two-dimensional, (*b*) axisymmetric, (*c*) three-dimensional.**

V9.1 Space shuttle landing

Even with a steady, uniform upstream flow, the flow in the vicinity of an object may be unsteady. Examples of this type of behavior include the flutter that is sometimes found in the flow past airfoils (wings), the regular oscillation of telephone wires that "sing" in a wind, and the irregular turbulent fluctuations in the wake regions behind bodies.

The structure of an external flow and the ease with which the flow can be described and analyzed often depend on the nature of the body in the flow. Three general categories of bodies are shown in Fig. 9.2. They include (a) two-dimensional objects (infinitely long and of constant cross-sectional size and shape), (b) axisymmetric bodies (formed by rotating their cross-sectional shape about the axis of symmetry), and (c) three-dimensional bodies that may or may not possess a line or plane of symmetry. In practice there can be no truly two-dimensional bodies—nothing extends to infinity. However, many objects are sufficiently long so that the end effects are negligibly small.

Another classification of body shape can be made depending on whether the body is streamlined or blunt. The flow characteristics depend strongly on the amount of streamlining present. In general, *streamlined bodies* (i.e., airfoils, racing cars, etc.) have little effect on the surrounding fluid, compared with the effect that *blunt bodies* (i.e., parachutes, buildings, etc.) have on the fluid. Usually, but not always, it is easier to force a streamlined body through a fluid than it is to force a similar-sized blunt body at the same velocity. There are important exceptions to this basic rule.

9.1.1 Lift and Drag Concepts

A body interacts with the surrounding fluid through pressure and shear stresses.

When any body moves through a fluid, an interaction between the body and the fluid occurs; this effect can be given in terms of the forces at the fluid–body interface. These forces can be described in terms of the stresses—wall shear stresses, τ_w, due to viscous effects and normal stresses due to the pressure, p. Typical shear stress and pressure distributions are shown in Figs. 9.3*a* and 9.3*b*. Both τ_w and p vary in magnitude and direction along the surface.

It is often useful to know the detailed distribution of shear stress and pressure over the surface of the body, although such information is difficult to obtain. Many times, however, only the

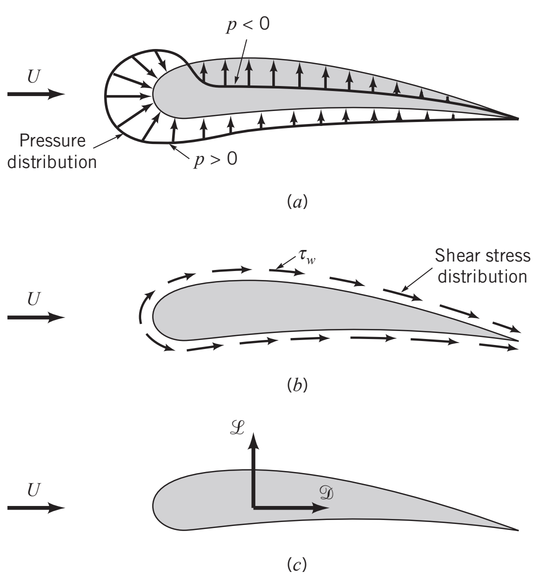

■ FIGURE 9.3 **Forces from the surrounding fluid on a two-dimensional object: (*a*) pressure force, (*b*) viscous force, (*c*) resultant force (lift and drag).**

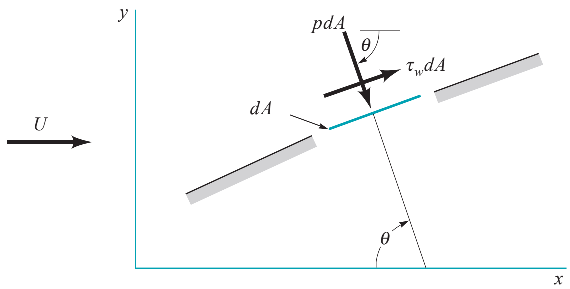

■ **FIGURE 9.4** **Pressure and shear forces on a small element of the surface of a body.**

integrated or resultant effects of these distributions are needed. The resultant force in the direction of the upstream velocity is termed the ***drag,*** $\mathscr{D}$, and the resultant force normal to the upstream velocity is termed the ***lift,*** $\mathscr{L}$, as is indicated in Fig. 9.3*c*. For some three-dimensional bodies there may also be a side force that is perpendicular to the plane containing $\mathscr{D}$ and $\mathscr{L}$.

The resultant of the shear stress and pressure distributions can be obtained by integrating the effect of these two quantities on the body surface as is indicated in Fig. 9.4. The x and y components of the fluid force on the small area element dA are

$$dF_x = (p\,dA)\cos\theta + (\tau_w\,dA)\sin\theta$$

and

$$dF_y = -(p\,dA)\sin\theta + (\tau_w\,dA)\cos\theta$$

Thus, the net x and y components of the force on the object are

$$\mathscr{D} = \int dF_x = \int p\cos\theta\,dA + \int \tau_w \sin\theta\,dA \qquad \textbf{(9.1)}$$

and

$$\mathscr{L} = \int dF_y = -\int p\sin\theta\,dA + \int \tau_w \cos\theta\,dA \qquad \textbf{(9.2)}$$

Lift and drag on a section of a body depend on the orientation of the surface.

Of course, to carry out the integrations and determine the lift and drag, we must know the body shape (i.e., θ as a function of location along the body) and the distribution of τ_w and p along the surface. These distributions are often extremely difficult to obtain, either experimentally or theoretically. The pressure distribution can be obtained experimentally by use of a series of static pressure taps along the body surface. On the other hand, it is usually quite difficult to measure the wall shear stress distribution.

Fluids in the News

Pressure-sensitive paint For many years, the conventional method for measuring *surface pressure* has been to use static pressure taps consisting of small holes on the surface connected by hoses from the holes to a pressure measuring device. Pressure-sensitive paint (PSP) is now gaining acceptance as an alternative to the static surface pressure ports. The PSP material is typically a luminescent compound that is sensitive to the pressure on it and can be excited by an appropriate light which is captured by special video imaging equipment. Thus, it provides a quantitative measure of the surface pressure. One of the biggest advantages of PSP is that it is a global measurement technique, measuring pressure over the entire surface, as opposed to discrete points. PSP also has the advantage of being nonintrusive to the flow field. Although static pressure port holes are small, they do alter the surface and can slightly alter the flow, thus affecting downstream ports. In addition, the use of PSP eliminates the need for a large number of pressure taps and connecting tubes. This allows pressure measurements to be made in less time and at a lower cost.

It is seen that both the shear stress and pressure force contribute to the lift and drag, since for an arbitrary body θ is neither zero nor 90° along the entire body. The exception is a flat plate aligned either parallel to the upstream flow ($\theta = 90°$) or normal to the upstream flow ($\theta = 0$) as is discussed in Example 9.1.

EXAMPLE 9.1 Drag from Pressure and Shear Stress Distributions

GIVEN Air at standard conditions flows past a flat plate as is indicated in Fig. E9.1. In case (a) the plate is parallel to the upstream flow, and in case (b) it is perpendicular to the upstream flow. The pressure and shear stress distributions on the surface are as indicated (obtained either by experiment or theory).

FIND Determine the lift and drag on the plate.

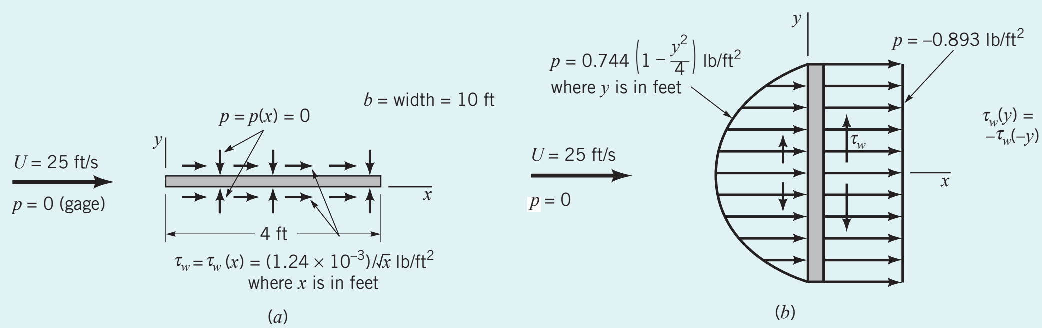

■ FIGURE E9.1

SOLUTION

For either orientation of the plate, the lift and drag are obtained from Eqs. 9.1 and 9.2. With the plate parallel to the upstream flow we have $\theta = 90°$ on the top surface and $\theta = 270°$ on the bottom surface so that the lift and drag are given by

$$\mathscr{L} = -\int_{\text{top}} p\, dA + \int_{\text{bottom}} p\, dA = 0$$

and

$$\mathscr{D} = \int_{\text{top}} \tau_w\, dA + \int_{\text{bottom}} \tau_w\, dA = 2\int_{\text{top}} \tau_w\, dA \qquad \textbf{(1)}$$

where we have used the fact that because of symmetry the shear stress distribution is the same on the top and the bottom surfaces, as is the pressure also [whether we use gage ($p = 0$) or absolute ($p = p_{\text{atm}}$) pressure]. There is no lift generated—the plate does not know up from down. With the given shear stress distribution, Eq. 1 gives

$$\mathscr{D} = 2\int_{x=0}^{4\text{ ft}} \left(\frac{1.24 \times 10^{-3}}{x^{1/2}}\ \text{lb/ft}^2\right)(10\text{ ft})\, dx$$

or

$$\mathscr{D} = 0.0992\text{ lb} \qquad \textbf{(Ans)}$$

With the plate perpendicular to the upstream flow, we have $\theta = 0°$ on the front and $\theta = 180°$ on the back. Thus, from Eqs. 9.1 and 9.2

$$\mathscr{L} = \int_{\text{front}} \tau_w\, dA - \int_{\text{back}} \tau_w\, dA = 0$$

and

$$\mathscr{D} = \int_{\text{front}} p\, dA - \int_{\text{back}} p\, dA$$

Again there is no lift because the pressure forces act parallel to the upstream flow (in the direction of $\mathscr{D}$ not $\mathscr{L}$) and the shear stress is symmetrical about the center of the plate. With the given relatively large pressure on the front of the plate (the center of the plate is a stagnation point) and the negative pressure (less than the upstream pressure) on the back of the plate, we obtain the following drag

$$\mathscr{D} = \int_{y=-2}^{2\text{ ft}} \left[0.744\left(1 - \frac{y^2}{4}\right)\text{lb/ft}^2 - (-0.893)\text{ lb/ft}^2\right](10\text{ ft})\, dy$$

or

$$\mathscr{D} = 55.6\text{ lb} \qquad \textbf{(Ans)}$$

COMMENTS Clearly there are two mechanisms responsible for the drag. On the ultimately streamlined body (a zero thickness flat plate parallel to the flow) the drag is entirely due to the shear stress at the surface and, in this example, is relatively small. For the ultimately blunted body (a flat plate normal to the upstream flow) the drag is entirely due to the pressure difference between the front and back portions of the object and, in this example, is relatively large.

If the flat plate were oriented at an arbitrary angle relative to the upstream flow as indicated in Fig. E9.1*c*, there would be both a lift and a drag, each of which would be dependent on both the shear stress and the pressure. Both the pressure and shear stress distributions would be different for the top and bottom surfaces.

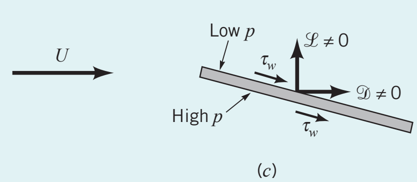

■ FIGURE E9.1 (*Continued*)

Although Eqs. 9.1 and 9.2 are valid for any body, the difficulty in their use lies in obtaining the appropriate shear stress and pressure distributions on the body surface. Considerable effort has gone into determining these quantities, but because of the various complexities involved, such information is available only for certain simple situations.

Lift coefficients and drag coefficients are dimensionless forms of lift and drag.

Without detailed information concerning the shear stress and pressure distributions on a body, Eqs. 9.1 and 9.2 cannot be used. The widely used alternative is to define dimensionless lift and drag coefficients and determine their approximate values by means of either a simplified analysis, some numerical technique, or an appropriate experiment. The ***lift coefficient,*** C_L, and ***drag coefficient,*** C_D, are defined as

$$C_L = \frac{\mathscr{L}}{\frac{1}{2}\rho U^2 A}$$

and

$$C_D = \frac{\mathscr{D}}{\frac{1}{2}\rho U^2 A}$$

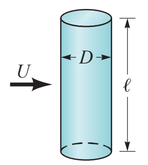

$A = D\ell$

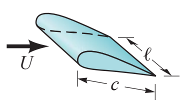

$A = c\ell$

where A is a characteristic area of the object (see Chapter 7). Typically, A is taken to be *frontal area*—the projected area seen by a person looking toward the object from a direction parallel to the upstream velocity, U, as indicated by the figure in the margin. It would be the area of the shadow of the object projected onto a screen normal to the upstream velocity as formed by a light shining along the upstream flow. In other situations A is taken to be the *planform area*—the projected area seen by an observer looking toward the object from a direction normal to the upstream velocity (i.e., from "above" it). Obviously, which characteristic area is used in the definition of the lift and drag coefficients must be clearly stated.

9.1.2 Characteristics of Flow Past an Object

External flows past objects encompass an extremely wide variety of fluid mechanics phenomena. Clearly the character of the flow field is a function of the shape of the body. Flows past relatively simple geometric shapes (i.e., a sphere or circular cylinder) are expected to have less complex flow fields than flows past a complex shape such as an airplane or a tree. However, even the simplest-shaped objects produce rather complex flows.

For a given-shaped object, the characteristics of the flow depend very strongly on various parameters such as size, orientation, speed, and fluid properties. As is discussed in Chapter 7, according to dimensional analysis arguments, the character of the flow should depend on the various dimensionless parameters involved. For typical external flows the most important of these parameters are the Reynolds number, $\text{Re} = \rho U\ell/\mu = U\ell/\nu$, the Mach number, $\text{Ma} = U/c$, and for flows with a free surface (i.e., flows with an interface between two fluids, such as the flow past a surface ship), the Froude number, $\text{Fr} = U/\sqrt{g\ell}$. (Recall that ℓ is some characteristic length of the object and c is the speed of sound.)

The character of flow past an object is dependent on the value of the Reynolds number.

For the present, we consider how the external flow and its associated lift and drag vary as a function of Reynolds number. Recall that the Reynolds number represents the ratio of inertial effects to viscous effects. In the absence of all viscous effects ($\mu = 0$), the Reynolds number is infinite. On the other hand, in the absence of all inertial effects (negligible mass or $\rho = 0$), the Reynolds number is zero. Clearly, any actual flow will have a Reynolds number between (but not including) these two extremes. The nature of the flow past a body depends strongly on whether $\text{Re} \gg 1$ or $\text{Re} \ll 1$.

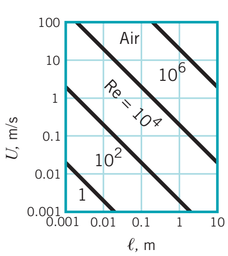

Most external flows with which we are familiar are associated with moderately sized objects with a characteristic length on the order of $0.01 \text{ m} < \ell < 10 \text{ m}$. In addition, typical upstream velocities are on the order of $0.01 \text{ m/s} < U < 100 \text{ m/s}$ and the fluids involved are typically water or air. The resulting Reynolds number range for such flows is approximately $10 < \text{Re} < 10^9$. This is shown by the figure in the margin for air. As a rule of thumb, flows with $\text{Re} > 100$ are dominated by inertial effects, whereas flows with $\text{Re} < 1$ are dominated by viscous effects. Hence, most familiar external flows are dominated by inertia.

On the other hand, there are many external flows in which the Reynolds number is considerably less than 1, indicating in some sense that viscous forces are more important than inertial forces. The gradual settling of small particles of dirt in a lake or stream is governed by low Reynolds number flow principles because of the small diameter of the particles and their small settling speed. Similarly, the Reynolds number for objects moving through large viscosity oils is small because μ is large. The general differences between small and large Reynolds number flow past streamlined and blunt objects can be illustrated by considering flows past two objects—one a flat plate parallel to the upstream velocity and the other a circular cylinder.

For low Reynolds number flows, viscous effects are felt far from the object.

Flows past three flat plates of length ℓ with $\mathrm{Re} = \rho U\ell/\mu = 0.1$, 10, and 10^7 are shown in Fig. 9.5. If the Reynolds number is small, the viscous effects are relatively strong and the plate affects the uniform upstream flow far ahead, above, below, and behind the plate. To reach that portion of the flow field where the velocity has been altered by less than 1% of its undisturbed value (i.e., $U - u < 0.01\ U$) we must travel relatively far from the plate. In low Reynolds number flows the viscous effects are felt far from the object in all directions.

As the Reynolds number is increased (by increasing U, for example), the region in which viscous effects are important becomes smaller in all directions except downstream, as is shown in

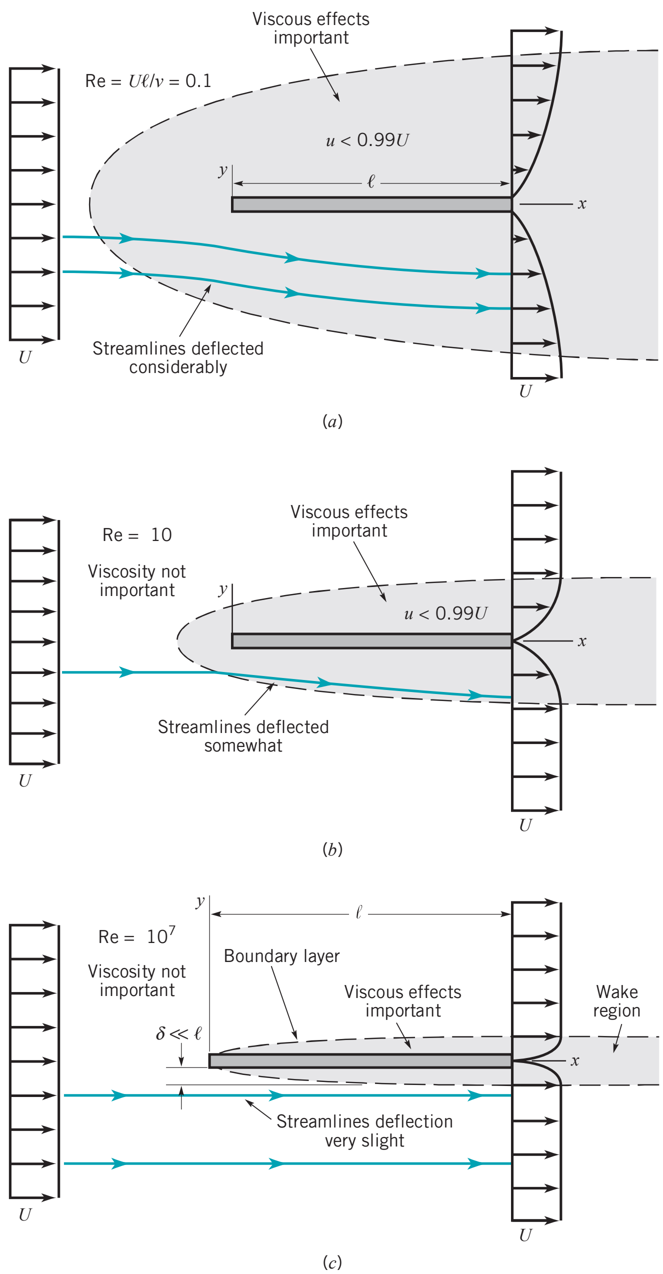

FIGURE 9.5 Character of the steady, viscous flow past a flat plate parallel to the upstream velocity: (*a*) low Reynolds number flow, (*b*) moderate Reynolds number flow, (*c*) large Reynolds number flow.

Fig. 9.5*b*. One does not need to travel very far ahead, above, or below the plate to reach areas in which the viscous effects of the plate are not felt. The streamlines are displaced from their original uniform upstream conditions, but the displacement is not as great as for the $\text{Re} = 0.1$ situation shown in Fig. 9.5*a*.

If the Reynolds number is large (but not infinite), the flow is dominated by inertial effects and the viscous effects are negligible everywhere except in a region very close to the plate and in the relatively thin ***wake region*** behind the plate, as shown in Fig. 9.5*c*. Since the fluid viscosity is not zero ($\text{Re} < \infty$), it follows that the fluid must stick to the solid surface (the no-slip boundary condition). There is a thin ***boundary layer*** region of thickness $\delta = \delta(x) \ll \ell$ (i.e., thin relative to the length of the plate) next to the plate in which the fluid velocity changes from the upstream value of $u = U$ to zero velocity on the plate. The thickness of this layer increases in the direction of flow, starting from zero at the forward or leading edge of the plate. The flow within the boundary layer may be laminar or turbulent, depending on various parameters involved.

The streamlines of the flow outside of the boundary layer are nearly parallel to the plate. As we will see in the next section, the slight displacement of the external streamlines that are outside of the boundary layer is due to the thickening of the boundary layer in the direction of flow. The existence of the plate has very little effect on the streamlines outside of the boundary layer—either ahead, above, or below the plate. On the other hand, the wake region is due entirely to the viscous interaction between the fluid and the plate.

Thin boundary layers may develop in large Reynolds number flows.

One of the great advancements in fluid mechanics occurred in 1904 as a result of the insight of Ludwig Prandtl (1875–1953), a German physicist and aerodynamicist. He conceived of the idea of the boundary layer—a thin region on the surface of a body in which viscous effects are very important and outside of which the fluid behaves essentially as if it were inviscid. Clearly the actual fluid viscosity is the same throughout; only the relative importance of the viscous effects (due to the velocity gradients) is different within or outside of the boundary layer. As is discussed in the next section, by using such a hypothesis it is possible to simplify the analysis of large Reynolds number flows, thereby allowing solution to external flow problems that are otherwise still unsolvable.

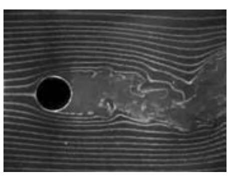

As with the flow past the flat plate described above, the flow past a blunt object (such as a circular cylinder) also varies with Reynolds number. In general, the larger the Reynolds number, the smaller the region of the flow field in which viscous effects are important. For objects that are not sufficiently streamlined, however, an additional characteristic of the flow is observed. This is termed *flow separation* and is illustrated by the figure in the margin and in Fig. 9.6.

Low Reynolds number flow ($\text{Re} = UD/\nu < 1$) past a circular cylinder is characterized by the fact that the presence of the cylinder and the accompanying viscous effects are felt throughout a relatively large portion of the flow field. As is indicated in Fig. 9.6*a*, for $\text{Re} = UD/\nu = 0.1$, the viscous effects are important several diameters in any direction from the cylinder. A somewhat surprising characteristic of this flow is that the streamlines are essentially symmetric about the center of the cylinder—the streamline pattern is the same in front of the cylinder as it is behind the cylinder.

As the Reynolds number is increased, the region ahead of the cylinder in which viscous effects are important becomes smaller, with the viscous region extending only a short distance ahead of the cylinder. The viscous effects are convected downstream and the flow loses its upstream to downstream symmetry. Another characteristic of external flows becomes important—the flow separates from the body at the *separation location* as indicated in Fig. 9.6*b*. With the increase in Reynolds number, the fluid inertia becomes more important and at some location on the body, denoted the separation location, the fluid's inertia is such that it cannot follow the curved path around to the rear of the body. The result is a separation bubble behind the cylinder in which some of the fluid is actually flowing upstream, against the direction of the upstream flow. (See the photograph at the beginning of this chapter.)

V9.2 Streamlined and blunt bodies

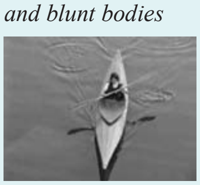

At still larger Reynolds numbers, the area affected by the viscous forces is forced farther downstream until it involves only a thin ($\delta \ll D$) boundary layer on the front portion of the cylinder and an irregular, unsteady (perhaps turbulent) wake region that extends far downstream of the cylinder. The fluid in the region outside of the boundary layer and wake region flows as if it were inviscid. Of course, the fluid viscosity is the same throughout the entire flow field. Whether viscous effects are important or not depends on which region of the flow field we consider. The velocity gradients within the boundary layer and wake regions are much larger than those in the remainder of the flow field.

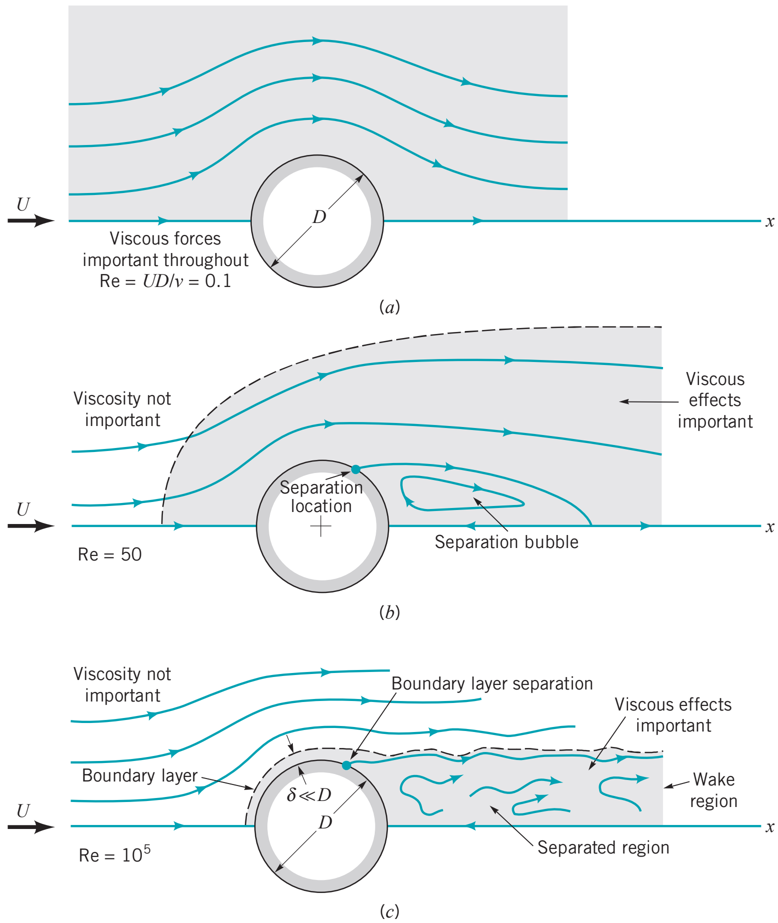

■ **FIGURE 9.6** **Character of the steady, viscous flow past a circular cylinder: (*a*) low Reynolds number flow, (*b*) moderate Reynolds number flow, (*c*) large Reynolds number flow.**

Since the shear stress (i.e., viscous effect) is the product of the fluid viscosity and the velocity gradient, it follows that viscous effects are confined to the boundary layer and wake regions.

Most familiar flows involve large Reynolds numbers.

The characteristics described in Figs. 9.5 and 9.6 for flow past a flat plate and a circular cylinder are typical of flows past streamlined and blunt bodies, respectively. The nature of the flow depends strongly on the Reynolds number. (See Ref. 31 for many examples illustrating this behavior.) Most familiar flows are similar to the large Reynolds number flows depicted in Figs. 9.5*c* and 9.6*c*, rather than the low Reynolds number flow situations. (See the photograph at the beginning of Chapters 7 and 11.) In the remainder of this chapter we will investigate more thoroughly these ideas and determine how to calculate the forces on immersed bodies.

EXAMPLE 9.2 Characteristics of Flow Past Objects

GIVEN It is desired to experimentally determine the various characteristics of flow past a car as shown in Fig E9.2. The following tests could be carried out: (a) $U = 20$ mm/s flow of glycerin past a scale model that is 34-mm tall, 100-mm long, and 40-mm wide, (b) $U = 20$ mm/s air flow past the same scale model, or (c) $U = 25$ m/s air flow past the actual car, which is 1.7-m tall, 5-m long, and 2-m wide.

FIND Would the flow characteristics for these three situations be similar? Explain.

■ **FIGURE E9.2**

SOLUTION

The characteristics of flow past an object depend on the Reynolds number. For this instance we could pick the characteristic length to be the height, h, width, b, or length, ℓ, of the car to obtain three possible Reynolds numbers, $\mathrm{Re}_h = Uh/\nu$, $\mathrm{Re}_b = Ub/\nu$, and $\mathrm{Re}_\ell = U\ell/\nu$. These numbers will be different because of the different values of h, b, and ℓ. Once we arbitrarily decide on the length we wish to use as the characteristic length, we must stick with it for all calculations when using comparisons between model and prototype.

With the values of kinematic viscosity for air and glycerin obtained from Tables 1.8 and 1.6 as $\nu_{\mathrm{air}} = 1.46 \times 10^{-5}\ \mathrm{m^2/s}$ and $\nu_{\mathrm{glycerin}} = 1.19 \times 10^{-3}\ \mathrm{m^2/s}$, we obtain the following Reynolds numbers for the flows described.

Reynolds Number	(a) Model in Glycerin	(b) Model in Air	(c) Car in Air
Re_h	0.571	46.6	2.91×10^6
Re_b	0.672	54.8	3.42×10^6
Re_ℓ	1.68	137.0	8.56×10^6

Clearly, the Reynolds numbers for the three flows are quite different (regardless of which characteristic length we choose). Based on the previous discussion concerning flow past a flat plate or flow past a circular cylinder, we would expect that the flow past the actual car would behave in some way similar to the flows shown in Figs. 9.5*c* or 9.6*c*. That is, we would expect some type of boundary layer characteristic in which viscous effects would be confined to relatively thin layers near the surface of the car and the wake region behind it. Whether the car would act more like a flat plate or a cylinder would depend on the amount of streamlining incorporated into the car's design.

Because of the small Reynolds number involved, the flow past the model car in glycerin would be dominated by viscous effects, in some way reminiscent of the flows depicted in Figs. 9.5*a* or 9.6*a*. Similarly, with the moderate Reynolds number involved for the air flow past the model, a flow with characteristics similar to those indicated in Figs. 9.5*b* and 9.6*b* would be expected. Viscous effects would be important—not as important as with the glycerin flow, but more important than with the full-sized car.

It would not be a wise decision to expect the flow past the full-sized car to be similar to the flow past either of the models. The same conclusions result regardless of whether we use Re_h, Re_b, or Re_ℓ. As is indicated in Chapter 7, the flows past the model car and the full-sized prototype will not be similar unless the Reynolds numbers for the model and prototype are the same. It is not always an easy task to ensure this condition. One (expensive) solution is to test full-sized prototypes in very large wind tunnels (see Fig. 9.1).

9.2 Boundary Layer Characteristics

Large Reynolds number flow fields may be divided into viscous and inviscid regions.

As was discussed in the previous section, it is often possible to treat flow past an object as a combination of viscous flow in the boundary layer and inviscid flow elsewhere. If the Reynolds number is large enough, viscous effects are important only in the boundary layer regions near the object (and in the wake region behind the object). The boundary layer is needed to allow for the no-slip boundary condition that requires the fluid to cling to any solid surface that it flows past. Outside of the boundary layer the velocity gradients normal to the flow are relatively small, and the fluid acts as if it were inviscid, even though the viscosity is not zero. A necessary condition for this structure of the flow is that the Reynolds number be large.

9.2.1 Boundary Layer Structure and Thickness on a Flat Plate

There can be a wide variety in the size of a boundary layer and the structure of the flow within it. Part of this variation is due to the shape of the object on which the boundary layer forms. In this section we consider the simplest situation, one in which the boundary layer is formed on an infinitely long flat plate along which flows a viscous, incompressible fluid as is shown in Fig. 9.7. If the surface were curved (i.e., a circular cylinder or an airfoil), the boundary layer structure would be more complex. Such flows are discussed in Section 9.2.6.

V9.3 Laminar boundary layer

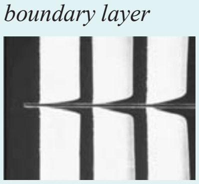

If the Reynolds number is sufficiently large, only the fluid in a relatively thin boundary layer on the plate will feel the effect of the plate. That is, except in the region next to the plate the flow velocity will be essentially $\mathbf{V} = U\hat{\mathbf{i}}$, the upstream velocity. For the infinitely long flat plate extending from $x = 0$ to $x = \infty$, it is not obvious how to define the Reynolds number because there is no characteristic length. The plate has no thickness and is not of finite length!

For a finite length plate, it is clear that the plate length, ℓ, can be used as the characteristic length. For an infinitely long plate we use x, the coordinate distance along the plate from the leading edge, as the characteristic length and define the Reynolds number as $\mathrm{Re}_x = Ux/\nu$. Thus, for

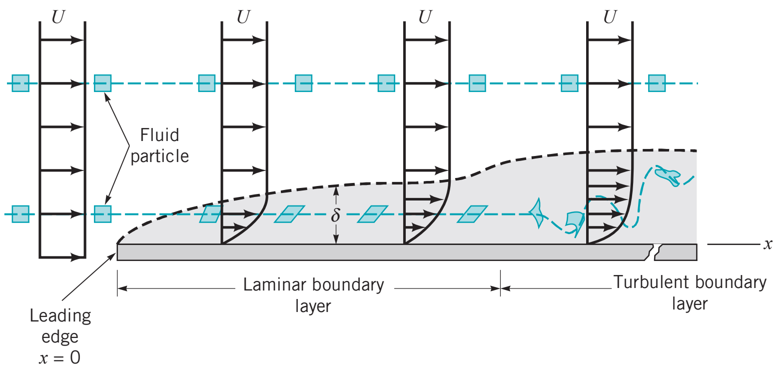

FIGURE 9.7 Distortion of a fluid particle as it flows within the boundary layer.

any fluid or upstream velocity the Reynolds number will be sufficiently large for boundary layer type flow (i.e., Fig. 9.5*c*) if the plate is long enough. Physically, this means that the flow situations illustrated in Fig. 9.5 could be thought of as occurring on the same plate, but should be viewed by looking at longer portions of the plate as we step away from the plate to see the flows in Fig. 9.5*a*, 9.5*b*, and 9.5*c*, respectively.

If the plate is sufficiently long, the Reynolds number $\mathrm{Re} = U\ell/\nu$ is sufficiently large so that the flow takes on its boundary layer character (except very near the leading edge). The details of the flow field near the leading edge are lost to our eyes because we are standing so far from the plate that we cannot make out these details. On this scale (Fig. 9.5*c*) the plate has negligible effect on the fluid ahead of the plate. The presence of the plate is felt only in the relatively thin boundary layer and wake regions. As previously noted, Prandtl in 1904 was the first to hypothesize such a concept. It has become one of the major turning points in fluid mechanics analysis.

Fluid particles within the boundary layer experience viscous effects.

A better appreciation of the structure of the boundary layer flow can be obtained by considering what happens to a fluid particle that flows into the boundary layer. As is indicated in Fig. 9.7, a small rectangular particle retains its original shape as it flows in the uniform flow outside of the boundary layer. Once it enters the boundary layer, the particle begins to distort because of the velocity gradient within the boundary layer—the top of the particle has a larger speed than its bottom. The fluid particles do not rotate as they flow along outside the boundary layer, but they begin to rotate once they pass through the fictitious boundary layer surface and enter the world of viscous flow. The flow is said to be irrotational outside the boundary layer and rotational within the boundary layer. (In terms of the kinematics of fluid particles as is discussed in Section 6.1, the flow outside the boundary layer has zero vorticity, and the flow within the boundary layer has nonzero vorticity.)

V9.4 Laminar/turbulent transition

At some distance downstream from the leading edge, the boundary layer flow becomes turbulent and the fluid particles become greatly distorted because of the random, irregular nature of the turbulence. One of the distinguishing features of turbulent flow is the occurrence of irregular mixing of fluid particles that range in size from the smallest fluid particles up to those comparable in size with the object of interest. For laminar flow, mixing occurs only on the molecular scale. This molecular scale is orders of magnitude smaller in size than typical size scales for turbulent flow mixing. The transition from a ***laminar boundary layer*** to a ***turbulent boundary layer*** occurs at a critical value of the Reynolds number, $\mathrm{Re}_{x\mathrm{cr}}$, on the order of 2×10^5 to 3×10^6, depending on the roughness of the surface and the amount of turbulence in the upstream flow, as is discussed in Section 9.2.4. As shown by the figure in the margin, the location along the plate where the flow becomes turbulent, x_{cr}, moves towards the leading edge as the free-stream velocity increases.

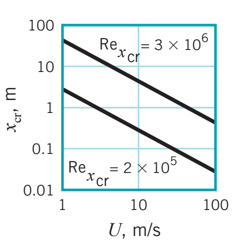

The purpose of the boundary layer is to allow the fluid to change its velocity from the upstream value of U to zero on the surface. Thus, $\mathbf{V} = 0$ at $y = 0$ and $\mathbf{V} \approx U\hat{\mathbf{i}}$ at the edge of the boundary layer, with the velocity profile, $u = u(x, y)$ bridging the boundary layer thickness. This boundary layer characteristic occurs in a variety of flow situations, not just on flat plates. For example, boundary layers form on the surfaces of cars, in the water running down the gutter of the street, and in the atmosphere as the wind blows across the surface of the earth (land or water).

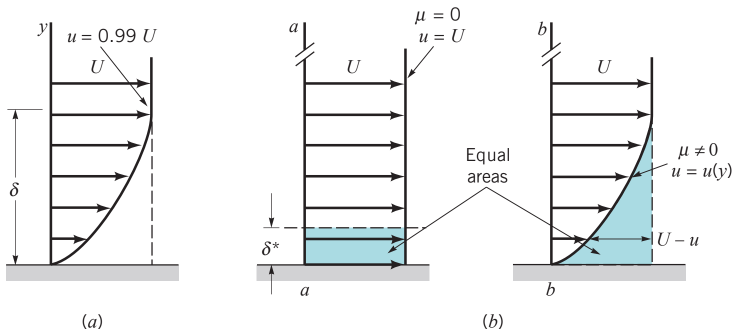

■ **FIGURE 9.8** **Boundary layer thickness: (*a*) standard boundary layer thickness, (*b*) boundary layer displacement thickness.**

Fluids in the News

The Albatross: Nature's Aerodynamic Solution for Long Flights The albatross is a phenomenal seabird that soars just above ocean waves, taking advantage of the local *boundary layer* to travel incredible distances with little to no wing flapping. This limited physical exertion results in minimal energy consumption and, combined with aerodynamic optimization, allows the albatross to easily travel 1000 km (620 miles) per day, with some tracking data showing almost double that amount. The albatross has high aspect ratio wings (up to 11 ft in wingspan) and a lift-to-drag ratio ($\mathscr{L}/\mathscr{D}$) of approximately 27, both similar to high-performance sailplanes. With this aerodynamic configuration, the albatross then makes use of a technique called "dynamic soaring" to take advantage of the wind profile over the ocean surface. Based on the boundary layer profile, the albatross uses the rule of dynamic soaring, which is to climb when pointed upwind and dive when pointed downwind, thus constantly exchanging kinetic and potential energy. Though the albatross loses energy to drag, it can periodically regain energy due to vertical and directional motions within the boundary layer by changing local airspeed and direction. This is not a direct line of travel, but it does provide the most fuel-efficient method of long-distance flight.

In actuality (both mathematically and physically), there is no sharp "edge" to the boundary layer; that is, $u \to U$ as we get farther from the plate. We define the ***boundary layer thickness,*** δ, as that distance from the plate at which the fluid velocity is within some arbitrary value of the upstream velocity. Typically, as indicated in Fig. 9.8*a,*

$$\delta = y \qquad \text{where} \qquad u = 0.99U$$

To remove this arbitrariness (i.e., what is so special about 99%; why not 98%?), the following definitions are introduced. Shown in Fig. 9.8*b* are two velocity profiles for flow past a flat plate—one if there were no viscosity (a uniform profile) and the other if there are viscosity and zero slip at the wall (the boundary layer profile). Because of the velocity deficit, $U - u$, within the boundary layer, the flowrate across section b–b is less than that across section a–a. However, if we displace the plate at section a–a by an appropriate amount δ^*, the *boundary layer displacement thickness*, the flowrates across each section will be identical. This is true if

The boundary layer displacement thickness is defined in terms of volumetric flowrate.

$$\delta^* b U = \int_0^\infty (U - u) b \, dy$$

where b is the plate width. Thus,

$$\delta^* = \int_0^\infty \left(1 - \frac{u}{U}\right) dy \tag{9.3}$$

The displacement thickness represents the amount that the thickness of the body must be increased so that the fictitious uniform inviscid flow has the same mass flowrate properties as the actual viscous flow. It represents the outward displacement of the streamlines caused by the viscous effects on the plate. This idea allows us to simulate the presence that the boundary layer has on the flow outside of the boundary layer by adding the displacement thickness to the actual wall and treating the flow over the thickened body as an inviscid flow. The displacement thickness concept is illustrated in Example 9.3.

EXAMPLE 9.3 Boundary Layer Displacement Thickness

GIVEN Air flowing into a 2-ft-square duct with a uniform velocity of 10 ft/s forms a boundary layer on the walls as shown in Fig. E9.3*a*. The fluid within the core region (outside the boundary layers) flows as if it were inviscid. From advanced calculations it is determined that for this flow the boundary layer displacement thickness is given by

$$\delta^* = 0.0070(x)^{1/2} \qquad \textbf{(1)}$$

where δ^* and x are in feet.

FIND Determine the velocity $U = U(x)$ of the air within the duct but outside of the boundary layer.

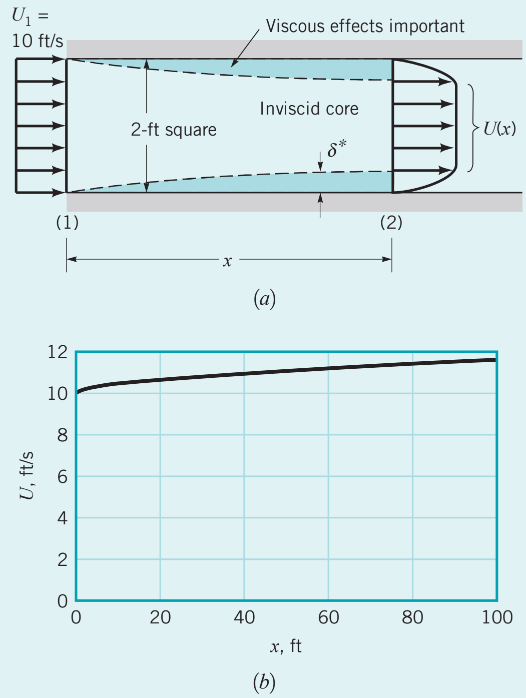

■ FIGURE E9.3

SOLUTION

If we assume incompressible flow (a reasonable assumption because of the low velocities involved), it follows that the volume flowrate across any section of the duct is equal to that at the entrance (i.e., $Q_1 = Q_2$). That is,

$$U_1A_1 = 10 \text{ ft/s } (2 \text{ ft})^2 = 40 \text{ ft}^3/\text{s} = \int_{(2)} u \, dA$$

According to the definition of the displacement thickness, δ^*, the flowrate across section (2) is the same as that for a uniform flow with velocity U through a duct whose walls have been moved inward by δ^*. That is,

$$40 \text{ ft}^3/\text{s} = \int_{(2)} u \, dA = U(2 \text{ ft} - 2\delta^*)^2 \qquad \textbf{(2)}$$

By combining Eqs. 1 and 2 we obtain

$$40 \text{ ft}^3/\text{s} = 4U(1 - 0.0070x^{1/2})^2$$

or

$$U = \frac{10}{(1 - 0.0070x^{1/2})^2} \text{ ft/s} \qquad \textbf{(Ans)}$$

COMMENTS Note that U increases in the downstream direction. For example, as shown in Fig. E9.3*b*, $U = 11.6$ ft/s at $x = 100$ ft. The viscous effects that cause the fluid to stick to the walls of the duct reduce the effective size of the duct, thereby (from conservation of mass principles) causing the fluid to accelerate. The pressure drop necessary to do this can be obtained by using the Bernoulli equation (Eq. 3.7) along the inviscid streamlines from section (1) to (2). (Recall that this equation is not valid for viscous flows within the boundary layer. It is, however, valid for the inviscid flow outside the boundary layer.) Thus,

$$p_1 + \tfrac{1}{2}\rho U_1^2 = p + \tfrac{1}{2}\rho U^2$$

Hence, with $\rho = 2.38 \times 10^{-3}$ slugs/ft^3 and $p_1 = 0$ we obtain

$$p = \frac{1}{2}\rho\,(U_1^2 - U^2)$$

$$= \frac{1}{2}(2.38 \times 10^{-3} \text{ slugs/ft}^3)$$

$$\times \left[(10 \text{ ft/s})^2 - \frac{10^2}{(1 - 0.0079x^{1/2})^4} \text{ ft}^2/\text{s}^2\right]$$

or

$$p = 0.119\left[1 - \frac{1}{(1 - 0.0070x^{1/2})^4}\right] \text{lb/ft}^2$$

For example, $p = -0.0401$ lb/ft^2 at $x = 100$ ft.

If it were desired to maintain a constant velocity along the centerline of this entrance region of the duct, the walls could be displaced outward by an amount equal to the boundary layer displacement thickness, δ^*.

Another boundary layer thickness definition, the *boundary layer momentum thickness*, Θ, is often used when determining the drag on an object. Again because of the velocity deficit, $U - u$, in the boundary layer, the momentum flux across section b–b in Fig. 9.8 is less than that across section a–a. This deficit in momentum flux for the actual boundary layer flow on a plate of width b is given by

$$\int \rho u(U - u)\, dA = \rho b \int_0^\infty u(U - u)\, dy$$

The boundary layer momentum thickness is defined in terms of momentum flux.

which by definition is the momentum flux in a layer of uniform speed U and thickness Θ. That is,

$$\rho b U^2 \Theta = \rho b \int_0^\infty u(U - u)\, dy$$

or

$$\Theta = \int_0^\infty \frac{u}{U}\left(1 - \frac{u}{U}\right) dy \tag{9.4}$$

All three boundary layer thickness definitions, δ, δ^*, and Θ, are of use in boundary layer analyses.

The boundary layer concept is based on the fact that the boundary layer is thin. For the flat plate flow this means that at any location x along the plate, $\delta \ll x$. Similarly, $\delta^* \ll x$ and $\Theta \ll x$. Again, this is true if we do not get too close to the leading edge of the plate (i.e., not closer than $\mathrm{Re}_x = Ux/\nu = 1000$ or so).

The structure and properties of the boundary layer flow depend on whether the flow is laminar or turbulent. As is illustrated in Fig. 9.9 and discussed in Sections 9.2.2 through 9.2.5, both the boundary layer thickness and the wall shear stress are different in these two regimes.

9.2.2 Prandtl/Blasius Boundary Layer Solution

In theory, the details of viscous, incompressible flow past any object can be obtained by solving the governing Navier–Stokes equations discussed in Section 6.8.2. For steady, two-dimensional laminar flows with negligible gravitational effects, these equations (Eqs. 6.127a, b, and c) reduce to the following:

$$u\frac{\partial u}{\partial x} + v\frac{\partial u}{\partial y} = -\frac{1}{\rho}\frac{\partial p}{\partial x} + \nu\left(\frac{\partial^2 u}{\partial x^2} + \frac{\partial^2 u}{\partial y^2}\right) \tag{9.5}$$

$$u\frac{\partial v}{\partial x} + v\frac{\partial v}{\partial y} = -\frac{1}{\rho}\frac{\partial p}{\partial y} + \nu\left(\frac{\partial^2 v}{\partial x^2} + \frac{\partial^2 v}{\partial y^2}\right) \tag{9.6}$$

which express Newton's second law. In addition, the conservation of mass equation, Eq. 6.31, for incompressible flow is

$$\frac{\partial u}{\partial x} + \frac{\partial v}{\partial y} = 0 \tag{9.7}$$

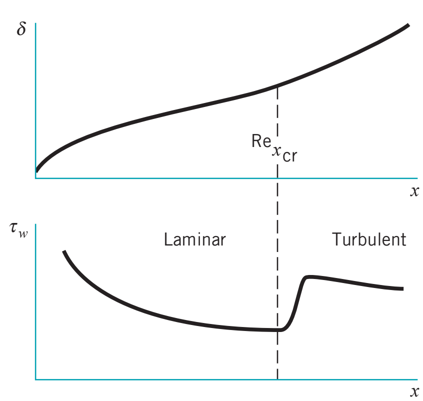

■ **FIGURE 9.9** **Typical characteristics of boundary layer thickness and wall shear stress for laminar and turbulent boundary layers.**

The appropriate boundary conditions are that the fluid velocity far from the body is the upstream velocity and that the fluid sticks to the solid body surfaces. Although the mathematical problem is well-posed, no one has obtained an analytical solution to these equations for flow past any shaped body! Currently much work is being done to obtain numerical solutions to these governing equations for many flow geometries.

By using boundary layer concepts introduced in the previous sections, Prandtl was able to impose certain approximations (valid for large Reynolds number flows), and thereby to simplify the governing equations. In 1908, H. Blasius (1883–1970), one of Prandtl's students, was able to solve these simplified equations for the boundary layer flow past a flat plate parallel to the flow. A brief outline of this technique and the results are presented below. Additional details may be found in the literature (Refs. 1–3).

Since the boundary layer is thin, it is expected that the component of velocity normal to the plate is much smaller than that parallel to the plate and that the rate of change of any parameter across the boundary layer should be much greater than that along the flow direction. That is,

$$v \ll u \quad \text{and} \quad \frac{\partial}{\partial x} \ll \frac{\partial}{\partial y}$$

Physically, the flow is primarily parallel to the plate and any fluid property is convected downstream much more quickly than it is diffused across the streamlines.

With these assumptions it can be shown that the governing equations (Eqs. 9.5, 9.6, and 9.7) reduce to the following boundary layer equations:

The Navier–Stokes equations can be simplified for boundary layer flow analysis.

$$\frac{\partial u}{\partial x} + \frac{\partial v}{\partial y} = 0 \tag{9.8}$$

$$u\,\frac{\partial u}{\partial x} + v\,\frac{\partial u}{\partial y} = \nu\,\frac{\partial^2 u}{\partial y^2} \tag{9.9}$$

Although both these boundary layer equations and the original Navier–Stokes equations are nonlinear partial differential equations, there are considerable differences between them. For one, the y momentum equation has been eliminated, leaving only the original, unaltered continuity equation and a modified x momentum equation. One of the variables, the pressure, has been eliminated, leaving only the x and y components of velocity as unknowns. For boundary layer flow over a flat plate the pressure is constant throughout the fluid. The flow represents a balance between viscous and inertial effects, with pressure playing no role.

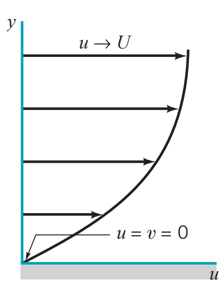

As shown by the figure in the margin, the boundary conditions for the governing boundary layer equations are that the fluid sticks to the plate

$$u = v = 0 \quad \text{on} \quad y = 0 \tag{9.10}$$

and that outside of the boundary layer the flow is the uniform upstream flow $u = U$. That is,

$$u \rightarrow U \quad \text{as} \quad y \rightarrow \infty \tag{9.11}$$

Mathematically, the upstream velocity is approached asymptotically as one moves away from the plate. Physically, the flow velocity is within 1% of the upstream velocity at a distance of δ from the plate.

In mathematical terms, the Navier–Stokes equations (Eqs. 9.5 and 9.6) and the continuity equation (Eq. 9.7) are elliptic equations, whereas the equations for boundary layer flow (Eqs. 9.8 and 9.9) are parabolic equations. The nature of the solutions to these two sets of equations, therefore, is different. Physically, this fact translates to the idea that what happens downstream of a given location in a boundary layer cannot affect what happens upstream of that point. That is, whether the plate shown in Fig. 9.5*c* ends with length ℓ or is extended to length 2ℓ, the flow within the first segment of length ℓ will be the same. In addition, the presence of the plate has no effect on the flow ahead of the plate. On the other hand, ellipticity allows flow information to propagate in all directions, including upstream.

In general, the solutions of nonlinear partial differential equations (such as the boundary layer equations, Eqs. 9.8 and 9.9) are extremely difficult to obtain. However, by applying a clever coordinate transformation and change of variables, Blasius reduced the partial differential equations to an ordinary differential equation that he was able to solve. A brief description of this process is given below. Additional details can be found in standard books dealing with boundary layer flow (Refs. 1, 2).

It can be argued that in dimensionless form the boundary layer velocity profiles on a flat plate should be similar regardless of the location along the plate. That is,

$$\frac{u}{U} = g\left(\frac{y}{\delta}\right)$$

where $g(y/\delta)$ is an unknown function to be determined. In addition, by applying an order of magnitude analysis of the forces acting on fluid within the boundary layer, it can be shown that the boundary layer thickness grows as the square root of x and inversely proportional to the square root of U. That is,

$$\delta \sim \left(\frac{\nu x}{U}\right)^{1/2}$$

Such a conclusion results from a balance between viscous and inertial forces within the boundary layer and from the fact that the velocity varies much more rapidly in the direction across the boundary layer than along it.

The boundary layer equations can be written in terms of a similarity variable.

Thus, we introduce the dimensionless *similarity variable* $\eta = (U/\nu x)^{1/2} y$ and the stream function $\psi = (\nu x U)^{1/2} f(\eta)$, where $f = f(\eta)$ is an unknown function. Recall from Section 6.2.3 that the velocity components for two-dimensional flow are given in terms of the stream function as $u = \partial\psi/\partial y$ and $v = -\partial\psi/\partial x$, which for this flow become

$$u = Uf'(\eta) \tag{9.12}$$

and

$$v = \left(\frac{\nu U}{4x}\right)^{1/2} (\eta f' - f) \tag{9.13}$$

with the notation $(\ )' = d/d\eta$. We substitute Eqs. 9.12 and 9.13 into the governing equations, Eqs. 9.8 and 9.9, to obtain (after considerable manipulation) the following nonlinear, third-order ordinary differential equation:

$$2f''' + ff'' = 0 \tag{9.14a}$$

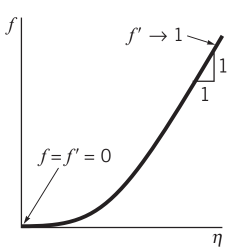

As shown by the figure in the margin, the boundary conditions given in Eqs. 9.10 and 9.11 can be written as

$$f = f' = 0 \text{ at } \eta = 0 \quad \text{and} \quad f' \to 1 \text{ as } \eta \to \infty \tag{9.14b}$$

The original partial differential equation and boundary conditions have been reduced to an ordinary differential equation by use of the similarity variable η. The two independent variables, x and y, were combined into the similarity variable in a fashion that reduced the partial differential equation (and boundary conditions) to an ordinary differential equation. This type of reduction is not generally possible. For example, this method does not work on the full Navier–Stokes equations, although it does on the boundary layer equations (Eqs. 9.8 and 9.9).

Although there is no known analytical solution to Eq. 9.14, it is relatively easy to integrate this equation on a computer. The dimensionless boundary layer profile, $u/U = f'(\eta)$, obtained by numerical solution of Eq. 9.14 (termed the Blasius solution), is sketched in Fig. 9.10*a* and is tabulated in Table 9.1. The velocity profiles at different x locations are similar in that there is only one curve necessary to describe the velocity at any point in the boundary layer. Because the similarity variable η contains both x and y, it is seen from Fig. 9.10*b* that the actual velocity profiles are a function of both x and y. The profile at location x_1 is the same as that at x_2 except that the y coordinate is stretched by a factor of $(x_2/x_1)^{1/2}$.

From the solution it is found that $u/U \approx 0.99$ when $\eta = 5.0$. Thus,

$$\delta = 5\sqrt{\frac{\nu x}{U}} \tag{9.15}$$

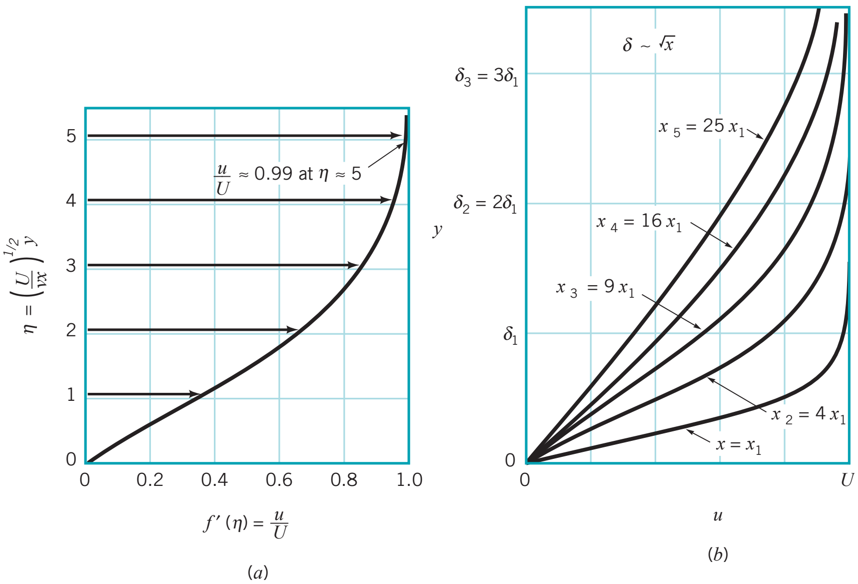

■ **FIGURE 9.10** **Blasius boundary layer profile: (*a*) boundary layer profile in dimensionless form using the similarity variable η, (*b*) similar boundary layer profiles at different locations along the flat plate.**

or

$$\frac{\delta}{x} = \frac{5}{\sqrt{\mathrm{Re}_x}}$$

where $\mathrm{Re}_x = Ux/\nu$. It can also be shown that the displacement and momentum thicknesses are given by

For large Reynolds numbers the boundary layer is relatively thin.

$$\frac{\delta^*}{x} = \frac{1.721}{\sqrt{\mathrm{Re}_x}} \tag{9.16}$$

and

$$\frac{\Theta}{x} = \frac{0.664}{\sqrt{\mathrm{Re}_x}} \tag{9.17}$$

As postulated, the boundary layer is thin provided that Re_x is large (i.e., $\delta/x \rightarrow 0$ as $\mathrm{Re}_x \rightarrow \infty$).

■ **TABLE 9.1**
Laminar Flow along a Flat Plate (the Blasius Solution)

$\eta = y(U/\nu x)^{1/2}$	$f'(\eta) = u/U$	η	$f'(\eta)$
0	0	3.6	0.9233
0.4	0.1328	4.0	0.9555
0.8	0.2647	4.4	0.9759
1.2	0.3938	4.8	0.9878
1.6	0.5168	5.0	0.9916
2.0	0.6298	5.2	0.9943
2.4	0.7290	5.6	0.9975
2.8	0.8115	6.0	0.9990
3.2	0.8761	∞	1.0000

With the velocity profile known, it is an easy matter to determine the wall shear stress, $\tau_w = \mu(\partial u/\partial y)_{y=0}$, where the velocity gradient is evaluated at the plate. The value of $\partial u/\partial y$ at $y = 0$ can be obtained from the Blasius solution to give

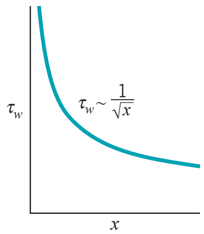

$$\tau_w = 0.332 U^{3/2} \sqrt{\frac{\rho\mu}{x}} \tag{9.18}$$

As indicated by Eq. 9.18 and illustrated in the figure in the margin, the shear stress decreases with increasing x because of the increasing thickness of the boundary layer—the velocity gradient at the wall decreases with increasing x. Also, τ_w varies as $U^{3/2}$, not as U as it does for fully developed laminar pipe flow. These variations are discussed in Section 9.2.3.

9.2.3 Momentum Integral Boundary Layer Equation for a Flat Plate

One of the important aspects of boundary layer theory is the determination of the drag caused by shear forces on a body. As was discussed in the previous section, such results can be obtained from the governing differential equations for laminar boundary layer flow. Since these solutions are extremely difficult to obtain, it is of interest to have an alternative approximate method. The momentum integral method described in this section provides such an alternative.

We consider the uniform flow past a flat plate and the fixed control volume as shown in Fig. 9.11. In agreement with advanced theory and experiment, we assume that the pressure is constant throughout the flow field. The flow entering the control volume at the leading edge of the plate [section (1)] is uniform, while the velocity of the flow exiting the control volume [section (2)] varies from the upstream velocity at the edge of the boundary layer to zero velocity on the plate.

The fluid adjacent to the plate makes up the lower portion of the control surface. The upper surface coincides with the streamline just outside the edge of the boundary layer at section (2). It need not (in fact, does not) coincide with the edge of the boundary layer except at section (2). If we apply the x component of the momentum equation (Eq. 5.22) to the steady flow of fluid within this control volume we obtain

$$\sum F_x = \rho \int_{(1)} u\mathbf{V} \cdot \hat{\mathbf{n}}\, dA + \rho \int_{(2)} u\mathbf{V} \cdot \hat{\mathbf{n}}\, dA$$

where for a plate of width b

$$\sum F_x = -\mathcal{D} = -\int_{\text{plate}} \tau_w\, dA = -b \int_{\text{plate}} \tau_w\, dx \tag{9.19}$$

and $\mathcal{D}$ is the drag that the plate exerts on the fluid. Note that the net force caused by the uniform pressure distribution does not contribute to this flow. Since the plate is solid and the upper surface of the control volume is a streamline, there is no flow through these areas. Thus,

$$-\mathcal{D} = \rho \int_{(1)} U(-U)\, dA + \rho \int_{(2)} u^2\, dA$$

The drag on a flat plate depends on the velocity profile within the boundary layer.

or

$$\mathcal{D} = \rho U^2 bh - \rho b \int_0^\delta u^2\, dy \tag{9.20}$$

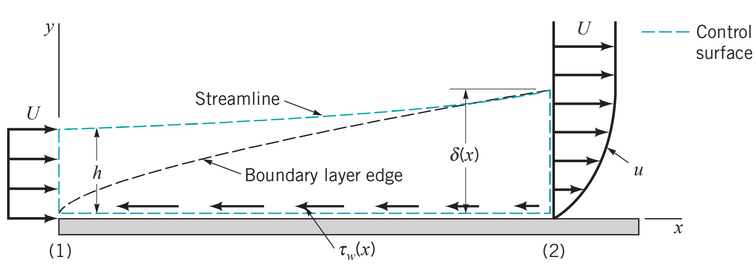

■ **FIGURE 9.11 Control volume used in the derivation of the momentum integral equation for boundary layer flow.**

Although the height h is not known, it is known that for conservation of mass the flowrate through section (1) must equal that through section (2), or

$$Uh = \int_0^\delta u\, dy$$

which can be written as

Drag on a flat plate is related to momentum deficit within the boundary layer.

$$\rho U^2 bh = \rho b \int_0^\delta Uu\, dy \tag{9.21}$$

Thus, by combining Eqs. 9.20 and 9.21 we obtain the drag in terms of the deficit of momentum flux across the outlet of the control volume as

$$\mathfrak{D} = \rho b \int_0^\delta u(U - u)\, dy \tag{9.22}$$

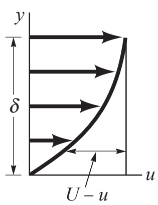

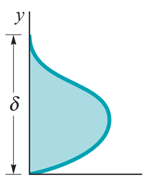

The idea of a momentum deficit is illustrated in the figure in the margin. If the flow were inviscid, the drag would be zero, since we would have $u \equiv U$ and the right-hand side of Eq. 9.22 would be zero. (This is consistent with the fact that $\tau_w = 0$ if $\mu = 0$.) Equation 9.22 points out the important fact that boundary layer flow on a flat plate is governed by a balance between shear drag (the left-hand side of Eq. 9.22) and a decrease in the momentum of the fluid (the right-hand side of Eq. 9.22). As x increases, δ increases and the drag increases. The thickening of the boundary layer is necessary to overcome the drag of the viscous shear stress on the plate. This is contrary to horizontal fully developed pipe flow in which the momentum of the fluid remains constant and the shear force is overcome by the pressure gradient along the pipe.

The development of Eq. 9.22 and its use was first put forth in 1921 by T. von Kármán (1881–1963), a Hungarian/German aerodynamicist. By comparing Eqs. 9.22 and 9.4 we see that the drag can be written in terms of the momentum thickness, Θ, as

$$\mathfrak{D} = \rho b U^2\, \Theta \tag{9.23}$$

Note that this equation is valid for laminar or turbulent flows.

The shear stress distribution can be obtained from Eq. 9.23 by differentiating both sides with respect to x to obtain

$$\frac{d\mathfrak{D}}{dx} = \rho b U^2 \frac{d\Theta}{dx} \tag{9.24}$$

The increase in drag per length of the plate, $d\mathfrak{D}/dx$, occurs at the expense of an increase of the momentum boundary layer thickness, which represents a decrease in the momentum of the fluid.

Since $d\mathfrak{D} = \tau_w\, b\, dx$ (see Eq. 9.19) it follows that

$$\frac{d\mathfrak{D}}{dx} = b\tau_w \tag{9.25}$$

Hence, by combining Eqs. 9.24 and 9.25 we obtain the *momentum integral equation* for the boundary layer flow on a flat plate

$$\tau_w = \rho U^2 \frac{d\Theta}{dx} \tag{9.26}$$

The usefulness of this relationship lies in the ability to obtain approximate boundary layer results easily by using rather crude assumptions. For example, if we knew the detailed velocity profile in the boundary layer (i.e., the Blasius solution discussed in the previous section), we could evaluate either the right-hand side of Eq. 9.23 to obtain the drag, or the right-hand side of Eq. 9.26 to obtain the shear stress. Fortunately, even a rather crude guess at the velocity profile will allow us to obtain reasonable drag and shear stress results from Eq. 9.26. This method is illustrated in Example 9.4.

EXAMPLE 9.4 Momentum Integral Boundary Layer Equation

GIVEN Consider the laminar flow of an incompressible fluid past a flat plate at $y = 0$. The boundary layer velocity profile is approximated as $u = Uy/\delta$ for $0 \le y \le \delta$ and $u = U$ for $y > \delta$, as is shown in Fig. E9.4.

FIND Determine the shear stress by using the momentum integral equation. Compare these results with the Blasius results given by Eq. 9.18.

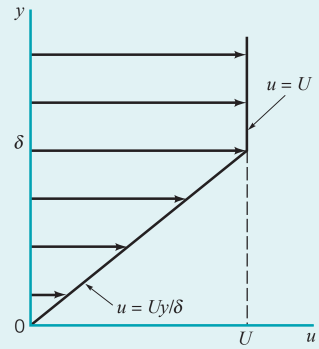

■ FIGURE E9.4

SOLUTION

From Eq. 9.26 the shear stress is given by

$$\tau_w = \rho U^2 \frac{d\Theta}{dx} \tag{1}$$

while for laminar flow we know that $\tau_w = \mu(\partial u/\partial y)_{y=0}$. For the assumed profile we have

$$\tau_w = \mu \frac{U}{\delta} \tag{2}$$

and from Eq. 9.4

$$\Theta = \int_0^\infty \frac{u}{U}\left(1 - \frac{u}{U}\right) dy = \int_0^\delta \frac{u}{U}\left(1 - \frac{u}{U}\right) dy$$

$$= \int_0^\delta \left(\frac{y}{\delta}\right)\left(1 - \frac{y}{\delta}\right) dy$$

or

$$\Theta = \frac{\delta}{6} \tag{3}$$

Note that as yet we do not know the value of δ (but suspect that it should be a function of x).

By combining Eqs. 1, 2, and 3 we obtain the following differential equation for δ:

$$\frac{\mu U}{\delta} = \frac{\rho U^2}{6}\frac{d\delta}{dx}$$

or

$$\delta\, d\delta = \frac{6\mu}{\rho U} dx$$

This can be integrated from the leading edge of the plate, $x = 0$ (where $\delta = 0$) to an arbitrary location x where the boundary layer thickness is δ. The result is

$$\frac{\delta^2}{2} = \frac{6\mu}{\rho U} x$$

or

$$\delta = 3.46 \sqrt{\frac{\nu x}{U}} \tag{4}$$

Note that this approximate result (i.e., the velocity profile is not actually the simple straight line we assumed) compares favorably with the (much more laborious to obtain) Blasius result given by Eq. 9.15.

The wall shear stress can also be obtained by combining Eqs. 1, 3, and 4 to give

$$\tau_w = 0.289 U^{3/2} \sqrt{\frac{\rho\mu}{x}} \qquad \textbf{(Ans)}$$

Again this approximate result is close (within 13%) to the Blasius value of τ_w given by Eq. 9.18.

As is illustrated in Example 9.4, the momentum integral equation, Eq. 9.26, can be used along with an assumed velocity profile to obtain reasonable, approximate boundary layer results. The accuracy of these results depends on how closely the shape of the assumed velocity profile approximates the actual profile.

Thus, we consider a general velocity profile

$$\frac{u}{U} = g(Y) \quad \text{for} \quad 0 \le Y \le 1$$

and

$$\frac{u}{U} = 1 \quad \text{for} \quad Y > 1$$

Approximate velocity profiles are used in the momentum integral equation.

where the dimensionless coordinate $Y = y/\delta$ varies from 0 to 1 across the boundary layer. The dimensionless function $g(Y)$ can be any shape we choose, although it should be a reasonable

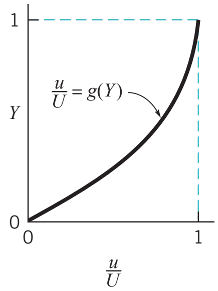

approximation to the boundary layer profile, as shown by the figure in the margin. In particular, it should certainly satisfy the boundary conditions $u = 0$ at $y = 0$ and $u = U$ at $y = \delta$. That is,

$$g(0) = 0 \quad \text{and} \quad g(1) = 1$$

The linear function $g(Y) = Y$ used in Example 9.4 is one such possible profile. Other conditions, such as $dg/dY = 0$ at $Y = 1$ (i.e., $\partial u/\partial y = 0$ at $y = \delta$), could also be incorporated into the function $g(Y)$ to more closely approximate the actual profile.

For a given $g(Y)$, the drag can be determined from Eq. 9.22 as

$$\mathscr{D} = \rho b \int_0^\delta u(U - u)\, dy = \rho b U^2 \delta \int_0^1 g(Y)[1 - g(Y)]\, dY$$

or

$$\mathscr{D} = \rho b U^2 \delta C_1 \tag{9.27}$$

where the dimensionless constant C_1 has the value

$$C_1 = \int_0^1 g(Y)[1 - g(Y)]\, dY$$

Also, the wall shear stress can be written as

$$\tau_w = \mu \left.\frac{\partial u}{\partial y}\right|_{y=0} = \frac{\mu U}{\delta} \left.\frac{dg}{dY}\right|_{Y=0} = \frac{\mu U}{\delta} C_2 \tag{9.28}$$

where the dimensionless constant C_2 has the value

$$C_2 = \left.\frac{dg}{dY}\right|_{Y=0}$$

By combining Eqs. 9.25, 9.27, and 9.28 we obtain

$$\delta\, d\delta = \frac{\mu C_2}{\rho U C_1} dx$$

which can be integrated from $\delta = 0$ at $x = 0$ to give

$$\delta = \sqrt{\frac{2\nu C_2 x}{U C_1}}$$

or

$$\frac{\delta}{x} = \frac{\sqrt{2C_2/C_1}}{\sqrt{\mathrm{Re}_x}} \tag{9.29}$$

By substituting this expression back into Eqs. 9.28 we obtain

$$\tau_w = \sqrt{\frac{C_1 C_2}{2}}\, U^{3/2} \sqrt{\frac{\rho\mu}{x}} \tag{9.30}$$

Approximate boundary layer results are obtained from the momentum integral equation.

To use Eqs. 9.29 and 9.30 we must determine the values of C_1 and C_2. Several assumed velocity profiles and the resulting values of δ are given in Fig. 9.12 and Table 9.2. The more closely the assumed shape approximates the actual (i.e., Blasius) profile, the more accurate the final results. For any assumed profile shape, the functional dependence of δ and τ_w on the physical parameters ρ, μ, U, and x is the same. Only the constants are different. That is, $\delta \sim (\mu x/\rho U)^{1/2}$ or $\delta \mathrm{Re}_x^{1/2}/x = \text{constant}$, and $\tau_w \sim (\rho\mu U^3/x)^{1/2}$, where $\mathrm{Re}_x = \rho U x/\mu$.

It is often convenient to use the dimensionless *local friction coefficient*, c_f, defined as

$$c_f = \frac{\tau_w}{\frac{1}{2}\rho U^2} \tag{9.31}$$

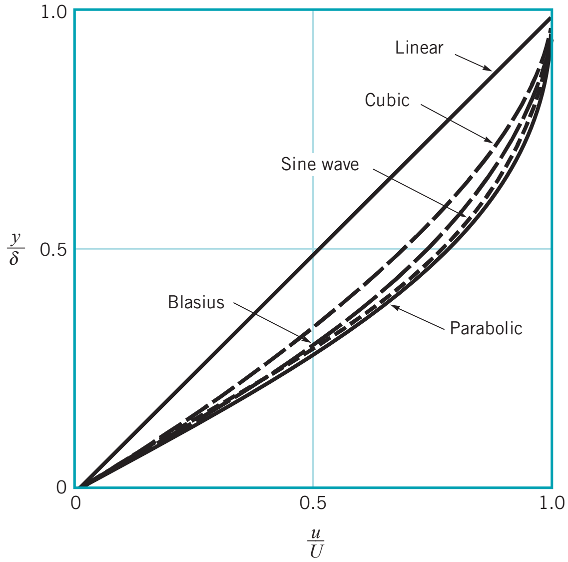

■ **FIGURE 9.12 Typical approximate boundary layer profiles used in the momentum integral equation.**

to express the wall shear stress. From Eq. 9.30 we obtain the approximate value

$$c_f = \sqrt{2C_1C_2}\sqrt{\frac{\mu}{\rho U x}} = \frac{\sqrt{2C_1C_2}}{\sqrt{\mathrm{Re}_x}}$$

while the Blasius solution result is given by

$$c_f = \frac{0.664}{\sqrt{\mathrm{Re}_x}} \tag{9.32}$$

These results are also indicated in Table 9.2.

For a flat plate of length ℓ and width b, the net friction drag, $\mathfrak{D}_f$, can be expressed in terms of the *friction drag coefficient*, C_{Df}, as

The friction drag coefficient is an integral of the local friction coefficient.

$$C_{Df} = \frac{\mathfrak{D}_f}{\frac{1}{2}\rho U^2 b\ell} = \frac{b\displaystyle\int_0^\ell \tau_w\,dx}{\frac{1}{2}\rho U^2 b\ell}$$

or

$$C_{Df} = \frac{1}{\ell}\int_0^\ell c_f\,dx \tag{9.33}$$

■ **TABLE 9.2**

Flat Plate Momentum Integral Results for Various Assumed Laminar Flow Velocity Profiles

Profile Character	$\delta \mathrm{Re}_x^{1/2}/x$	$c_f \mathrm{Re}_x^{1/2}$	$C_{Df}\mathrm{Re}_\ell^{1/2}$
a. Blasius solution	5.00	0.664	1.328
b. Linear $u/U = y/\delta$	3.46	0.578	1.156
c. Parabolic $u/U = 2y/\delta - (y/\delta)^2$	5.48	0.730	1.460
d. Cubic $u/U = 3(y/\delta)/2 - (y/\delta)^3/2$	4.64	0.646	1.292
e. Sine wave $u/U = \sin[\pi(y/\delta)/2]$	4.79	0.655	1.310

We use the above approximate value of $c_f = (2C_1C_2\mu/\rho Ux)^{1/2}$ to obtain

$$C_{Df} = \frac{\sqrt{8C_1C_2}}{\sqrt{\text{Re}_\ell}}$$

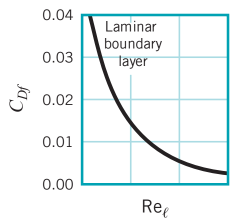

where $\text{Re}_\ell = U\ell/\nu$ is the Reynolds number based on the plate length. The corresponding value obtained from the Blasius solution (Eq. 9.32) and shown by the figure in the margin gives

$$C_{Df} = \frac{1.328}{\sqrt{\text{Re}_\ell}}$$

These results are also indicated in Table 9.2.

The momentum integral boundary layer method provides a relatively simple technique to obtain useful boundary layer results. As is discussed in Sections 9.2.5 and 9.2.6, this technique can be extended to boundary layer flows on curved surfaces (where the pressure and fluid velocity at the edge of the boundary layer are not constant) and to turbulent flows.

9.2.4 Transition from Laminar to Turbulent Flow

The boundary layer on a flat plate will become turbulent if the plate is long enough.

The analytical results given in Table 9.2 are restricted to laminar boundary layer flows along a flat plate with zero pressure gradient. They agree quite well with experimental results up to the point where the boundary layer flow becomes turbulent, which will occur for any free-stream velocity and any fluid provided the plate is long enough. This is true because the parameter that governs the ***transition*** to turbulent flow is the Reynolds number—in this case the Reynolds number based on the distance from the leading edge of the plate, $\text{Re}_x = Ux/\nu$.

The value of the Reynolds number at the transition location is a rather complex function of various parameters involved, including the roughness of the surface, the curvature of the surface (for example, a flat plate or a sphere), and some measure of the disturbances in the flow outside the boundary layer. On a flat plate with a sharp leading edge in a typical airstream, the transition takes place at a distance x from the leading edge given by $\text{Re}_{xcr} = 2 \times 10^5$ to 3×10^6. Unless otherwise stated, we will use $\text{Re}_{xcr} = 5 \times 10^5$ in our calculations.

The actual transition from laminar to turbulent boundary layer flow may occur over a region of the plate, not at a specific single location. This occurs, in part, because of the spottiness of the transition. Typically, the transition begins at random locations on the plate in the vicinity of $\text{Re}_x = \text{Re}_{xcr}$. These spots grow rapidly as they are convected downstream until the entire width of the plate is covered with turbulent flow. The photo shown in Fig. 9.13 illustrates this transition process.

The complex process of transition from laminar to turbulent flow involves the instability of the flow field. Small disturbances imposed on the boundary layer flow (i.e., from a vibration of the plate, a roughness of the surface, or a "wiggle" in the flow past the plate) will either grow (instability) or decay (stability), depending on where the disturbance is introduced into the flow. If these disturbances occur at a location with $\text{Re}_x < \text{Re}_{xcr}$ they will die out, and the boundary layer will return to laminar flow at that location. Disturbances imposed at a location with $\text{Re}_x > \text{Re}_{xcr}$ will grow and transform the boundary layer flow downstream of this location into turbulence. The study of the initiation, growth, and structure of these turbulent bursts or spots is an active area of fluid mechanics research.

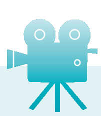

V9.5 Transition on flat plate

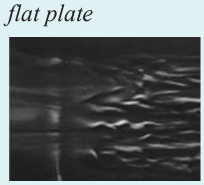

FIGURE 9.13 Turbulent spots and the transition from laminar to turbulent boundary layer flow on a flat plate. Flow from left to right. (Photograph courtesy of B. Cantwell, Stanford University.)

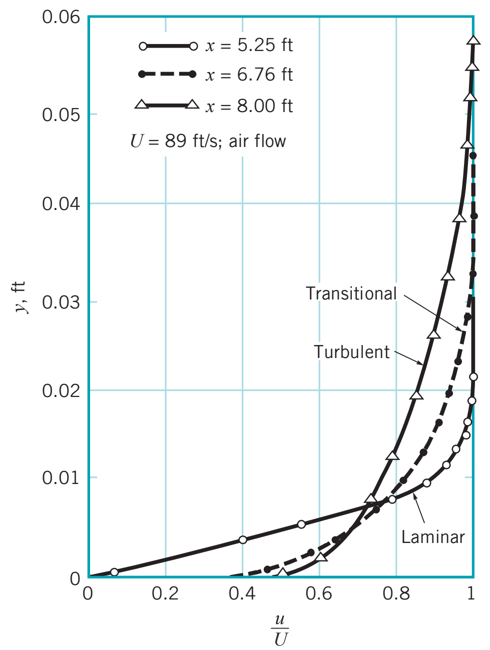

■ **FIGURE 9.14** **Typical boundary layer profiles on a flat plate for laminar, transitional, and turbulent flow (Ref. 1).**

Transition from laminar to turbulent flow also involves a noticeable change in the shape of the boundary layer velocity profile. Typical profiles obtained in the neighborhood of the transition location are indicated in Fig. 9.14. The turbulent profiles are flatter, have a larger velocity gradient at the wall, and produce a larger boundary layer thickness than do the laminar profiles.

EXAMPLE 9.5 Boundary Layer Transition

GIVEN A fluid flows steadily past a flat plate with a velocity of $U = 10$ ft/s.

FIND At approximately what location will the boundary layer become turbulent, and how thick is the boundary layer at that point if the fluid is (a) water at 60 °F, (b) standard air, or (c) glycerin at 68 °F?

SOLUTION

For any fluid, the laminar boundary layer thickness is found from Eq. 9.15 as

$$\delta = 5\sqrt{\frac{\nu x}{U}}$$

The boundary layer remains laminar up to

$$x_{\text{cr}} = \frac{\nu \text{Re}_{x\text{cr}}}{U}$$

Thus, if we assume $\text{Re}_{x\text{cr}} = 5 \times 10^5$ we obtain

$$x_{\text{cr}} = \frac{5 \times 10^5}{10 \text{ ft/s}} \nu = 5 \times 10^4 \nu$$

and

$$\delta_{\text{cr}} \equiv \delta|_{x=x_{\text{cr}}} = 5\left[\frac{\nu}{10}(5 \times 10^4 \nu)\right]^{1/2} = 354 \nu$$

where ν is in ft²/s and x_{cr} and δ_{cr} are in feet. The values of the kinematic viscosity obtained from Tables 1.5 and 1.7 are listed in Table E9.5 along with the corresponding x_{cr} and δ_{cr}.

■ **TABLE E9.5**

Fluid	ν (ft²/s)	x_{cr} (ft)	δ_{cr} (ft)
a. Water	1.21×10^{-5}	0.605	0.00428
b. Air	1.57×10^{-4}	7.85	0.0556
c. Glycerin	1.28×10^{-2}	640.0	4.53

(Ans)

COMMENT Laminar flow can be maintained on a longer portion of the plate if the viscosity is increased. However, the boundary layer flow eventually becomes turbulent, provided the plate is long enough. Similarly, the boundary layer thickness is greater if the viscosity is increased.

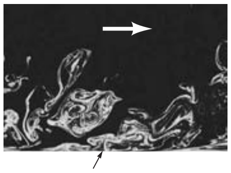

Random transport of finite-sized fluid particles occurs within turbulent boundary layers.

9.2.5 Turbulent Boundary Layer Flow

The structure of turbulent boundary layer flow is very complex, random, and irregular. It shares many of the characteristics described for turbulent pipe flow in Section 8.3. In particular, the velocity at any given location in the flow is unsteady in a random fashion. The flow can be thought of as a jumbled mix of intertwined eddies (or swirls) of different sizes (diameters and angular velocities). The figure in the margin shows a laser-induced fluorescence visualization of a turbulent boundary layer on a flat plate (side view). The various fluid quantities involved (i.e., mass, momentum, energy) are convected downstream in the free-stream direction as in a laminar boundary layer. For turbulent flow they are also convected across the boundary layer (in the direction perpendicular to the plate) by the random transport of finite-sized fluid particles associated with the turbulent eddies. There is considerable mixing involved with these finite-sized eddies—considerably more than is associated with the mixing found in laminar flow where it is confined to the molecular scale. Although there is considerable random motion of fluid particles perpendicular to the plate, there is very little net transfer of mass across the boundary layer—the largest flowrate by far is parallel to the plate.

There is, however, a considerable net transfer of x component of momentum perpendicular to the plate because of the random motion of the particles. Fluid particles moving toward the plate (in the negative y direction) have some of their excess momentum (they come from areas of higher velocity) removed by the plate. Conversely, particles moving away from the plate (in the positive y direction) gain momentum from the fluid (they come from areas of lower velocity). The net result is that the plate acts as a momentum sink, continually extracting momentum from the fluid. For laminar flows, such cross-stream transfer of these properties takes place solely on the molecular scale. For turbulent flow the randomness is associated with fluid particle mixing. Consequently, the shear force for turbulent boundary layer flow is considerably greater than it is for laminar boundary layer flow (see Section 8.3.2).

There are no "exact" solutions for turbulent boundary layer flow. As is discussed in Section 9.2.2, it is possible to solve the Prandtl boundary layer equations for laminar flow past a flat plate to obtain the Blasius solution (which is "exact" within the framework of the assumptions involved in the boundary layer equations). Since there is no precise expression for the shear stress in turbulent flow (see Section 8.3), solutions are not available for turbulent flow. However, considerable headway has been made in obtaining numerical (computer) solutions for turbulent flow by using approximate shear stress relationships. Also, progress is being made in the area of direct, full numerical integration of the basic governing equations, the Navier–Stokes equations.

Approximate turbulent boundary layer results can also be obtained by use of the momentum integral equation, Eq. 9.26, which is valid for either laminar or turbulent flow. What is needed for the use of this equation are reasonable approximations to the velocity profile $u = U\,g(Y)$, where $Y = y/\delta$ and u is the time-averaged velocity (the overbar notation, $\overline{u}$, of Section 8.3.2 has been dropped for convenience), and a functional relationship describing the wall shear stress. For laminar flow the wall shear stress was used as $\tau_w = \mu(\partial u/\partial y)_{y=0}$. In theory, such a technique should work for turbulent boundary layers also. However, as is discussed in Section 8.3, the details of the velocity gradient at the wall are not well understood for turbulent flow. Thus, it is necessary to use some empirical relationship for the wall shear stress. This is illustrated in Example 9.6.

EXAMPLE 9.6 Turbulent Boundary Layer Properties

GIVEN Consider turbulent flow of an incompressible fluid past a flat plate. The boundary layer velocity profile is assumed to be $u/U = (y/\delta)^{1/7} = Y^{1/7}$ for $Y = y/\delta \le 1$ and $u = U$ for $Y > 1$ as shown in Fig. E9.6. This is a reasonable approximation of experimentally observed profiles, except very near the plate where this formula gives $\partial u/\partial y = \infty$ at $y = 0$. Note the differences between the assumed turbulent profile and the laminar profile. Also assume that the shear stress agrees with the experimentally determined formula:

$$\tau_w = 0.0225\rho U^2 \left(\frac{\nu}{U\delta}\right)^{1/4} \tag{1}$$

FIND Determine the boundary layer thicknesses δ, δ^*, and Θ and the wall shear stress, τ_w, as a function of x. Determine the friction drag coefficient, C_{Df}.

Solution

Whether the flow is laminar or turbulent, it is true that the drag force is accounted for by a reduction in the momentum of the fluid flowing past the plate. The shear is obtained from Eq. 9.26 in terms of the rate at which the momentum boundary layer thickness, Θ, increases with distance along the plate as

$$\tau_w = \rho U^2 \frac{d\Theta}{dx}$$

For the assumed velocity profile, the boundary layer momentum thickness is obtained from Eq. 9.4 as

$$\Theta = \int_0^\infty \frac{u}{U}\left(1 - \frac{u}{U}\right) dy = \delta \int_0^1 \frac{u}{U}\left(1 - \frac{u}{U}\right) dY$$

or by integration

$$\Theta = \delta \int_0^1 Y^{1/7}(1 - Y^{1/7})\, dY = \frac{7}{72}\delta \qquad \textbf{(2)}$$

where δ is an unknown function of x. By combining the assumed shear force dependence (Eq. 1) with Eq. 2, we obtain the following differential equation for δ:

$$0.0225\rho U^2 \left(\frac{\nu}{U\delta}\right)^{1/4} = \frac{7}{72}\rho U^2 \frac{d\delta}{dx}$$

or

$$\delta^{1/4}\, d\delta = 0.231 \left(\frac{\nu}{U}\right)^{1/4} dx$$

This can be integrated from $\delta = 0$ at $x = 0$ to obtain

$$\delta = 0.370 \left(\frac{\nu}{U}\right)^{1/5} x^{4/5} \qquad \textbf{(3)} \quad \textbf{(Ans)}$$

or in dimensionless form

$$\frac{\delta}{x} = \frac{0.370}{\mathrm{Re}_x^{1/5}}$$

Strictly speaking, the boundary layer near the leading edge of the plate is laminar, not turbulent, and the precise boundary condition should be the matching of the initial turbulent boundary layer thickness (at the transition location) with the thickness of the laminar boundary layer at that point. In practice, however, the laminar boundary layer often exists over a relatively short portion of the plate, and the error associated with starting the turbulent boundary layer with $\delta = 0$ at $x = 0$ can be negligible.

The displacement thickness, δ^*, and the momentum thickness, Θ, can be obtained from Eqs. 9.3 and 9.4 by integrating as follows:

$$\delta^* = \int_0^\infty \left(1 - \frac{u}{U}\right) dy = \delta \int_0^1 \left(1 - \frac{u}{U}\right) dY$$

$$= \delta \int_0^1 (1 - Y^{1/7})\, dY = \frac{\delta}{8}$$

Thus, by combining this with Eq. 3 we obtain

$$\delta^* = 0.0463 \left(\frac{\nu}{U}\right)^{1/5} x^{4/5} \qquad \textbf{(Ans)}$$

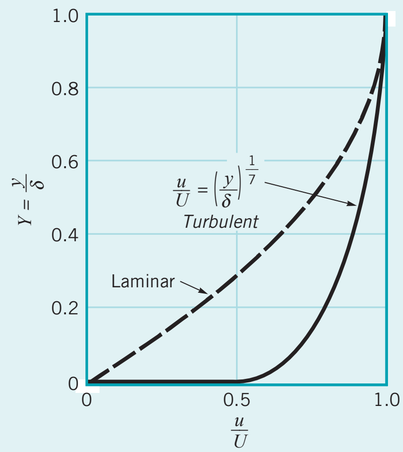

■ **FIGURE E9.6**

Similarly, from Eq. 2,

$$\Theta = \tfrac{7}{72}\delta = 0.0360 \left(\frac{\nu}{U}\right)^{1/5} x^{4/5} \qquad \textbf{(4)} \quad \textbf{(Ans)}$$

The functional dependence for δ, δ^*, and Θ is the same; only the constants of proportionality are different. Typically, $\Theta < \delta^* < \delta$.

By combining Eqs. 1 and 3, we obtain the following result for the wall shear stress

$$\tau_w = 0.0225\rho U^2 \left[\frac{\nu}{U(0.370)(\nu/U)^{1/5} x^{4/5}}\right]^{1/4}$$

$$= \frac{0.0288\rho U^2}{\mathrm{Re}_x^{1/5}} \qquad \textbf{(Ans)}$$

This can be integrated over the length of the plate to obtain the friction drag on one side of the plate, $\mathscr{D}_f$, as

$$\mathscr{D}_f = \int_0^\ell b\tau_w\, dx = b(0.0288\rho U^2)\int_0^\ell \left(\frac{\nu}{Ux}\right)^{1/5} dx$$

or

$$\mathscr{D}_f = 0.0360\rho U^2 \frac{A}{\mathrm{Re}_\ell^{1/5}}$$

where $A = b\ell$ is the area of the plate. (This result can also be obtained by combining Eq. 9.23 and the expression for the momentum thickness given in Eq. 4.) The corresponding friction drag coefficient, C_{Df}, is

$$C_{Df} = \frac{\mathscr{D}_f}{\frac{1}{2}\rho U^2 A} = \frac{0.0720}{\mathrm{Re}_\ell^{1/5}} \qquad \textbf{(Ans)}$$

COMMENT Note that for the turbulent boundary layer flow the boundary layer thickness increases with x as $\delta \sim x^{4/5}$ and the shear stress decreases as $\tau_w \sim x^{-1/5}$. For laminar flow these dependencies are $x^{1/2}$ and $x^{-1/2}$, respectively. The random character of the turbulent flow causes a different structure of the flow.

Obviously the results presented in this example are valid only in the range of validity of the original data—the assumed velocity profile and shear stress. This range covers smooth flat plates with $5 \times 10^5 < \mathrm{Re}_\ell < 10^7$.

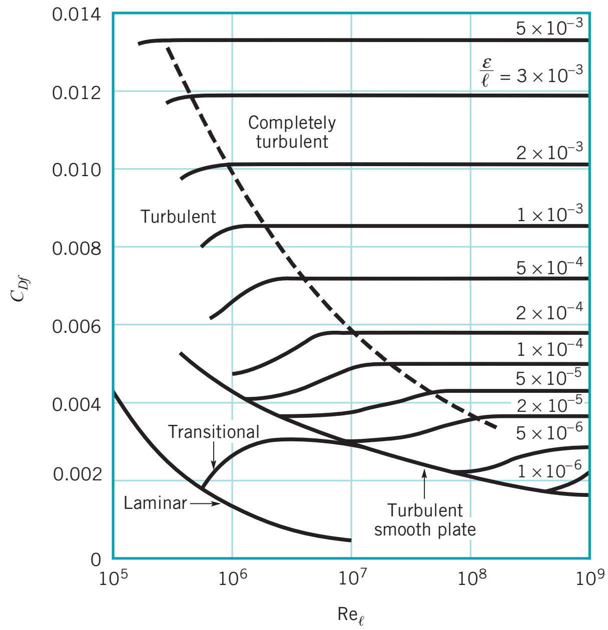

FIGURE 9.15 Friction drag coefficient for a flat plate parallel to the upstream flow (Ref. 18, with permission).

The flat plate drag coefficient is a function of relative roughness and Reynolds number.

In general, the drag coefficient for a flat plate of length ℓ is a function of the Reynolds number, Re_ℓ, and the relative roughness, ε/ℓ. The results of numerous experiments covering a wide range of the parameters of interest are shown in Fig. 9.15. For laminar boundary layer flow the drag coefficient is a function of only the Reynolds number—surface roughness is not important. This is similar to laminar flow in a pipe. However, for turbulent flow, the surface roughness does affect the shear stress and, hence, the drag coefficient. This is similar to turbulent pipe flow in which the surface roughness may protrude into or through the viscous sublayer next to the wall and alter the flow in this thin, but very important, layer (see Section 8.4.1). Values of the roughness, ε, for different materials can be obtained from Table 8.1.

The drag coefficient diagram of Fig. 9.15 (boundary layer flow) shares many characteristics in common with the familiar Moody diagram (pipe flow) of Fig. 8.23, even though the mechanisms governing the flow are quite different. Fully developed horizontal pipe flow is governed by a balance between pressure forces and viscous forces. The fluid inertia remains constant throughout the flow. Boundary layer flow on a horizontal flat plate is governed by a balance between inertia effects and viscous forces. The pressure remains constant throughout the flow. (As is discussed in Section 9.2.6, for boundary layer flow on curved surfaces, the pressure is not constant.)

It is often convenient to have an equation for the drag coefficient as a function of the Reynolds number and relative roughness rather than the graphical representation given in Fig. 9.15. Although there is not one equation valid for the entire $\mathrm{Re}_\ell - \varepsilon/\ell$ range, the equations presented in Table 9.3 do work well for the conditions indicated.

TABLE 9.3
Empirical Equations for the Flat Plate Drag Coefficient (Ref. 1)

Equation	Flow Conditions
$C_{Df} = 1.328/(\mathrm{Re}_\ell)^{0.5}$	Laminar flow
$C_{Df} = 0.455/(\log \mathrm{Re}_\ell)^{2.58} - 1700/\mathrm{Re}_\ell$	Transitional with $\mathrm{Re}_{xcr} = 5 \times 10^5$
$C_{Df} = 0.455/(\log \mathrm{Re}_\ell)^{2.58}$	Turbulent, smooth plate
$C_{Df} = [1.89 - 1.62 \log(\varepsilon/\ell)]^{-2.5}$	Completely turbulent

EXAMPLE 9.7 Drag on a Flat Plate

GIVEN The water ski shown in Fig. E9.7*a* moves through 70 °F water with a velocity U.

FIND Estimate the drag caused by the shear stress on the bottom of the ski for $0 < U < 30$ ft/s.

SOLUTION

Clearly the ski is not a flat plate, and it is not aligned exactly parallel to the upstream flow. However, we can obtain a reasonable approximation to the shear force by using the flat plate results. That is, the friction drag, $\mathfrak{D}_f$, caused by the shear stress on the bottom of the ski (the wall shear stress) can be determined as

$$\mathfrak{D}_f = \tfrac{1}{2}\rho U^2 \ell b C_{Df}$$

With $A = \ell b = 4 \text{ ft} \times 0.5 \text{ ft} = 2 \text{ ft}^2$, $\rho = 1.94 \text{ slugs/ft}^3$, and $\mu = 2.04 \times 10^{-5} \text{ lb} \cdot \text{s/ft}^2$ (see Table B.1) we obtain

$$\begin{aligned}\mathfrak{D}_f &= \tfrac{1}{2}(1.94 \text{ slugs/ft}^3)(2.0 \text{ ft}^2)U^2 C_{Df} \\ &= 1.94\, U^2 C_{Df} \qquad (1)\end{aligned}$$

where $\mathfrak{D}_f$ and U are in pounds and ft/s, respectively.

The friction coefficient, C_{Df}, can be obtained from Fig. 9.15 or from the appropriate equations given in Table 9.3. As we will see, for this problem, much of the flow lies within the transition regime where both the laminar and turbulent portions of the boundary layer flow occupy comparable lengths of the plate. We choose to use the values of C_{Df} from the table.

For the given conditions we obtain

$$\text{Re}_\ell = \frac{\rho U \ell}{\mu} = \frac{(1.94 \text{ slugs/ft}^3)(4 \text{ ft})U}{2.04 \times 10^{-5} \text{ lb} \cdot \text{s/ft}^2} = 3.80 \times 10^5\, U$$

where U is in ft/s. With $U = 10$ ft/s, or $\text{Re}_\ell = 3.80 \times 10^6$, we obtain from Table 9.3 $C_{Df} = 0.455/(\log \text{Re}_\ell)^{2.58} - 1700/\text{Re}_\ell = 0.00308$. From Eq. 1 the corresponding drag is

$$\mathfrak{D}_f = 1.94(10)^2(0.00308) = 0.598 \text{ lb}$$

By covering the range of upstream velocities of interest we obtain the results shown in Fig. E9.7*b*. **(Ans)**

COMMENTS If $\text{Re} \lesssim 1000$, the results of boundary layer theory are not valid—inertia effects are not dominant enough and the boundary layer is not thin compared with the length of the plate. For our problem this corresponds to $U = 2.63 \times 10^{-3}$ ft/s. For all practical purposes U is greater than this value, and the flow past the ski is of the boundary layer type.

The approximate location of the transition from laminar to turbulent boundary layer flow as defined by $\text{Re}_{\text{cr}} = \rho U x_{\text{cr}}/\mu = 5 \times 10^5$ is indicated in Fig. E9.7*b*. Up to $U = 1.31$ ft/s the entire boundary layer is laminar. The fraction of the boundary layer that is laminar decreases as U increases until only the front 0.18 ft is laminar when $U = 30$ ft/s.

For anyone who has water skied, it is clear that it can require considerably more force to be pulled along at 30 ft/s than the $2 \times 4.88 \text{ lb} = 9.76$ lb (two skis) indicated in Fig. E9.7*b*. As is discussed in Section 9.3, the total drag on an object such as a water ski consists of more than just the friction drag. Other components, including pressure drag and wave-making drag, add considerably to the total resistance.

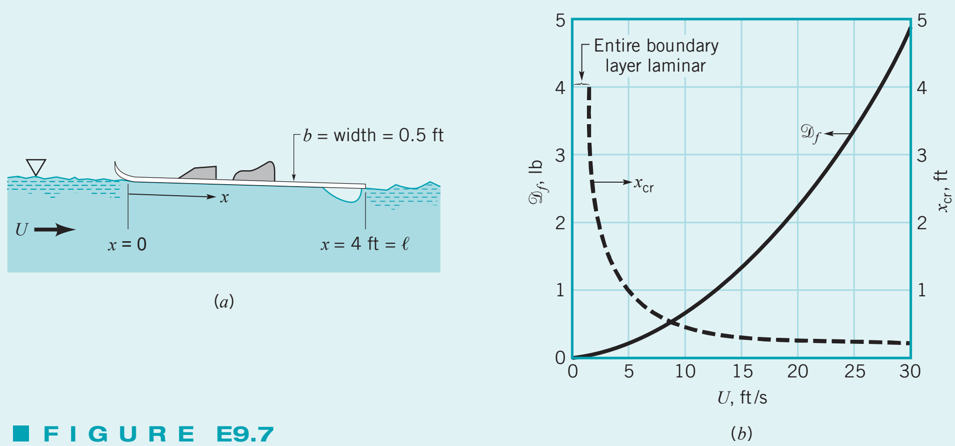

■ FIGURE E9.7

9.2.6 Effects of Pressure Gradient

The boundary layer discussions in the previous parts of Section 9.2 have dealt with flow along a flat plate in which the pressure is constant throughout the fluid. In general, when a fluid flows past an object other than a flat plate, the pressure field is not uniform. As shown in Fig. 9.6, if the Reynolds number is large, relatively thin boundary layers will develop along the surfaces. Within

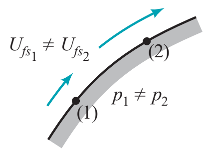

these layers the component of the pressure gradient in the streamwise direction (i.e., along the body surface) is not zero, although the pressure gradient normal to the surface is negligibly small. That is, if we were to measure the pressure while moving across the boundary layer from the body to the boundary layer edge, we would find that the pressure is essentially constant. However, the pressure does vary in the direction along the body surface if the body is curved, as shown by the figure in the margin. The variation in the ***free-stream velocity,*** U_{fs}, the fluid velocity at the edge of the boundary layer, is the cause of the pressure gradient in this direction. The characteristics of the entire flow (both within and outside of the boundary layer) are often highly dependent on the pressure gradient effects on the fluid within the boundary layer.

The free-stream velocity on a curved surface is not constant.

For a flat plate parallel to the upstream flow, the upstream velocity (that far ahead of the plate) and the free-stream velocity (that at the edge of the boundary layer) are equal—$U = U_{fs}$. This is a consequence of the negligible thickness of the plate. For bodies of nonzero thickness, these two velocities are different. This can be seen in the flow past a circular cylinder of diameter D. The upstream velocity and pressure are U and p_0, respectively. If the fluid were completely inviscid ($\mu = 0$), the Reynolds number would be infinite ($\text{Re} = \rho UD/\mu = \infty$) and the streamlines would be symmetrical, as are shown in Fig. 9.16*a*. The fluid velocity along the surface would vary from $U_{fs} = 0$ at the very front and rear of the cylinder (points A and F are stagnation points) to a maximum of $U_{fs} = 2U$ at the top and bottom of the cylinder (point C). This is also indicated in the figure in the margin. The pressure on the surface of the cylinder would be symmetrical about the vertical midplane of the cylinder, reaching a maximum value of $p_0 + \rho U^2/2$ (the stagnation pressure) at both the front and back of the cylinder, and a minimum of $p_0 - 3\rho U^2/2$ at the top and bottom of the cylinder. The pressure and free-stream velocity distributions are shown in Figs. 9.16*b* and 9.16*c*. These characteristics can be obtained from potential flow analysis of Section 6.6.3.

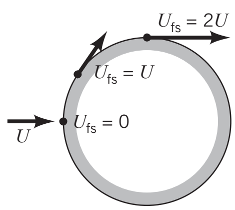

Because of the absence of viscosity (therefore, $\tau_w = 0$) and the symmetry of the pressure distribution for inviscid flow past a circular cylinder, it is clear that the drag on the cylinder is zero. Although it is not obvious, it can be shown that the drag is zero for any object that does not produce a lift (symmetrical or not) in an inviscid fluid (Ref. 4). Based on experimental evidence, however, we know that there must be a net drag. Clearly, since there is no purely inviscid fluid, the reason for the observed drag must lie on the shoulders of the viscous effects.

To test this hypothesis, we could conduct an experiment by measuring the drag on an object (such as a circular cylinder) in a series of fluids with decreasing values of viscosity. To our initial surprise we would find that no matter how small we make the viscosity (provided it is not precisely zero) we would measure a finite drag, essentially independent of the value of μ. As was noted in Section 6.6.3, this leads to what has been termed *d'Alembert's paradox*—the drag on an

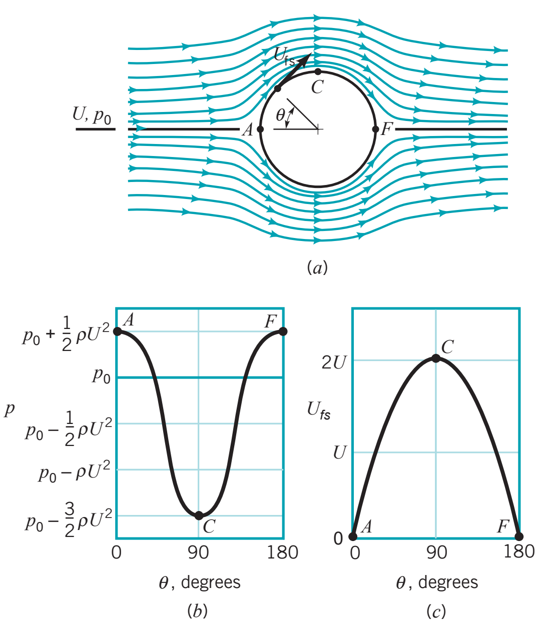

FIGURE 9.16 **Inviscid flow past a circular cylinder: (*a*) streamlines for the flow if there were no viscous effects, (*b*) pressure distribution on the cylinder's surface, (*c*) free-stream velocity on the cylinder's surface.**

object in an inviscid fluid is zero, but the drag on an object in a fluid with vanishingly small (but nonzero) viscosity is not zero.

The reason for the above paradox can be described in terms of the effect of the pressure gradient on boundary layer flow. Consider large Reynolds number flow of a real (viscous) fluid past a circular cylinder. As was discussed in Section 9.1.2, we expect the viscous effects to be confined to thin boundary layers near the surface. This allows the fluid to stick ($\mathbf{V} = 0$) to the surface—a necessary condition for any fluid, provided $\mu \neq 0$. The basic idea of boundary layer theory is that the boundary layer is thin enough so that it does not greatly disturb the flow outside the boundary layer. Based on this reasoning, for large Reynolds numbers the flow throughout most of the flow field would be expected to be as is indicated in Fig. 9.16*a*, the inviscid flow field.

The pressure gradient in the external flow is imposed throughout the boundary layer fluid.

The pressure distribution indicated in Fig. 9.16*b* is imposed on the boundary layer flow along the surface of the cylinder. In fact, there is negligible pressure variation across the thin boundary layer so that the pressure within the boundary layer is that given by the inviscid flow field. This pressure distribution along the cylinder is such that the stationary fluid at the nose of the cylinder ($U_{fs} = 0$ at $\theta = 0$) is accelerated to its maximum velocity ($U_{fs} = 2U$ at $\theta = 90°$) and then is decelerated back to zero velocity at the rear of the cylinder ($U_{fs} = 0$ at $\theta = 180°$). This is accomplished by a balance between pressure and inertia effects; viscous effects are absent for the inviscid flow outside the boundary layer.

Physically, in the absence of viscous effects, a fluid particle traveling from the front to the back of the cylinder coasts down the "pressure hill" from $\theta = 0$ to $\theta = 90°$ (from point A to C in Fig. 9.16*b*) and then back up the hill to $\theta = 180°$ (from point C to F) without any loss of energy. There is an exchange between kinetic and pressure energy, but there are no energy losses. The same pressure distribution is imposed on the viscous fluid within the boundary layer. The decrease in pressure in the direction of flow along the front half of the cylinder is termed a ***favorable pressure gradient***. The increase in pressure in the direction of flow along the rear half of the cylinder is termed an ***adverse pressure gradient***.

Consider a fluid particle within the boundary layer indicated in Fig. 9.17*a*. In its attempt to flow from A to F it experiences the same pressure distribution as the particles in the free stream immediately outside the boundary layer—the inviscid flow field pressure. However, because of the viscous effects involved, the particle in the boundary layer experiences a loss of energy as it flows along. This loss means that the particle does not have enough energy to coast all of the way up the pressure hill (from C to F) and to reach point F at the rear of the cylinder. This kinetic energy deficit is seen in the velocity profile detail at point C, shown in Fig. 9.17*a*. Because of friction, the boundary layer fluid cannot travel from the front to the rear of the cylinder. (This conclusion can also be obtained from the concept that due to viscous effects the particle at C does not have enough momentum to allow it to coast up the pressure hill to F.)

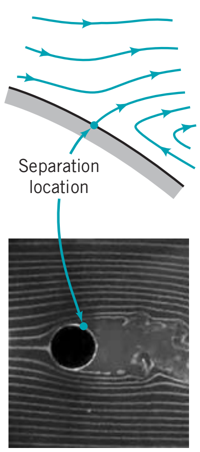

The situation is similar to a bicyclist coasting down a hill and up the other side of the valley. If there were no friction, the rider starting with zero speed could reach the same height from which he or she started. Clearly friction (rolling resistance, aerodynamic drag, etc.) causes a loss of energy (and momentum), making it impossible for the rider to reach the height from which he or she started without supplying additional energy (i.e., pedaling). The fluid within the boundary layer does not have such an energy supply. Thus, the fluid flows against the increasing pressure as far as it can, at which point the boundary layer separates from (lifts off) the surface. This ***boundary layer separation*** is indicated in Fig. 9.17*a* as well as the figures in the margin. (See the photograph at the beginning of Chapters 7, 9, and 11.) Typical velocity profiles at representative locations along the surface are shown in Fig. 9.17*b*. At the separation location (profile D), the velocity gradient at the wall and the wall shear stress are zero. Beyond that location (from D to E) there is reverse flow in the boundary layer.

V9.6 Snow drifts

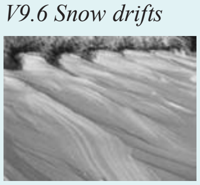

As is indicated in Fig. 9.17*c*, because of the boundary layer separation, the average pressure on the rear half of the cylinder is considerably less than that on the front half. Thus, a large pressure drag is developed, even though (because of small viscosity) the viscous shear drag may be quite small. D'Alembert's paradox is explained. No matter how small the viscosity, provided it is not zero, there will be a boundary layer that separates from the surface, giving a drag that is, for the most part, independent of the value of μ.

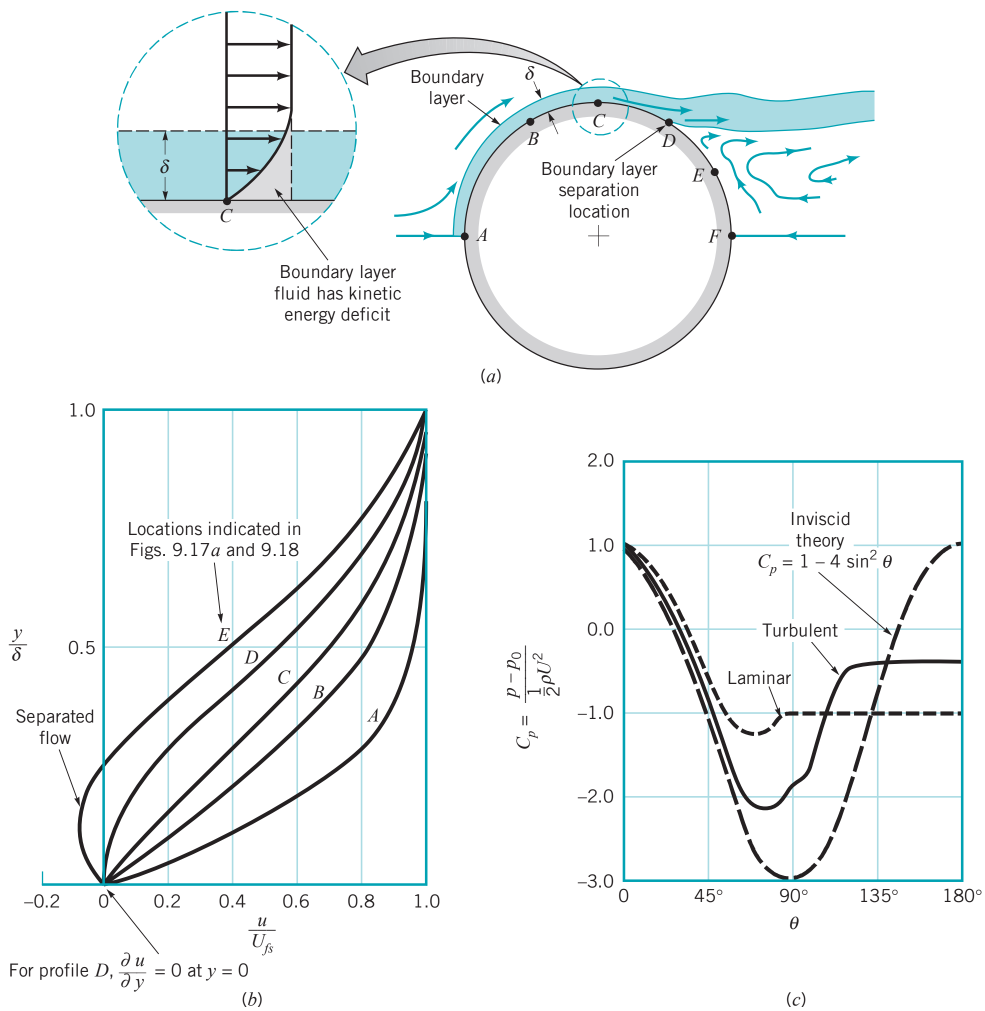

■ **FIGURE 9.17** **Boundary layer characteristics on a circular cylinder: (*a*) boundary layer separation location, (*b*) typical boundary layer velocity profiles at various locations on the cylinder, (*c*) surface pressure distributions for inviscid flow and boundary layer flow.**

Fluids in the News

Increasing truck mpg A large portion of the aerodynamic drag on semis (tractor-trailer rigs) is a result of the low pressure on the flat back end of the trailer. Researchers have recently developed a drag-reducing attachment that could reduce fuel costs on these big rigs by 10 percent. The device consists of a set of flat plates (attached to the rear of the trailer) that fold out into a box shape, thereby making the originally flat rear of the trailer a somewhat more "aerodynamic" shape. Based on thorough wind tunnel testing and actual tests conducted with a prototype design used in a series of cross-country runs, it is estimated that trucks using the device could save approximately \$6,000 a year in fuel costs.

Viscous effects within the boundary layer cause boundary layer separation.

The location of separation, the width of the wake region behind the object, and the pressure distribution on the surface depend on the nature of the boundary layer flow. Compared with a laminar boundary layer, a turbulent boundary layer flow has more kinetic energy and momentum associated with it because: (1) as is indicated in Fig. E9.6, the velocity profile is fuller, more nearly like the ideal uniform profile, and (2) there can be considerable energy associated with the swirling, random components of the velocity that do not appear in the time-averaged x component of velocity. Thus, as is indicated in Fig. 9.17*c*, the turbulent boundary layer can flow farther around the cylinder (farther up the pressure hill) before it separates than can the laminar boundary layer.

The structure of the flow field past a circular cylinder is completely different for a zero viscosity fluid than it is for a viscous fluid, no matter how small the viscosity is, provided it is not

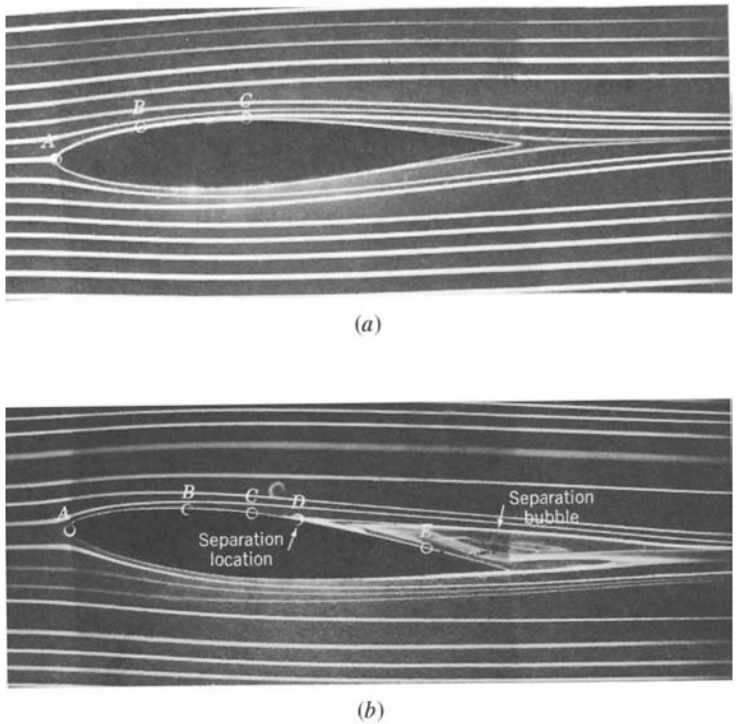

■ FIGURE 9.18 **Flow visualization photographs of flow past an airfoil (the boundary layer velocity profiles for the points indicated are similar to those indicated in Fig. 9.17*b*): (*a*) zero angle of attack, no separation, (*b*) 5° angle of attack, flow separation. Dye in water. (Photograph courtesy of ONERA, France.)**

zero. This is due to boundary layer separation. Similar concepts hold for other shaped bodies as well. The flow past an airfoil at zero *angle of attack* (the angle between the upstream flow and the axis of the object) is shown in Fig. 9.18*a*; flow past the same airfoil at a 5° angle of attack is shown in Fig. 9.18*b*. Over the front portion of the airfoil the pressure decreases in the direction of flow—a favorable pressure gradient. Over the rear portion the pressure increases in the direction of flow—an adverse pressure gradient. The boundary layer velocity profiles at representative locations are similar to those indicated in Fig. 9.17*b* for flow past a circular cylinder. If the adverse pressure gradient is not too great (because the body is not too "thick" in some sense), the boundary layer fluid can flow into the slightly increasing pressure region (i.e., from *C* to the trailing edge in Fig. 9.18*a*) without separating from the surface. However, if the pressure gradient is too adverse (because the angle of attack is too large), the boundary layer will separate from the surface as indicated in Fig. 9.18*b*. Such situations can lead to the catastrophic loss of lift called *stall*, which is discussed in Section 9.4.

Streamlined bodies generally have no separated flow.

Streamlined bodies are generally those designed to eliminate (or at least to reduce) the effects of separation, whereas nonstreamlined bodies generally have relatively large drag due to the low pressure in the separated regions (the wake). Although the boundary layer may be quite thin, it can appreciably alter the entire flow field because of boundary layer separation. These ideas are discussed in Section 9.3.

9.2.7 Momentum Integral Boundary Layer Equation with Nonzero Pressure Gradient

The boundary layer results discussed in Sections 9.2.2 and 9.2.3 are valid only for boundary layers with zero pressure gradients. They correspond to the velocity profile labeled *C* in Fig. 9.17*b*. Boundary layer characteristics for flows with nonzero pressure gradients can be obtained from nonlinear, partial differential boundary layer equations similar to Eqs. 9.8 and 9.9, provided the pressure gradient is appropriately accounted for. Such an approach is beyond the scope of this book (Refs. 1, 2).

An alternative approach is to extend the momentum integral boundary layer equation technique (Section 9.2.3) so that it is applicable for flows with nonzero pressure gradients. The momentum integral equation for boundary layer flows with zero pressure gradient, Eq. 9.26, is a statement of the balance between the shear force on the plate (represented by τ_w) and rate of change of momentum of the fluid within the boundary layer [represented by $\rho U^2\,(d\Theta/dx)$]. For such flows the free-stream velocity is constant ($U_{fs} = U$). If the free-stream velocity is not constant [$U_{fs} = U_{fs}(x)$, where x is the distance measured along the curved body], the pressure will not be constant. This follows from the Bernoulli equation with negligible gravitational effects, since $p + \rho U_{fs}^2/2$ is constant along the streamlines outside the boundary layer. Thus,

$$\frac{dp}{dx} = -\rho U_{fs} \frac{dU_{fs}}{dx} \tag{9.34}$$

For a given body the free-stream velocity and the corresponding pressure gradient on the surface can be obtained from inviscid flow techniques (potential flow) discussed in Section 6.7. (This is how the circular cylinder results of Fig. 9.16 were obtained.)

Flow in a boundary layer with nonzero pressure gradient is very similar to that shown in Fig. 9.11, except that the upstream velocity, U, is replaced by the free-stream velocity, $U_{fs}(x)$, and the pressures at sections (1) and (2) are not necessarily equal. By using the x component of the momentum equation (Eq. 5.22) with the appropriate shear forces and pressure forces acting on the control surface indicated in Fig. 9.11, the following integral momentum equation for boundary layer flows is obtained:

Pressure gradient effects can be included in the momentum integral equation.

$$\tau_w = \rho \frac{d}{dx}(U_{fs}^2\,\Theta) + \rho\delta^*\,U_{fs}\frac{dU_{fs}}{dx} \tag{9.35}$$

The derivation of this equation is similar to that of the corresponding equation for constant-pressure boundary layer flow, Eq. 9.26, although the inclusion of the pressure gradient effect brings in additional terms (Refs. 1, 2, 3). For example, both the boundary layer momentum thickness, Θ, and the displacement thickness, δ^*, are involved.

Equation 9.35, the general momentum integral equation for two-dimensional boundary layer flow, represents a balance between viscous forces (represented by τ_w), pressure forces (represented by $\rho U_{fs}\,dU_{fs}/dx = -dp/dx$), and the fluid momentum (represented by Θ, the boundary layer momentum thickness). In the special case of a flat plate, $U_{fs} = U =$ constant, and Eq. 9.35 reduces to Eq. 9.26.

Equation 9.35 can be used to obtain boundary layer information in a manner similar to that done for the flat plate boundary layer (Section 9.2.3). That is, for a given body shape the free-stream velocity, U_{fs}, is determined, and a family of approximate boundary layer profiles is assumed. Equation 9.35 is then used to provide information about the boundary layer thickness, wall shear stress, and other properties of interest. The details of this technique are not within the scope of this book (Refs. 1, 3).

9.3 Drag

As was discussed in Section 9.1, any object moving through a fluid will experience a drag, $\mathscr{D}$—a net force in the direction of flow due to the pressure and shear forces on the surface of the object. This net force, a combination of flow direction components of the normal and tangential forces on the body, can be determined by use of Eqs. 9.1 and 9.2, provided the distributions of pressure, p, and wall shear stress, τ_w, are known. Only in very rare instances can these distributions be determined analytically. The boundary layer flow past a flat plate parallel to the upstream flow as is discussed in Section 9.2 is one such case. Current advances in computational fluid dynamics, CFD, (i.e., the use of computers to solve the governing equations of the flow field) have provided encouraging results for more complex shapes. However, much work in this area remains.

Most of the information pertaining to drag on objects is a result of numerous experiments with wind tunnels, water tunnels, towing tanks, and other ingenious devices that are used to measure the drag on scale models. As was discussed in Chapter 7, these data can be put into dimensionless form and the results can be appropriately ratioed for prototype calculations. Typically, the result for a given-shaped object is a drag coefficient, C_D, where

$$C_D = \frac{\mathcal{D}}{\frac{1}{2}\rho U^2 A} \tag{9.36}$$

and C_D is a function of other dimensionless parameters such as Reynolds number, Re, Mach number, Ma, Froude number, Fr, and relative roughness of the surface, ε/ℓ. That is,

$$C_D = \phi(\text{shape, Re, Ma, Fr}, \varepsilon/\ell)$$

The character of C_D as a function of these parameters is discussed in this section.

9.3.1 Friction Drag

Friction drag, $\mathcal{D}_f$, is that part of the drag that is due directly to the shear stress, τ_w, on the object. It is a function of not only the magnitude of the wall shear stress, but also of the orientation of the surface on which it acts. This is indicated by the factor $\tau_w \sin\theta$ in Eq. 9.1. If the surface is parallel to the upstream velocity, the entire shear force contributes directly to the drag. This is true for the flat plate parallel to the flow as was discussed in Section 9.2. If the surface is perpendicular to the upstream velocity, the shear stress contributes nothing to the drag. Such is the case for a flat plate normal to the upstream velocity as was discussed in Section 9.1.

In general, the surface of a body will contain portions parallel to and normal to the upstream flow, as well as any direction in between. A circular cylinder is such a body. Because the viscosity of most common fluids is small, the contribution of the shear force to the overall drag on a body is often quite small. Such a statement should be worded in dimensionless terms. That is, because the Reynolds number of most familiar flows is quite large, the percent of the drag caused directly by the shear stress is often quite small. For highly streamlined bodies or for low Reynolds number flow, however, most of the drag may be due to friction drag.

The friction drag on a flat plate of width b and length ℓ oriented parallel to the upstream flow can be calculated from

$$\mathcal{D}_f = \tfrac{1}{2}\rho U^2 b\ell C_{Df}$$

where C_{Df} is the friction drag coefficient. The value of C_{Df}, given as a function of Reynolds number, $\text{Re}_\ell = \rho U\ell/\mu$, and relative surface roughness, ε/ℓ, in Fig. 9.15 and Table 9.3, is a result of boundary layer analysis and experiments (see Section 9.2). Typical values of roughness, ε, for various surfaces are given in Table 8.1. As with the pipe flow discussed in Chapter 8, the flow is divided into two distinct categories—laminar or turbulent, with a transitional regime connecting them. The drag coefficient (and, hence, the drag) is not a function of the plate roughness if the flow is laminar. However, for turbulent flow the roughness does considerably affect the value of C_{Df}. As with pipe flow, this dependence is a result of the surface roughness elements protruding into or through the laminar sublayer (see Section 8.3).

Friction (viscous) drag is the drag produced by viscous shear stresses.

Most objects are not flat plates parallel to the flow; instead, they are curved surfaces along which the pressure varies. As was discussed in Section 9.2.6, this means that the boundary layer character, including the velocity gradient at the wall, is different for most objects from that for a flat plate. This can be seen in the change of shape of the boundary layer profile along the cylinder in Fig. 9.17*b*.

The precise determination of the shear stress along the surface of a curved body is quite difficult to obtain. Although approximate results can be obtained by a variety of techniques (Refs. 1, 2), these are outside the scope of this text. As is shown by the following example, if the shear stress is known, its contribution to the drag can be determined.

EXAMPLE 9.8 Drag Coefficient Based on Friction Drag

GIVEN A viscous, incompressible fluid flows past the circular cylinder shown in Fig. E9.8*a*. According to a more advanced theory of boundary layer flow, the boundary layer remains attached to the cylinder up to the separation location at $\theta \approx 108.8°$, with the dimensionless wall shear stress as is indicated in Fig. E9.8*b* (Ref. 1). The shear stress on the cylinder in the wake region, $108.8 < \theta < 180°$, is negligible.

FIND Determine C_{Df}, the drag coefficient for the cylinder based on the friction drag only.

Solution

The friction drag, $\mathscr{D}_f$, can be determined from Eq. 9.1 as

$$\mathscr{D}_f = \int \tau_w \sin\theta \, dA = 2\left(\frac{D}{2}\right) b \int_0^{\pi} \tau_w \sin\theta \, d\theta$$

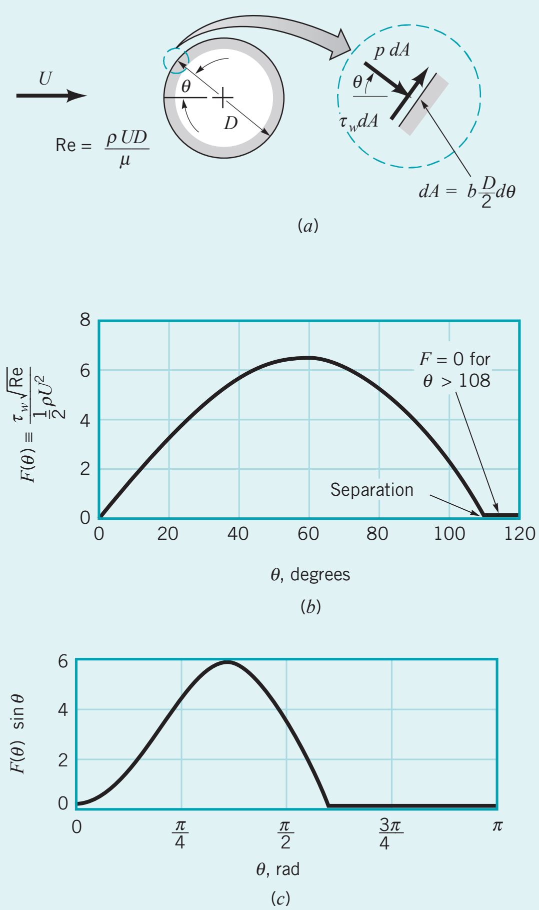

■ FIGURE E9.8

where b is the length of the cylinder. Note that θ is in radians (not degrees) to ensure the proper dimensions of $dA = 2\,(D/2)\,b\,d\theta$. Thus,

$$C_{Df} = \frac{\mathscr{D}_f}{\frac{1}{2}\rho U^2 bD} = \frac{2}{\rho U^2}\int_0^{\pi} \tau_w \sin\theta \, d\theta$$

This can be put into dimensionless form by using the dimensionless shear stress parameter, $F(\theta) = \tau_w\sqrt{\text{Re}}/(\rho U^2/2)$, given in Fig. E9.8*b* as follows:

$$C_{Df} = \int_0^{\pi} \frac{\tau_w}{\frac{1}{2}\rho U^2}\sin\theta\, d\theta = \frac{1}{\sqrt{\text{Re}}}\int_0^{\pi} \frac{\tau_w\sqrt{\text{Re}}}{\frac{1}{2}\rho U^2}\sin\theta\, d\theta$$

where $\text{Re} = \rho UD/\mu$. Thus,

$$C_{Df} = \frac{1}{\sqrt{\text{Re}}}\int_0^{\pi} F(\theta)\sin\theta\, d\theta \tag{1}$$

The function $F(\theta)\sin\theta$, obtained from Fig. E9.8*b*, is plotted in Fig. E9.8*c*. The necessary integration to obtain C_{Df} from Eq. 1 can be done by an appropriate numerical technique or by an approximate graphical method to determine the area under the given curve.

The result is $\int_0^{\pi} F(\theta)\sin\theta\, d\theta = 5.93$, or

$$C_{Df} = \frac{5.93}{\sqrt{\text{Re}}} \qquad \textbf{(Ans)}$$

COMMENTS Note that the total drag must include both the shear stress (friction) drag and the pressure drag. As we will see in Example 9.9, for the circular cylinder most of the drag is due to the pressure force.

The above friction drag result is valid only if the boundary layer flow on the cylinder is laminar. As is discussed in Section 9.3.3, for a smooth cylinder this means that $\text{Re} = \rho UD/\mu < 3 \times 10^5$. It is also valid only for flows that have a Reynolds number sufficiently large to ensure the boundary layer structure to the flow. For the cylinder, this means $\text{Re} > 100$.

9.3.2 Pressure Drag

Pressure (form) drag is the drag produced by normal stresses.

Pressure drag, $\mathscr{D}_p$, is that part of the drag that is due directly to the pressure, p, on an object. It is often referred to as *form drag* because of its strong dependency on the shape or form of the object. Pressure drag is a function of the magnitude of the pressure and the orientation of the surface element on which the pressure force acts. For example, the pressure force on either side of a flat plate parallel to the flow may be very large, but it does not contribute to the drag because it acts in the direction normal to the upstream velocity. On the other hand, the pressure force on a flat plate normal to the flow provides the entire drag.

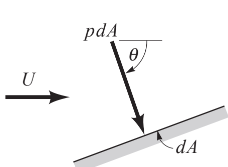

As previously noted, for most bodies, there are portions of the surface that are parallel to the upstream velocity, others normal to the upstream velocity, and the majority of which are at some angle in between, as shown by the figure in the margin. The pressure drag can be obtained from Eq. 9.1 provided a detailed description of the pressure distribution and the body shape is given. That is,

$$\mathscr{D}_p = \int p\cos\theta\, dA$$

which can be rewritten in terms of the *pressure drag coefficient*, C_{Dp}, as

$$C_{Dp} = \frac{\mathscr{D}_p}{\frac{1}{2}\rho U^2 A} = \frac{\int p \cos\theta \, dA}{\frac{1}{2}\rho U^2 A} = \frac{\int C_p \cos\theta \, dA}{A} \tag{9.37}$$

The pressure coefficient is a dimensionless form of the pressure.

Here $C_p = (p - p_0)/(\rho U^2/2)$ is the *pressure coefficient*, where p_0 is a reference pressure. The level of the reference pressure does not influence the drag directly because the net pressure force on a body is zero if the pressure is constant (i.e., p_0) on the entire surface.

For flows in which inertial effects are large relative to viscous effects (i.e., large Reynolds number flows), the pressure difference, $p - p_0$, scales directly with the dynamic pressure, $\rho U^2/2$, and the pressure coefficient is independent of Reynolds number. In such situations we expect the drag coefficient to be relatively independent of Reynolds number.

For flows in which viscous effects are large relative to inertial effects (i.e., very small Reynolds number flows), it is found that both the pressure difference and wall shear stress scale with the characteristic viscous stress, $\mu U/\ell$, where ℓ is a characteristic length. In such situations we expect the drag coefficient to be proportional to 1/Re. That is, $C_D \sim \mathscr{D}/(\rho U^2/2) \sim (\mu U/\ell)/(\rho U^2/2) \sim \mu/\rho U\ell = 1/\text{Re}$. These characteristics are similar to the friction factor dependence of $f \sim 1/\text{Re}$ for laminar pipe flow and $f \sim$ constant for large Reynolds number flow (see Section 8.4).

If the viscosity were zero, the pressure drag on any shaped object (symmetrical or not) in a steady flow would be zero. There perhaps would be large pressure forces on the front portion of the object, but there would be equally large (and oppositely directed) pressure forces on the rear portion. If the viscosity is not zero, the net pressure drag may be nonzero because of boundary layer separation as is discussed in Section 9.2.6. Example 9.9 illustrates this.

EXAMPLE 9.9 Drag Coefficient Based on Pressure Drag

GIVEN A viscous, incompressible fluid flows past the circular cylinder shown in Fig. E9.8*a*. The pressure coefficient on the surface of the cylinder (as determined from experimental measurements) is as indicated in Fig. E9.9*a*.

FIND Determine the pressure drag coefficient for this flow. Combine the results of Examples 9.8 and 9.9 to determine the drag coefficient for a circular cylinder. Compare your results with those given in Fig. 9.21.

SOLUTION

The pressure (form) drag coefficient, C_{Dp}, can be determined from Eq. 9.37 as

$$C_{Dp} = \frac{1}{A}\int C_p \cos\theta \, dA = \frac{1}{bD}\int_0^{2\pi} C_p \cos\theta \, b\left(\frac{D}{2}\right) d\theta$$

or because of symmetry

$$C_{Dp} = \int_0^{\pi} C_p \cos\theta \, d\theta$$

where b and D are the length and diameter of the cylinder. To obtain C_{Dp}, we must integrate the $C_p \cos\theta$ function from $\theta = 0$ to $\theta = \pi$ radians. Again, this can be done by some numerical integration scheme or by determining the area under the curve shown in Fig. E9.9*b*. The result is

$$C_{Dp} = 1.17 \tag{1}$$ **(Ans)**

Note that the positive pressure on the front portion of the cylinder $(0 \leq \theta \leq 30°)$ and the negative pressure (less than the upstream value) on the rear portion $(90 \leq \theta \leq 180°)$ produce positive contributions to the drag. The negative pressure on the front portion of the cylinder $(30 < \theta < 90°)$ reduces the drag by pulling on the cylinder in the upstream direction. The positive area under the $C_p \cos\theta$ curve is greater than the negative area—there is a net pressure drag. In the absence of viscosity, these two contributions would be equal—there would be no pressure (or friction) drag.

The net drag on the cylinder is the sum of friction and pressure drag. Thus, from Eq. 1 of Example 9.8 and Eq. 1 of this example, we obtain the drag coefficient

$$C_D = C_{Df} + C_{Dp} = \frac{5.93}{\sqrt{\text{Re}}} + 1.17 \tag{2}$$ **(Ans)**

This result is compared with the standard experimental value (obtained from Fig. 9.21) in Fig. E9.9*c*. The agreement is very good over a wide range of Reynolds numbers. For Re < 10 the curves diverge because the flow is not a boundary layer type flow—the shear stress and pressure distributions used to obtain Eq. 2 are not valid in this range. The drastic divergence in the curves for Re $> 3 \times 10^5$ is due to the change from a laminar to turbulent boundary layer, with the corresponding change in the pressure distribution. This is discussed in Section 9.3.3.

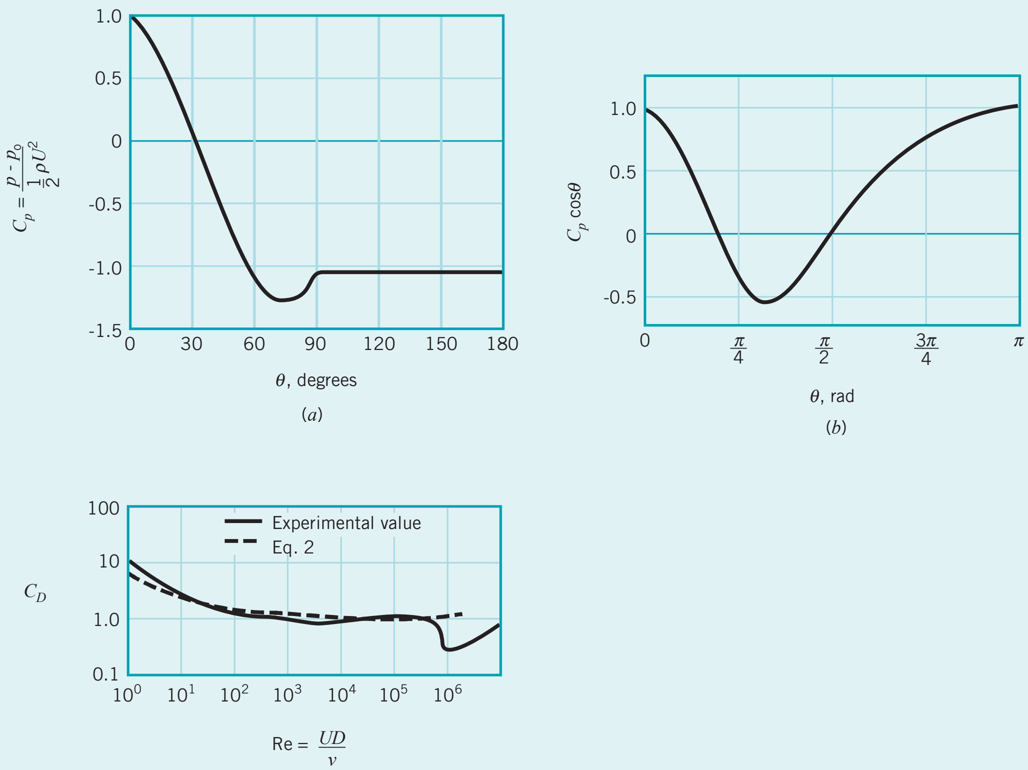

■ **FIGURE E9.9**

COMMENT It is of interest to compare the friction drag to the total drag on the cylinder. That is,

$$\frac{\mathcal{D}_f}{\mathcal{D}} = \frac{C_{Df}}{C_D} = \frac{5.93/\sqrt{\text{Re}}}{(5.93/\sqrt{\text{Re}}) + 1.17} = \frac{1}{1 + 0.197\sqrt{\text{Re}}}$$

For Re $= 10^3$, 10^4, and 10^5 this ratio is 0.138, 0.0483, and 0.0158, respectively. Most of the drag on the blunt cylinder is pressure drag—a result of the boundary layer separation.

9.3.3 Drag Coefficient Data and Examples

As was discussed in previous sections, the net drag is produced by both pressure and shear stress effects. In most instances these two effects are considered together, and an overall drag coefficient, C_D, as defined in Eq. 9.36 is used. There is an abundance of such drag coefficient data available in the literature. This information covers incompressible and compressible viscous flows past objects of almost any shape of interest—both man-made and natural objects. In this section we consider a small portion of this information for representative situations. Additional data can be obtained from various sources (Refs. 5, 6).

V9.7 Skydiving practice

Shape Dependence. Clearly the drag coefficient for an object depends on the shape of the object, with shapes ranging from those that are streamlined to those that are blunt. The drag on an ellipse with aspect ratio ℓ/D, where D and ℓ are the thickness and length parallel to the flow, illustrates this dependence. The drag coefficient $C_D = \mathcal{D}/(\rho U^2 bD/2)$, based on the frontal area, $A = bD$, where b is the length normal to the flow, is as shown in Fig. 9.19. The more blunt the body, the larger the drag coefficient. With $\ell/D = 0$ (i.e., a flat plate normal to the flow) we obtain the flat plate value of $C_D = 1.9$. With $\ell/D = 1$ the corresponding value for a circular cylinder is obtained. As ℓ/D becomes larger the value of C_D decreases.

The drag coefficient may be based on the frontal area or the planform area.

For very large aspect ratios ($\ell/D \to \infty$) the ellipse behaves as a flat plate parallel to the flow. For such cases, the friction drag is greater than the pressure drag, and the value of C_D based on the frontal area, $A = bD$, would increase with increasing ℓ/D. (This occurs for larger ℓ/D values than those shown in the figure.) For such extremely thin bodies (i.e., an ellipse with $\ell/D \to \infty$, a flat plate, or very thin airfoils) it is customary to use the planform area, $A = b\ell$, in defining the drag coefficient.

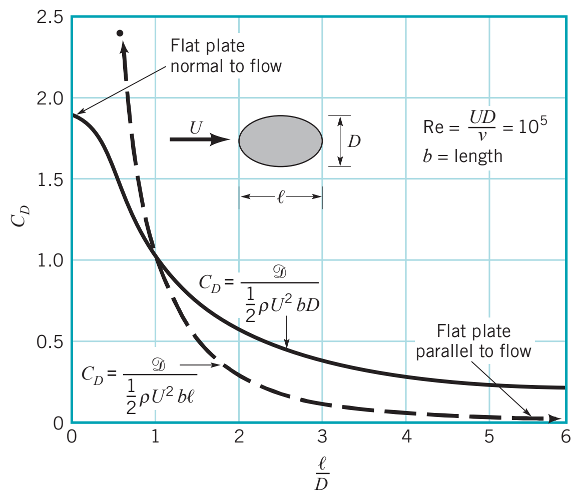

■ **FIGURE 9.19** **Drag coefficient for an ellipse with the characteristic area either the frontal area, $A = bD$, or the planform area, $A = b\ell$ (Ref. 5).**

After all, it is the planform area on which the shear stress acts, rather than the much smaller (for thin bodies) frontal area. The ellipse drag coefficient based on the planform area, $C_D = \mathcal{D}/(\rho U^2 b\ell/2)$, is also shown in Fig. 9.19. Clearly the drag obtained by using either of these drag coefficients would be the same. They merely represent two different ways to package the same information.

The amount of streamlining can have a considerable effect on the drag. Incredibly, the drag on the two two-dimensional objects drawn to scale in Fig. 9.20 is the same. The width of the wake for the streamlined strut is very thin, on the order of that for the much smaller diameter circular cylinder.

Reynolds Number Dependence. Another parameter on which the drag coefficient can be very dependent is the Reynolds number. The main categories of Reynolds number dependence are (1) very low Reynolds number flow, (2) moderate Reynolds number flow (laminar boundary layer), and (3) very large Reynolds number flow (turbulent boundary layer). Examples of these three situations are discussed below.

Low Reynolds number flows ($\text{Re} < 1$) are governed by a balance between viscous and pressure forces. Inertia effects are negligibly small. In such instances the drag on a three-dimensional body is expected to be a function of the upstream velocity, U, the body size, ℓ, and the viscosity, μ. Thus, for a small grain of sand settling in a lake (see margin figure)

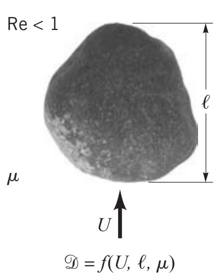

$$\mathcal{D} = f(U, \ell, \mu)$$

From dimensional considerations (see Section 7.7.1)

$$\mathcal{D} = C\mu\ell U \tag{9.38}$$

where the value of the constant C depends on the shape of the body. If we put Eq. 9.38 into dimensionless form using the standard definition of the drag coefficient, we obtain

$$C_D = \frac{\mathcal{D}}{\frac{1}{2}\rho U^2 \ell^2} = \frac{2C\mu\ell U}{\rho U^2 \ell^2} = \frac{2C}{\text{Re}}$$

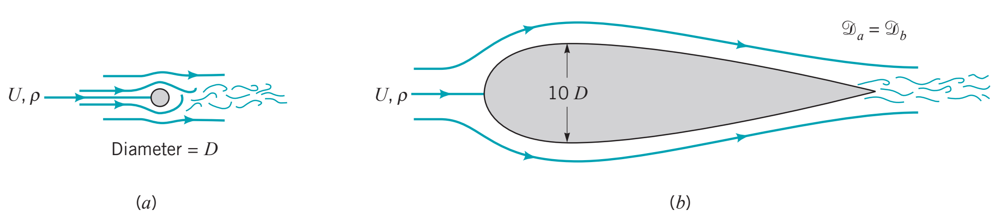

■ **FIGURE 9.20** **Two objects of considerably different size that have the same drag force: (*a*) circular cylinder $C_D = 1.2$; (*b*) streamlined strut $C_D = 0.12$.**

TABLE 9.4

Low Reynolds Number Drag Coefficients (Ref. 7) ($\mathrm{Re} = \rho UD/\mu$, $A = \pi D^2/4$)

Object	$C_D = \mathcal{D}/(\rho U^2 A/2)$ (for $\mathrm{Re} \lesssim 1$)	Object	C_D
a. Circular disk normal to flow	20.4/Re	c. Sphere	24.0/Re
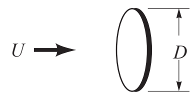		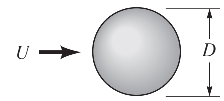	
b. Circular disk parallel to flow	13.6/Re	d. Hemisphere	22.2/Re
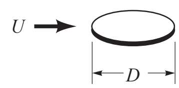		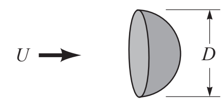	

where $\mathrm{Re} = \rho U\ell/\mu$. The use of the dynamic pressure, $\rho U^2/2$, in the definition of the drag coefficient is somewhat misleading in the case of creeping flows ($\mathrm{Re} < 1$) because it introduces the fluid density, which is not an important parameter for such flows (inertia is not important). Use of this standard drag coefficient definition gives the 1/Re dependence for small Re drag coefficients.

For very small Reynolds number flows, the drag coefficient varies inversely with the Reynolds number.

Typical values of C_D for low Reynolds number flows past a variety of objects are given in Table 9.4. It is of interest that the drag on a disk normal to the flow is only 1.5 times greater than that on a disk parallel to the flow. For large Reynolds number flows this ratio is considerably larger (see Example 9.1). Streamlining (i.e., making the body slender) can produce a considerable drag reduction for large Reynolds number flows; for very small Reynolds number flows it can actually increase the drag because of an increase in the area on which shear forces act. For most objects, the low Reynolds number flow results are valid up to a Reynolds number of about 1.

EXAMPLE 9.10 Low Reynolds Number Flow Drag

GIVEN A small grain of sand, diameter $D = 0.10$ mm and specific gravity $SG = 2.3$, settles to the bottom of a lake after having been stirred up by a passing boat.

FIND Determine how fast it falls through the still water.

SOLUTION

A free-body diagram of the particle (relative to the moving particle) is shown in Fig. E9.10*a*. The particle moves downward with a constant velocity U that is governed by a balance between the weight of the particle, $\mathcal{W}$, the buoyancy force of the surrounding water, F_B, and the drag of the water on the particle, $\mathcal{D}$.

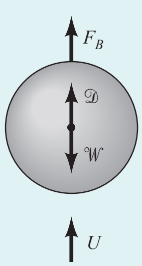

FIGURE E9.10*a*

From the free-body diagram, we obtain

$$\mathcal{W} = \mathcal{D} + F_B$$

where

$$\mathcal{W} = \gamma_{\text{sand}}\mathcal{V} = SG\,\gamma_{H_2O}\frac{\pi}{6}D^3 \tag{1}$$

and

$$F_B = \gamma_{H_2O}\mathcal{V} = \gamma_{H_2O}\frac{\pi}{6}D^3 \tag{2}$$

We assume (because of the smallness of the object) that the flow will be creeping flow ($\mathrm{Re} < 1$) with $C_D = 24/\mathrm{Re}$ (see Table 9.4) so that

$$\mathcal{D} = \frac{1}{2}\rho_{H_2O}U^2\frac{\pi}{4}D^2C_D = \frac{1}{2}\rho_{H_2O}U^2\frac{\pi}{4}D^2\left(\frac{24}{\rho_{H_2O}UD/\mu_{H_2O}}\right)$$

or

$$\mathcal{D} = 3\pi\mu_{H_2O}UD \quad (3)$$

We must eventually check to determine if this assumption (Re < 1) is valid or not. Equation 3 is called Stokes's law in honor of G. G. Stokes (1819–1903), a British mathematician and physicist. By combining Eqs. 1, 2, and 3, we obtain

$$SG\,\gamma_{H_2O}\frac{\pi}{6}D^3 = 3\pi\mu_{H_2O}UD + \gamma_{H_2O}\frac{\pi}{6}D^3$$

or, since $\gamma = \rho g$,

$$U = \frac{(SG - 1)\rho_{H_2O}\,gD^2}{18\,\mu} \quad (4)$$

From Table 1.6 for water at 15.6 °C we obtain $\rho_{H_2O} = 999 \text{ kg/m}^3$ and $\mu_{H_2O} = 1.12 \times 10^{-3} \text{ N} \cdot \text{s/m}^2$. Thus, from Eq. 4 we obtain

$$U = \frac{(2.3 - 1)(999 \text{ kg/m}^3)(9.81 \text{ m/s}^2)(0.10 \times 10^{-3} \text{ m})^2}{18(1.12 \times 10^{-3} \text{ N} \cdot \text{s/m}^2)}$$

or

$$U = 6.32 \times 10^{-3} \text{ m/s} \quad \textbf{(Ans)}$$

Since

$$\text{Re} = \frac{\rho DU}{\mu} = \frac{(999 \text{ kg/m}^3)(0.10 \times 10^{-3} \text{ m})(0.00632 \text{ m/s})}{1.12 \times 10^{-3} \text{ N} \cdot \text{s/m}^2} = 0.564$$

we see that Re < 1, and the form of the drag coefficient used is valid.

COMMENTS By repeating the calculations for various particle diameters, D, the results shown in Fig. E9.10*b* are obtained. Note that very small particles fall extremely slowly. Thus, it can take considerable time for silt to settle to the bottom of a river or lake.

Note that if the density of the particle were the same as the surrounding water (i.e., $SG = 1$), from Eq. 4 we would obtain $U = 0$. This is reasonable since the particle would be neutrally buoyant and there would be no force to overcome the motion-induced drag. Note also that we have assumed that the particle falls at its steady terminal velocity. That is, we have neglected the acceleration of the particle from rest to its terminal velocity. Since the terminal velocity is small, this acceleration time is quite small. For faster objects (such as a free-falling sky diver) it may be important to consider the acceleration portion of the fall.

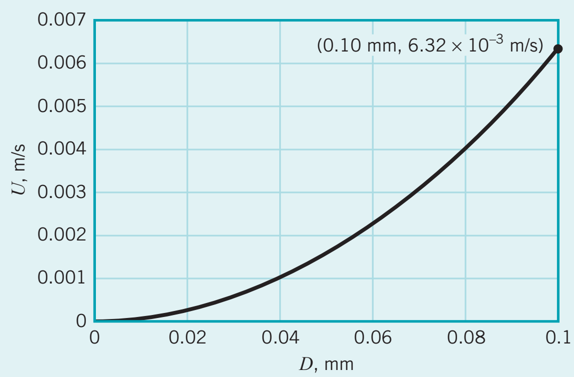

■ **F I G U R E E9.10*b***

Flow past a cylinder can take on a variety of different structures.

V9.8 Karman vortex street

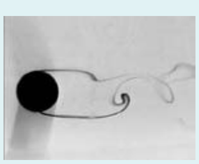

Moderate Reynolds number flows tend to take on a boundary layer flow structure. For such flows past streamlined bodies, the drag coefficient tends to decrease slightly with Reynolds number. The $C_D \sim \text{Re}^{-1/2}$ dependence for a laminar boundary layer on a flat plate (see Table 9.3) is such an example. Moderate Reynolds number flows past blunt bodies generally produce drag coefficients that are relatively constant. The C_D values for the spheres and circular cylinders shown in Fig. 9.21*a* indicate this character in the range $10^3 < \text{Re} < 10^5$.

The structure of the flow field at selected Reynolds numbers indicated in Fig. 9.21*a* is shown in Fig. 9.21*b*. For a given object there is a wide variety of flow situations, depending on the Reynolds number involved. The curious reader is strongly encouraged to study the many beautiful photographs and videos of these (and other) flow situations found in Refs. 8 and 31. (See also the photograph at the beginning of Chapter 7.)

For many shapes there is a sudden change in the character of the drag coefficient when the boundary layer becomes turbulent. This is illustrated in Fig. 9.15 for the flat plate and in Fig. 9.21 for the sphere and the circular cylinder. The Reynolds number at which this transition takes place is a function of the shape of the body.

For streamlined bodies, the drag coefficient increases when the boundary layer becomes turbulent because most of the drag is due to the shear force, which is greater for turbulent flow than for laminar flow. On the other hand, the drag coefficient for a relatively blunt object, such as a cylinder or sphere, actually decreases when the boundary layer becomes turbulent. As is discussed in Section 9.2.6, a turbulent boundary layer can travel further along the surface into the adverse pressure gradient on the rear portion of the cylinder before separation occurs. The result is a thinner wake and smaller pressure drag for turbulent boundary layer flow. This is indicated in Fig. 9.21

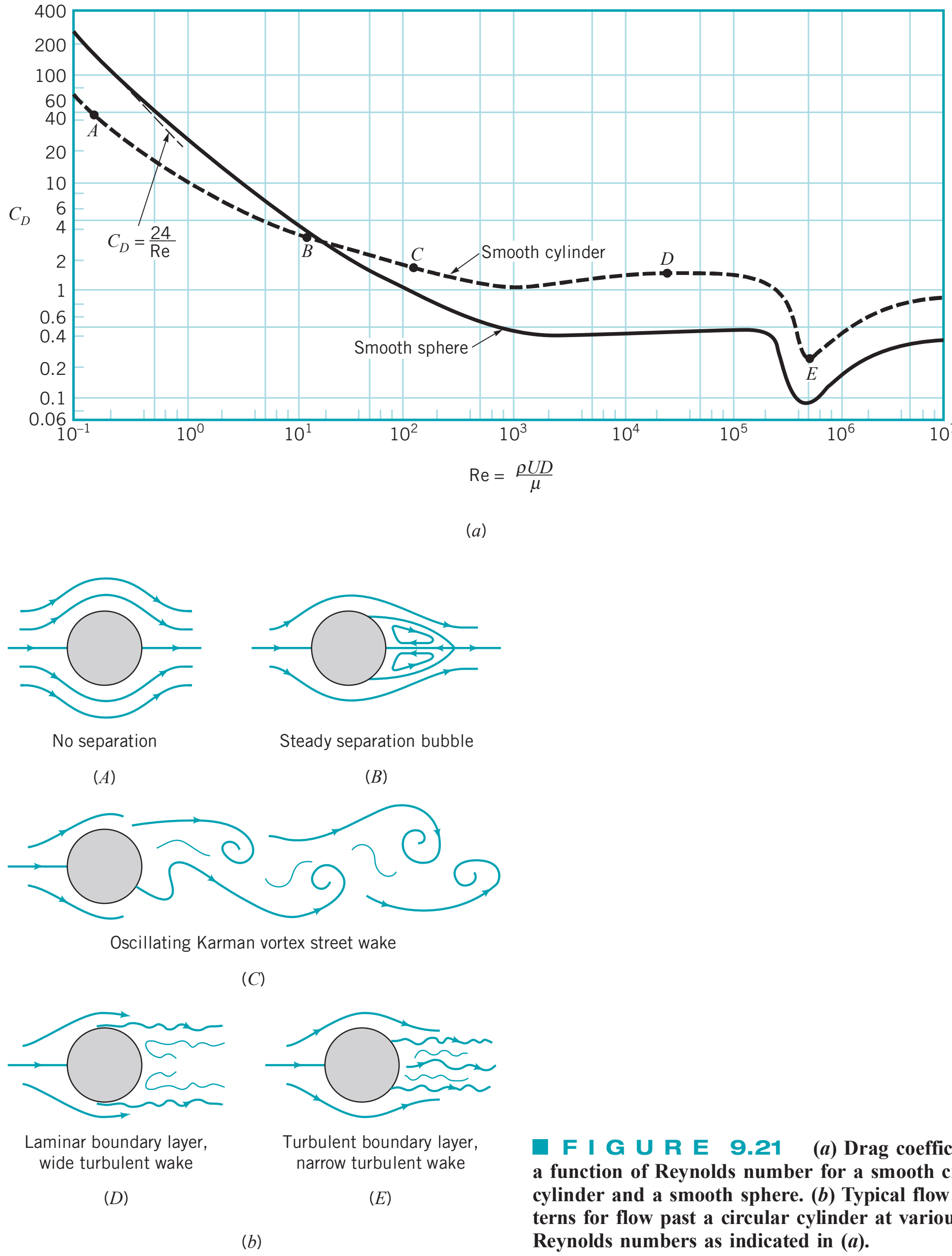

FIGURE 9.21 **(*a*) Drag coefficient as a function of Reynolds number for a smooth circular cylinder and a smooth sphere. (*b*) Typical flow patterns for flow past a circular cylinder at various Reynolds numbers as indicated in (*a*).**

V9.9 Oscillating sign

V9.10 Flow past a flat plate

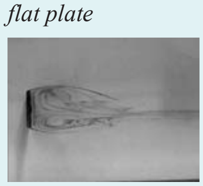

by the sudden decrease in C_D for $10^5 < \text{Re} < 10^6$. In a portion of this range the actual drag (not just the drag coefficient) decreases with increasing speed. It would be very difficult to control the steady flight of such an object in this range—an increase in velocity requires a decrease in thrust (drag). In all other Reynolds number ranges the drag increases with an increase in the upstream velocity (even though C_D may decrease with Re).

For extremely blunt bodies, like a flat plate perpendicular to the flow, the flow separates at the edge of the plate regardless of the nature of the boundary layer flow. Thus, the drag coefficient shows very little dependence on the Reynolds number.

The drag coefficients for a series of two-dimensional bodies of varying bluntness are given as a function of Reynolds number in Fig. 9.22. The characteristics described above are evident.

V9.11 Flow past an ellipse

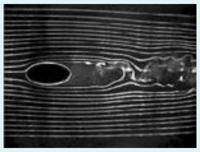

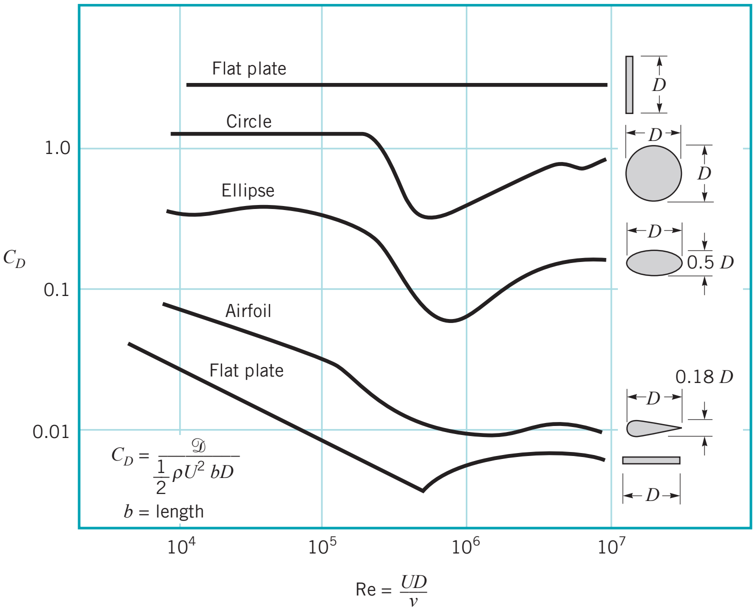

■ **FIGURE 9.22** **Character of the drag coefficient as a function of Reynolds number for objects with various degrees of streamlining, from a flat plate normal to the upstream flow to a flat plate parallel to the flow (two-dimensional flow) (Ref. 5).**

EXAMPLE 9.11 Terminal Velocity of a Falling Object

GIVEN Hail is produced by the repeated rising and falling of ice particles in the updraft of a thunderstorm, as is indicated in Fig. E9.11*a*. When the hail becomes large enough, the aerodynamic drag from the updraft can no longer support the weight of the hail, and it falls from the storm cloud.

FIND Estimate the velocity, U, of the updraft needed to make D = 1.5-in.-diameter (i.e., "golf ball-sized") hail.

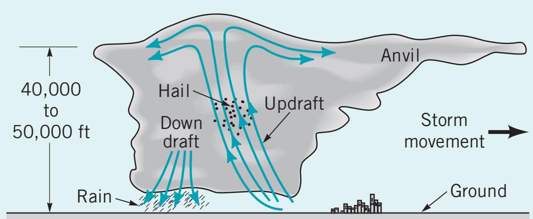

■ **FIGURE E9.11*a***

SOLUTION

As is discussed in Example 9.10, for steady-state conditions a force balance on an object falling through a fluid at its terminal velocity, U, gives

$$\mathscr{W} = \mathscr{D} + F_B$$

where $F_B = \gamma_{\text{air}} \forall$ is the buoyant force of the air on the particle, $\mathscr{W} = \gamma_{\text{ice}} \forall$ is the particle weight, and $\mathscr{D}$ is the aerodynamic drag. This equation can be rewritten as

$$\tfrac{1}{2}\rho_{\text{air}} U^2 \frac{\pi}{4} D^2 C_D = \mathscr{W} - F_B \qquad (1)$$

With $\forall = \pi D^3/6$ and since $\gamma_{\text{ice}} \gg \gamma_{\text{air}}$ (i.e., $\mathscr{W} \gg F_B$), Eq. 1 can be simplified to

$$U = \left(\frac{4}{3}\frac{\rho_{\text{ice}}}{\rho_{\text{air}}}\frac{gD}{C_D}\right)^{1/2} \qquad (2)$$

By using $\rho_{\text{ice}} = 1.84$ slugs/ft^3, $\rho_{\text{air}} = 2.38 \times 10^{-3}$ slugs/ft^3, and D = 1.5 in. = 0.125 ft, Eq. 2 becomes

$$U = \left[\frac{4(1.84 \text{ slugs/ft}^3)(32.2 \text{ ft/s}^2)(0.125 \text{ ft})}{3(2.38 \times 10^{-3} \text{ slugs/ft}^3)C_D}\right]^{1/2}$$

or

$$U = \frac{64.5}{\sqrt{C_D}} \qquad (3)$$

where U is in ft/s. To determine U, we must know C_D. Unfortunately, C_D is a function of the Reynolds number (see Fig. 9.21), which is not known unless U is known. Thus, we must use an iterative technique similar to that done with the Moody chart for certain types of pipe flow problems (see Section 8.5).

From Fig. 9.21 we expect that C_D is on the order of 0.5. Thus, we assume $C_D = 0.5$ and from Eq. 3 obtain

$$U = \frac{64.5}{\sqrt{0.5}} = 91.2 \text{ ft/s}$$

The corresponding Reynolds number (assuming $\nu = 1.57 \times 10^{-4}$ ft^2/s) is

$$\text{Re} = \frac{UD}{\nu} = \frac{91.2 \text{ ft/s } (0.125 \text{ ft})}{1.57 \times 10^{-4} \text{ ft}^2\text{/s}} = 7.26 \times 10^4$$

For this value of Re we obtain from Fig. 9.21, $C_D = 0.5$. Thus, our assumed value of $C_D = 0.5$ was correct. The corresponding value of U is

$$U = 91.2 \text{ ft/s} = 62.2 \text{ mph} \qquad \textbf{(Ans)}$$

COMMENTS By repeating the calculations for various altitudes, z, above sea level (using the properties of the U.S. Standard Atmosphere given in Appendix C), the results shown in Fig. E9.11*b* are obtained. Because of the decrease in density with altitude, the hail falls even faster through the upper portions of the storm than when it hits the ground.

Clearly, an airplane flying through such an updraft would feel its effects (even if it were able to dodge the hail). As seen from Eq. 2, the larger the hail, the stronger the necessary updraft. Hailstones greater than 6 in. in diameter have been reported. In reality, a hailstone is seldom spherical and often not smooth. However, the calculated updraft velocities are in agreement with measured values.

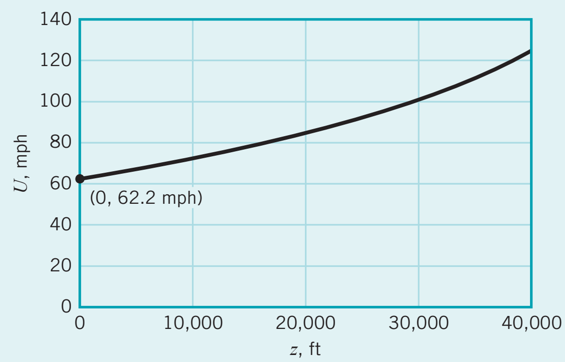

■ **FIGURE E9.11*b***

Compressibility Effects. The above discussion is restricted to incompressible flows. If the velocity of the object is sufficiently large, compressibility effects become important and the drag coefficient becomes a function of the Mach number, $\text{Ma} = U/c$, where c is the speed of sound in the fluid. The introduction of Mach number effects complicates matters because the drag coefficient for a given object is then a function of both Reynolds number and Mach number—$C_D = \phi(\text{Re}, \text{Ma})$. The Mach number and Reynolds number effects are often closely connected because both are directly proportional to the upstream velocity. For example, both Re and Ma increase with increasing flight speed of an airplane. The changes in C_D due to a change in U are due to changes in both Re and Ma.

The drag coefficient is usually independent of Mach number for Mach numbers up to approximately 0.5.

The precise dependence of the drag coefficient on Re and Ma is generally quite complex (Ref. 13). However, the following simplifications are often justified. For low Mach numbers, the drag coefficient is essentially independent of Ma as is indicated in Fig. 9.23. For this situation, if $\text{Ma} < 0.5$ or so, compressibility effects are unimportant. On the other hand, for larger Mach number flows, the drag coefficient can be strongly dependent on Ma, with only secondary Reynolds number effects.

For most objects, values of C_D increase dramatically in the vicinity of $\text{Ma} = 1$ (i.e., sonic flow). This change in character, indicated by Fig. 9.24, is due to the existence of shock waves as

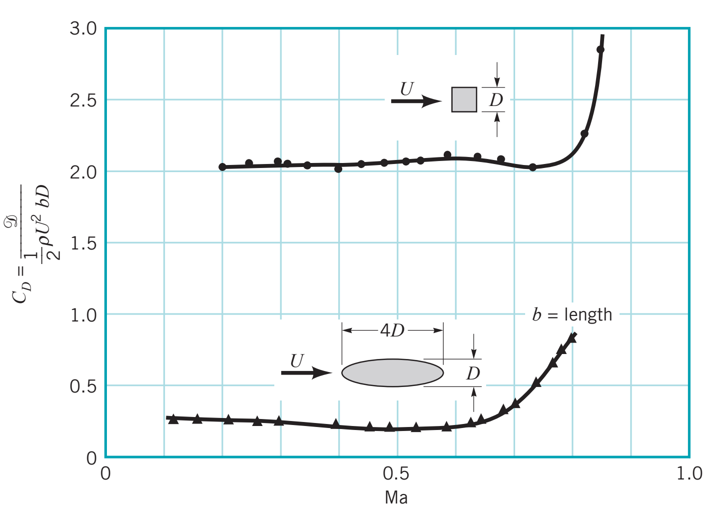

■ **FIGURE 9.23** **Drag coefficient as a function of Mach number for two-dimensional objects in subsonic flow (Ref. 5).**

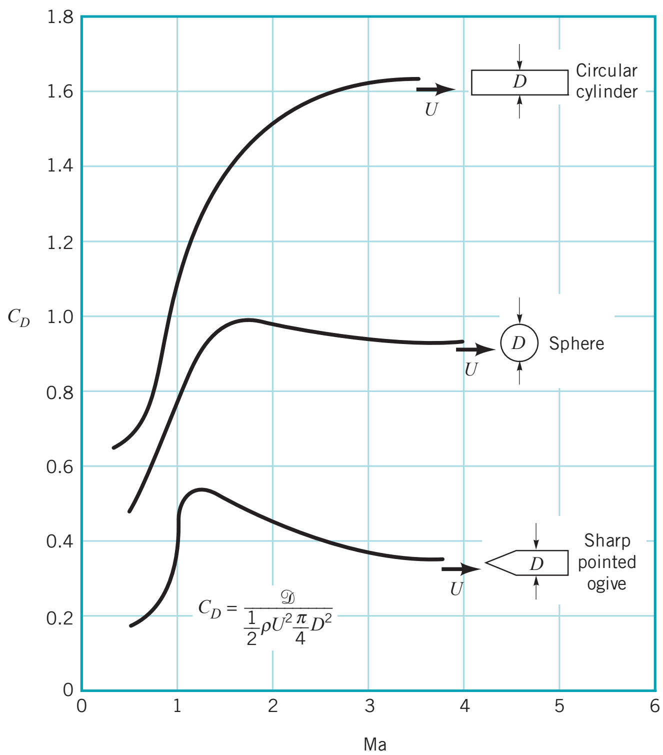

■ FIGURE 9.24 **Drag coefficient as a function of Mach number for supersonic flow (adapted from Ref. 19).**

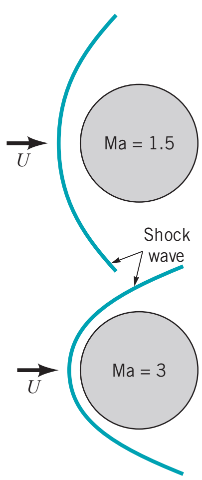

indicated by the figure in the margin. Shock waves are extremely narrow regions in the flow field across which the flow parameters change in a nearly discontinuous manner, which are discussed in Chapter 11. Shock waves, which cannot exist in subsonic flows, provide a mechanism for the generation of drag that is not present in the relatively low-speed subsonic flows. (See the photograph at the beginning of Chapter 11.)

The character of the drag coefficient as a function of Mach number is different for blunt bodies than for sharp bodies. As is shown in Fig. 9.24, sharp-pointed bodies develop their maximum drag coefficient in the vicinity of Ma $= 1$ (sonic flow), whereas the drag coefficient for blunt bodies increases with Ma far above Ma $= 1$. This behavior is due to the nature of the shock wave structure and the accompanying flow separation. The leading edges of wings for subsonic aircraft are usually quite rounded and blunt, while those of supersonic aircraft tend to be quite pointed and sharp. More information on these important topics can be found in standard texts about compressible flow and aerodynamics (Refs. 9, 10, 29).

Surface Roughness. As is indicated in Fig. 9.15, the drag on a flat plate parallel to the flow is quite dependent on the surface roughness, provided the boundary layer flow is turbulent. In such cases the surface roughness protrudes through the laminar sublayer adjacent to the surface (see Section 8.4) and alters the wall shear stress. In addition to the increased turbulent shear stress, surface roughness can alter the Reynolds number at which the boundary layer flow becomes turbulent. Thus, a rough flat plate may have a larger portion of its length covered by a turbulent boundary layer than does the corresponding smooth plate. This also acts to increase the net drag on the plate.

Depending on the body shape, an increase in surface roughness may increase or decrease drag.

In general, for streamlined bodies, the drag increases with increasing surface roughness. Great care is taken to design the surfaces of airplane wings to be as smooth as possible, since protruding rivets or screw heads can cause a considerable increase in the drag. On the other hand, for an extremely blunt body, such as a flat plate normal to the flow, the drag is independent of the surface roughness, since the shear stress is not in the upstream flow direction and contributes nothing to the drag.

For blunt bodies like a circular cylinder or sphere, an increase in surface roughness can actually cause a decrease in the drag. This is illustrated for a sphere in Fig. 9.25. As is discussed in Section 9.2.6, when the Reynolds number reaches the critical value (Re $= 3 \times 10^5$ for a smooth sphere),

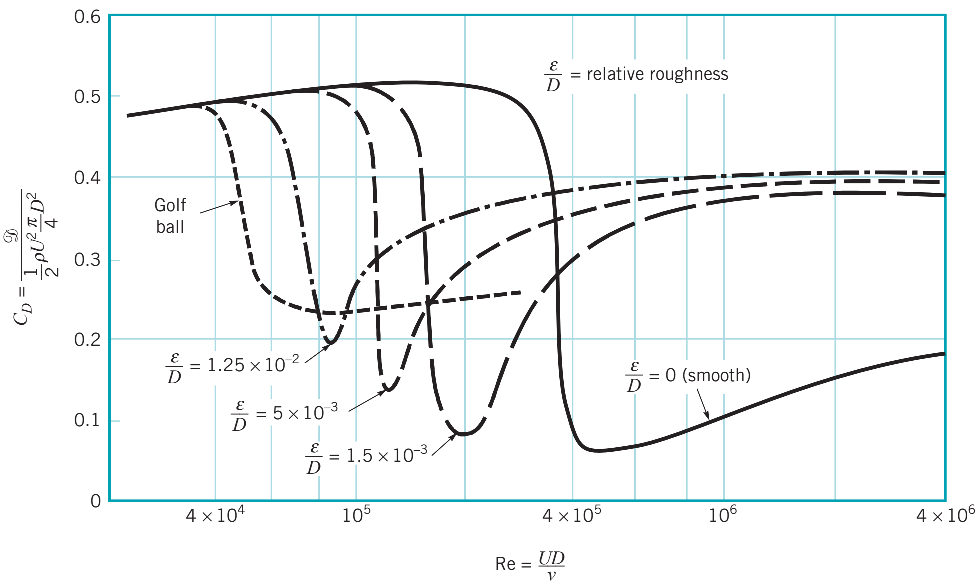

FIGURE 9.25 **The effect of surface roughness on the drag coefficient of a sphere in the Reynolds number range for which the laminar boundary layer becomes turbulent (Ref. 5).**

the boundary layer becomes turbulent and the wake region behind the sphere becomes considerably narrower than if it were laminar (see Fig. 9.17). The result is a considerable drop in pressure drag with a slight increase in friction drag, combining to give a smaller overall drag (and C_D).

Surface roughness can cause the boundary layer to become turbulent.

The boundary layer can be tripped into turbulence at a smaller Reynolds number by using a rough-surfaced sphere. For example, the critical Reynolds number for a golf ball is approximately $\mathrm{Re} = 4 \times 10^4$. In the range $4 \times 10^4 < \mathrm{Re} < 4 \times 10^5$, the drag on the standard rough (i.e., dimpled) golf ball is considerably less ($C_{D\text{rough}}/C_{D\text{smooth}} \approx 0.25/0.5 = 0.5$) than for the smooth ball. As is shown in Example 9.12, this is precisely the Reynolds number range for well-hit golf balls—hence, a reason for dimples on golf balls. The Reynolds number range for well-hit table tennis balls is less than $\mathrm{Re} = 4 \times 10^4$. Thus, table tennis balls are smooth.

EXAMPLE 9.12 Effect of Surface Roughness

GIVEN A well-hit golf ball (diameter $D = 1.69$ in., weight $\mathcal{W} = 0.0992$ lb) can travel at $U = 200$ ft/s as it leaves the tee. A well-hit table tennis ball (diameter $D = 1.50$ in., weight $\mathcal{W} = 0.00551$ lb) can travel at $U = 60$ ft/s as it leaves the paddle.

FIND Determine the drag on a standard golf ball, a smooth golf ball, and a table tennis ball for the conditions given. Also determine the deceleration of each ball for these conditions.

SOLUTION

For either ball, the drag can be obtained from

$$\mathfrak{D} = \frac{1}{2}\rho U^2 \frac{\pi}{4} D^2 C_D \qquad \textbf{(1)}$$

where the drag coefficient, C_D, is given in Fig. 9.25 as a function of the Reynolds number and surface roughness. For the golf ball in standard air

$$\mathrm{Re} = \frac{UD}{\nu} = \frac{(200 \text{ ft/s})(1.69/12 \text{ ft})}{1.57 \times 10^{-4} \text{ ft}^2\text{/s}} = 1.79 \times 10^5$$

while for the table tennis ball

$$\mathrm{Re} = \frac{UD}{\nu} = \frac{(60 \text{ ft/s})(1.50/12 \text{ ft})}{1.57 \times 10^{-4} \text{ ft}^2\text{/s}} = 4.78 \times 10^4$$

The corresponding drag coefficients are $C_D = 0.25$ for the standard golf ball, $C_D = 0.51$ for the smooth golf ball, and $C_D = 0.50$ for the table tennis ball. Hence, from Eq. 1 for the standard golf ball

$$\mathfrak{D} = \frac{1}{2}(0.00238 \text{ slugs/ft}^3)(200 \text{ ft/s})^2 \frac{\pi}{4}\left(\frac{1.69}{12} \text{ ft}\right)^2 (0.25)$$
$$= 0.185 \text{ lb} \qquad \textbf{(Ans)}$$

for the smooth golf ball

$$\mathfrak{D} = \frac{1}{2}(0.00238 \text{ slugs/ft}^3)(200 \text{ ft/s})^2 \frac{\pi}{4}\left(\frac{1.69}{12} \text{ ft}\right)^2 (0.51)$$

$$= 0.378 \text{ lb} \qquad \textbf{(Ans)}$$

and for the table tennis ball

$$\mathfrak{D} = \frac{1}{2}(0.00238 \text{ slugs/ft}^3)(60 \text{ ft/s})^2 \frac{\pi}{4}\left(\frac{1.50}{12} \text{ ft}\right)^2 (0.50)$$

$$= 0.0263 \text{ lb} \qquad \textbf{(Ans)}$$

The corresponding decelerations are $a = \mathfrak{D}/m = g\mathfrak{D}/\mathcal{W}$, where m is the mass of the ball. Thus, the deceleration relative to the acceleration of gravity, a/g (i.e., the number of g's deceleration) is $a/g = \mathfrak{D}/\mathcal{W}$ or

$$\frac{a}{g} = \frac{0.185 \text{ lb}}{0.0992 \text{ lb}} = 1.86 \text{ for the standard golf ball} \qquad \textbf{(Ans)}$$

$$\frac{a}{g} = \frac{0.378 \text{ lb}}{0.0992 \text{ lb}} = 3.81 \text{ for the smooth golf ball} \qquad \textbf{(Ans)}$$

$$\frac{a}{g} = \frac{0.0263 \text{ lb}}{0.00551 \text{ lb}} = 4.77 \text{ for the table tennis ball} \qquad \textbf{(Ans)}$$

COMMENTS Note that there is a considerably smaller deceleration for the rough golf ball than for the smooth one. Because of its much larger drag-to-mass ratio, the table tennis ball slows down relatively quickly and does not travel as far as the golf ball. Note that with $U = 60$ ft/s the standard golf ball has a drag of $\mathfrak{D} = 0.0200$ lb and a deceleration of $a/g = 0.202$, considerably less than the $a/g = 4.77$ of the table tennis ball. Conversely, a table tennis ball hit from a tee at 200 ft/s would decelerate at a rate of $a = 1740$ ft/s^2, or $a/g = 54.1$. It would not travel nearly as far as the golf ball.

By repeating the above calculations, the drag as a function of speed for both a standard golf ball and a smooth golf ball is shown in Fig. E9.12.

The Reynolds number range for which a rough golf ball has smaller drag than a smooth one (i.e., 4×10^4 to 3.6×10^5) corresponds to a flight velocity range of $45 < U < 400$ ft/s. This is comfortably within the range of most golfers. (The fastest tee shot by top professional golfers is approximately 280 ft/s.) As discussed in Section 9.4.2, the dimples (roughness) on a golf ball also help produce a lift (due to the spin of the ball) that allows the ball to travel farther than a smooth ball.

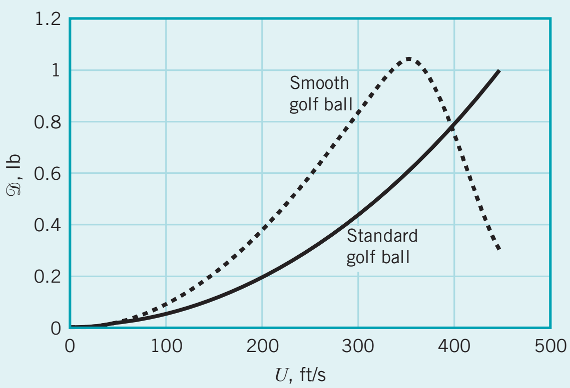

■ FIGURE E9.12

Fluids in the News

Dimpled baseball bats For many years it has been known that dimples on golf balls can create a *turbulent boundary layer* and reduce the aerodynamic drag, allowing longer drives than with smooth balls. Thus, why not put dimples on baseball bats so that tomorrow's baseball sluggers can swing the bat faster and, therefore, hit the ball farther? MIT instructor Jeffery De Tullio pondered that question, performed experiments with dimpled bats to determine the answer, and received a patent for his dimpled bat invention. The result is that a batter can swing a dimpled bat approximately 3 to 5% faster than a smooth bat. Theoretically, this extra speed will translate to an extra 10 to 15 ft distance on a long hit. (See Problem 9.89.)

V9.12 Jet ski

Froude Number Effects. Another parameter on which the drag coefficient may be strongly dependent is the Froude number, $\text{Fr} = U/\sqrt{g\ell}$. As is discussed in Chapter 10, the Froude number is a ratio of the free-stream speed to a typical wave speed on the interface of two fluids, such as the surface of the ocean. An object moving on the surface, such as a ship, often produces waves that require a source of energy to generate. This energy comes from the ship and is manifest as a drag. [Recall that the rate of energy production (power) equals speed times force.] The nature of the waves produced often depends on the Froude number of the flow and the shape of the object—the waves generated by a water skier "plowing" through the water at a low speed (low Fr) are different than those generated by the skier "planing" along the surface at high speed (large Fr).

The drag coefficient for surface ships is a function of the Froude number.

Thus, the drag coefficient for surface ships is a function of Reynolds number (viscous effects) and Froude number (wave-making effects); $C_D = \phi(\text{Re}, \text{Fr})$. As was discussed in Chapter 7, it is often quite difficult to run model tests under conditions similar to those of the prototype (i.e., same Re and Fr for surface ships). Fortunately, the viscous and wave effects can often be separated, with the total drag being the sum of the drag of these individual effects. A detailed account of this important topic can be found in standard texts (Ref. 11).

As is indicated in Fig. 9.26, the wave-making drag, $\mathfrak{D}_w$, can be a complex function of the Froude number and the body shape. The rather "wiggly" dependence of the wave drag coefficient,

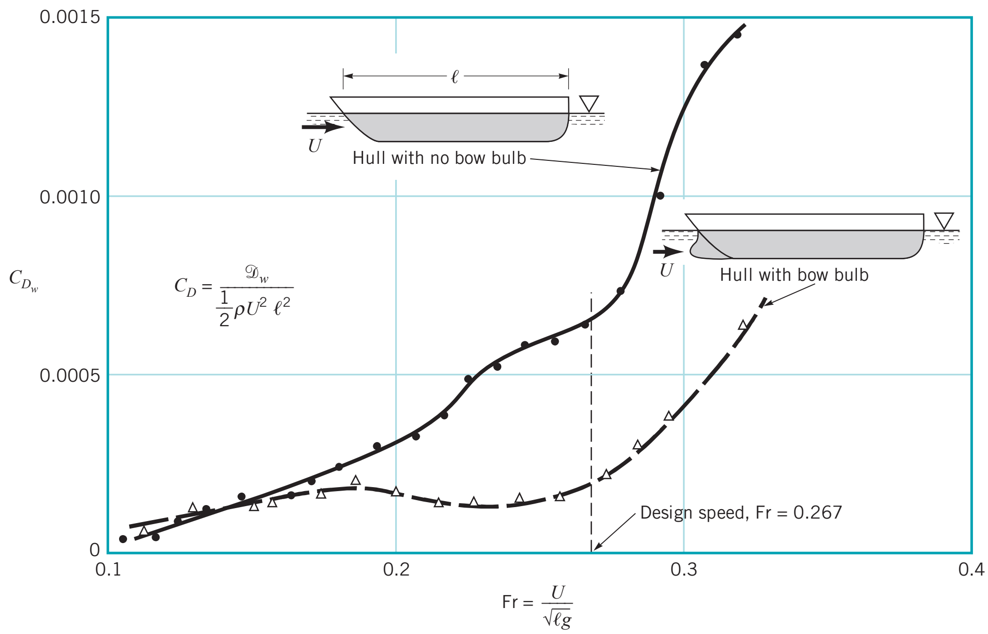

■ **FIGURE 9.26** **Typical drag coefficient data as a function of Froude number and hull characteristics for that portion of the drag due to the generation of waves (adapted from Ref. 25).**

$C_{Dw} = \mathscr{D}_w/(\rho U^2 \ell^2/2)$, on the Froude number shown is typical. It results from the fact that the structure of the waves produced by the hull is a strong function of the ship speed or, in dimensionless form, the Froude number. This wave structure is also a function of the body shape. For example, the bow wave, which is often the major contributor to the wave drag, can be reduced by use of an appropriately designed bulb on the bow, as is indicated in Fig. 9.26. In this instance the streamlined body (hull without a bulb) has more drag than the less streamlined one.

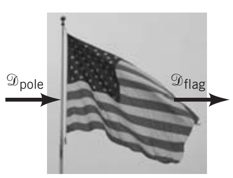

The drag on a complex body can be approximated as the sum of the drag on its parts.

Composite Body Drag. Approximate drag calculations for a complex body can often be obtained by treating the body as a composite collection of its various parts. For example, the total force on a flag pole because of the wind (see the figure in the margin) can be approximated by adding the aerodynamic drag produced by the various components involved—the drag on the flag and the drag on the pole. In some cases considerable care must be taken in such an approach because of the interactions between the various parts. It may not be correct to merely add the drag of the components to obtain the drag of the entire object, although such approximations are often reasonable.

EXAMPLE 9.13 Drag on a Composite Body

GIVEN A 60-mph (i.e., 88-fps) wind blows past the water tower shown in Fig. E9.13*a*.

FIND Estimate the moment (torque), M, needed at the base to keep the tower from tipping over.

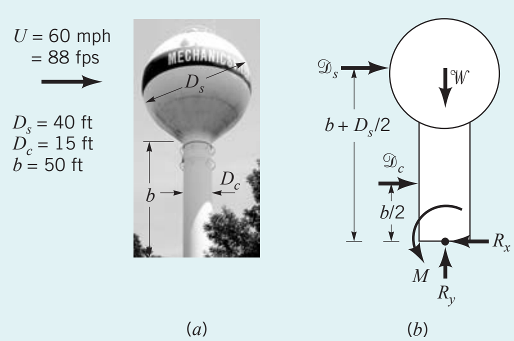

■ **FIGURE E9.13**

SOLUTION

We treat the water tower as a sphere resting on a circular cylinder and assume that the total drag is the sum of the drag from these parts. The free-body diagram of the tower is shown in Fig.

E9.13*b*. By summing moments about the base of the tower, we obtain

$$M = \mathscr{D}_s\left(b + \frac{D_s}{2}\right) + \mathscr{D}_c\left(\frac{b}{2}\right) \quad \textbf{(1)}$$

where

$$\mathscr{D}_s = \frac{1}{2}\rho U^2 \frac{\pi}{4} D_s^2 C_{Ds} \quad \textbf{(2)}$$

and

$$\mathscr{D}_c = \frac{1}{2}\rho U^2 b D_c C_{Dc} \quad \textbf{(3)}$$

are the drag on the sphere and cylinder, respectively. For standard atmospheric conditions, the Reynolds numbers are

$$\mathrm{Re}_s = \frac{UD_s}{\nu} = \frac{(88 \text{ ft/s})(40 \text{ ft})}{1.57 \times 10^{-4} \text{ ft}^2\text{/s}} = 2.24 \times 10^7$$

and

$$\mathrm{Re}_c = \frac{UD_c}{\nu} = \frac{(88 \text{ ft/s})(15 \text{ ft})}{1.57 \times 10^{-4} \text{ ft}^2\text{/s}} = 8.41 \times 10^6$$

The corresponding drag coefficients, C_{Ds} and C_{Dc}, can be approximated from Fig. 9.21 as

$$C_{Ds} \approx 0.3 \quad \text{and} \quad C_{Dc} \approx 0.7$$

Note that the value of C_{Ds} was obtained by an extrapolation of the given data to Reynolds numbers beyond those given (a potentially dangerous practice!). From Eqs. 2 and 3 we obtain

$$\mathscr{D}_s = 0.5(0.00238 \text{ slugs/ft}^3)(88 \text{ ft/s})^2 \frac{\pi}{4}(40 \text{ ft})^2(0.3)$$
$$= 3470 \text{ lb}$$

and

$$\mathscr{D}_c = 0.5(0.00238 \text{ slugs/ft}^3)(88 \text{ ft/s})^2(50 \text{ ft} \times 15 \text{ ft})(0.7)$$
$$= 4840 \text{ lb}$$

From Eq. 1 the corresponding moment needed to prevent the tower from tipping is

$$M = 3470 \text{ lb}\left(50 \text{ ft} + \frac{40}{2} \text{ ft}\right) + 4840 \text{ lb}\left(\frac{50}{2} \text{ ft}\right)$$
$$= 3.64 \times 10^5 \text{ ft} \cdot \text{lb} \qquad \textbf{(Ans)}$$

COMMENT The above result is only an estimate because (a) the wind is probably not uniform from the top of the tower to the ground, (b) the tower is not exactly a combination of a smooth sphere and a circular cylinder, (c) the cylinder is not of infinite length, (d) there will be some interaction between the flow past the cylinder and that past the sphere so that the net drag is not exactly the sum of the two, and (e) a drag coefficient value was obtained by extrapolation of the given data. However, such approximate results are often quite accurate.

V9.13 Drag on a truck

V9.14 Automobile streamlining

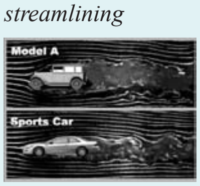

The aerodynamic drag on automobiles provides an example of the use of adding component drag forces. The power required to move a car along a level street is used to overcome the rolling resistance and the aerodynamic drag. For speeds above approximately 30 mph, the aerodynamic drag becomes a significant contribution to the net propulsive force needed. The contribution of the drag due to various portions of car (i.e., front end, windshield, roof, rear end, windshield peak, rear roof/trunk, and cowl) have been determined by numerous model and full-sized tests as well as by

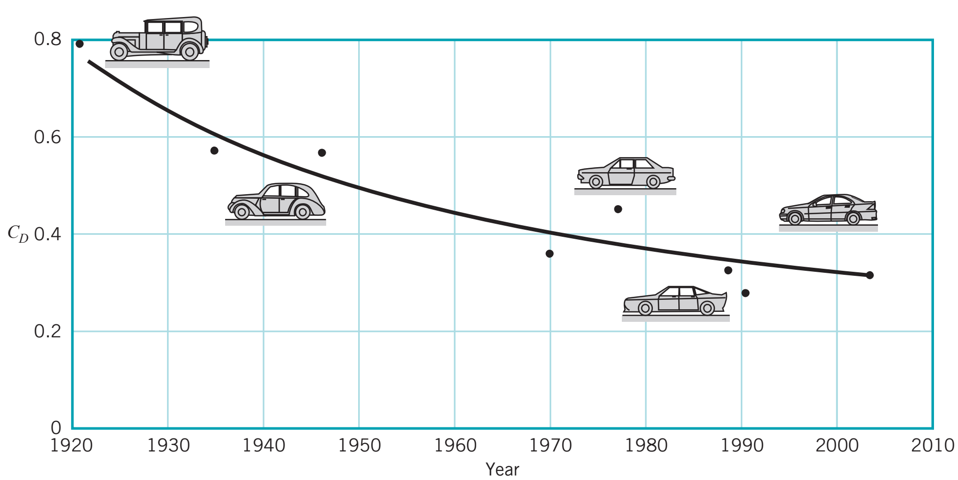

■ **FIGURE 9.27 The historical trend of streamlining automobiles to reduce their aerodynamic drag and increase their miles per gallon (adapted from Ref. 5).**

Considerable effort has gone into reducing the aerodynamic drag of automobiles.

numerical calculations. As a result it is possible to predict the aerodynamic drag on cars of a wide variety of body styles.

As is indicated in Fig. 9.27, the drag coefficient for cars has decreased rather continuously over the years. This reduction is a result of careful design of the shape and the details (such as window molding, rear view mirrors, etc.). An additional reduction in drag has been accomplished by a reduction of the projected area. The net result is a considerable increase in the gas mileage, especially at highway speeds. Considerable additional information about the aerodynamics of road vehicles can be found in the literature (Ref. 30).

Fluids in the News

At 10,240 mpg it doesn't cost much to "fill 'er up" Typical gas consumption for a Formula 1 racer, a sports car, and a sedan is approximately 2 mpg, 15 mpg, and 30 mpg, respectively. Thus, just how did the winning entry in the 2002 Shell Eco-Marathon achieve an incredible 10,240 mpg? To be sure, this vehicle is not as fast as a Formula 1 racer (although the rules require it to average at least 15 mph) and it can't carry as large a load as your family sedan can (the vehicle has barely enough room for the driver). However, by using a number of clever engineering design considerations, this amazing fuel efficiency was obtained. The type (and number) of tires, the appropriate engine power and weight, the specific chassis design, and the design of the body shell are all important and interrelated considerations. To reduce *drag*, the aerodynamic shape of the high-efficiency vehicle was given special attention through theoretical considerations and wind tunnel model testing. The result is an amazing vehicle that can travel a long distance without hearing the usual "fill 'er up." (See Problem 9.90.)

The effect of several important parameters (shape, Re, Ma, Fr, and roughness) on the drag coefficient for various objects has been discussed in this section. As stated previously, drag coefficient information for a very wide range of objects is available in the literature. Some of this information is given in Figs. 9.28, 9.29, and 9.30 below for a variety of two- and three-dimensional, natural and man-made objects. Recall that a drag coefficient of unity is equivalent to the drag produced by the dynamic pressure acting on an area of size A. That is, $\mathcal{D} = \frac{1}{2}\rho U^2 A C_D = \frac{1}{2}\rho U^2 A$ if $C_D = 1$. Typical nonstreamlined objects have drag coefficients on this order.

9.4 Lift

As is indicated in Section 9.1, any object moving through a fluid will experience a net force of the fluid on the object. For objects symmetrical perpendicular to the upstream flow, this force will be in the direction of the free stream—a drag, $\mathcal{D}$. If the object is not symmetrical (or if it does not produce a symmetrical flow field, such as the flow around a rotating sphere), there may also be a force normal to the free stream—a lift, $\mathcal{L}$. Considerable effort has been put forth to understand the various properties of the generation of lift. Some objects, such as an airfoil, are designed to generate lift. Other objects are designed to reduce the lift generated. For example, the lift on a car tends to reduce the contact force between the wheels and the ground, causing reduction in traction and cornering ability. It is desirable to reduce this lift.

9.4.1 Surface Pressure Distribution

The lift can be determined from Eq. 9.2 if the distributions of pressure and wall shear stress around the entire body are known. As is indicated in Section 9.1, such data are usually not known. Typically, the lift is given in terms of the lift coefficient,

The lift coefficient is a dimensionless form of the lift.

$$\boxed{C_L = \frac{\mathcal{L}}{\frac{1}{2}\rho U^2 A}} \qquad \textbf{(9.39)}$$

Shape	Reference area A (b = length)	Drag coefficient $C_D = \dfrac{\mathfrak{D}}{\frac{1}{2}\rho U^2 A}$	Reynolds number $\mathrm{Re} = \rho UD/\mu$
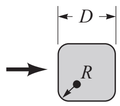 Square rod with rounded corners	$A = bD$	R/D | C_D 0 | 2.2 0.02 | 2.0 0.17 | 1.2 0.33 | 1.0	$\mathrm{Re} = 10^5$
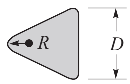 Rounded equilateral triangle	$A = bD$	R/D | C_D (→) | C_D (←) 0 | 1.4 | 2.1 0.02 | 1.2 | 2.0 0.08 | 1.3 | 1.9 0.25 | 1.1 | 1.3	$\mathrm{Re} = 10^5$
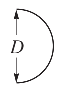 Semicircular shell	$A = bD$	→ 2.3 ← 1.1	$\mathrm{Re} = 2 \times 10^4$
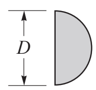 Semicircular cylinder	$A = bD$	→ 2.15 ← 1.15	$\mathrm{Re} > 10^4$
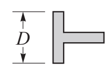 T-beam	$A = bD$	→ 1.80 ← 1.65	$\mathrm{Re} > 10^4$
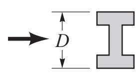 I-beam	$A = bD$	2.05	$\mathrm{Re} > 10^4$
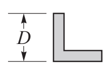 Angle	$A = bD$	→ 1.98 ← 1.82	$\mathrm{Re} > 10^4$
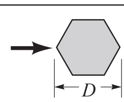 Hexagon	$A = bD$	1.0	$\mathrm{Re} > 10^4$
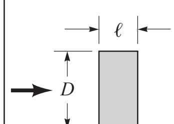 Rectangle	$A = bD$	ℓ/D | C_D ≤0.1 | 1.9 0.5 | 2.5 0.65 | 2.9 1.0 | 2.2 2.0 | 1.6 3.0 | 1.3	$\mathrm{Re} = 10^5$

■ **FIGURE 9.28 Typical drag coefficients for regular two-dimensional objects (Refs. 5, 6).**

which is obtained from experiments, advanced analysis, or numerical considerations. The lift coefficient is a function of the appropriate dimensionless parameters and, as the drag coefficient, can be written as

The lift coefficient is a function of other dimensionless parameters.

$$C_L = \phi(\text{shape, Re, Ma, Fr}, \varepsilon/\ell)$$

The Froude number, Fr, is important only if there is a free surface present, as with an underwater "wing" used to support a high-speed hydrofoil surface ship. Often the surface roughness, ε, is relatively unimportant in terms of lift—it has more of an effect on the drag. The Mach number, Ma, is of importance for relatively high-speed subsonic and supersonic flows (i.e., $\mathrm{Ma} > 0.8$), and the Reynolds number effect is often not great. The most important parameter that affects the lift coefficient is the shape of the object. Considerable effort has gone into designing optimally shaped lift-producing devices. We will emphasize the effect of the shape on lift—the effects of the other dimensionless parameters can be found in the literature (Refs. 13, 14, 29).

Shape	Reference area A	Drag coefficient C_D	Reynolds number $\mathrm{Re} = \rho UD/\mu$
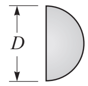 Solid hemisphere	$A = \frac{\pi}{4}D^2$	→ 1.17 ← 0.42	$\mathrm{Re} > 10^4$
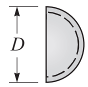 Hollow hemisphere	$A = \frac{\pi}{4}D^2$	→ 1.42 ← 0.38	$\mathrm{Re} > 10^4$
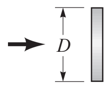 Thin disk	$A = \frac{\pi}{4}D^2$	1.1	$\mathrm{Re} > 10^3$
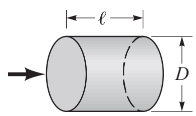 Circular rod parallel to flow	$A = \frac{\pi}{4}D^2$	ℓ/D | C_D 0.5 | 1.1 1.0 | 0.93 2.0 | 0.83 4.0 | 0.85	$\mathrm{Re} > 10^5$
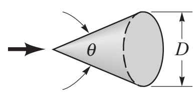 Cone	$A = \frac{\pi}{4}D^2$	θ, degrees | C_D 10 | 0.30 30 | 0.55 60 | 0.80 90 | 1.15	$\mathrm{Re} > 10^4$
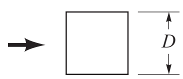 Cube	$A = D^2$	1.05	$\mathrm{Re} > 10^4$
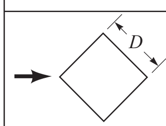 Cube	$A = D^2$	0.80	$\mathrm{Re} > 10^4$
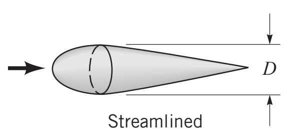 Streamlined body	$A = \frac{\pi}{4}D^2$	0.04	$\mathrm{Re} > 10^5$

■ **FIGURE 9.29** **Typical drag coefficients for regular three-dimensional objects (Ref. 5).**

Usually most lift comes from pressure forces, not viscous forces.

Most common lift-generating devices (i.e., airfoils, fans, spoilers on cars, etc.) operate in the large Reynolds number range in which the flow has a boundary layer character, with viscous effects confined to the boundary layers and wake regions. For such cases the wall shear stress, τ_w, contributes little to the lift. Most of the lift comes from the surface pressure distribution. A typical pressure distribution on a moving car is shown in Fig. 9.31. The distribution, for the most part, is consistent with simple Bernoulli equation analysis. Locations with high-speed flow (i.e., over the roof and hood) have low pressure, while locations with low-speed flow (i.e., on the grill and windshield) have high pressure. It is easy to believe that the integrated effect of this pressure distribution would provide a net upward force.

For objects operating in very low Reynolds number regimes (i.e., $\mathrm{Re} < 1$), viscous effects are important, and the contribution of the shear stress to the lift may be as important as that of the pressure. Such situations include the flight of minute insects and the swimming of microscopic organisms. The relative importance of τ_w and p in the generation of lift in a typical large Reynolds number flow is shown in Example 9.14.

Shape	Reference area	Drag coefficient C_D
 Parachute	Frontal area $A = \frac{\pi}{4}D^2$	1.4
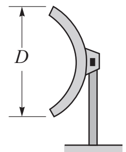 Porous parabolic dish	Frontal area $A = \frac{\pi}{4}D^2$	Porosity: 0 / 0.2 / 0.5 → : 1.42 / 1.20 / 0.82 ← : 0.95 / 0.90 / 0.80 Porosity = open area/total area
 Average person	Standing Sitting Crouching	$C_DA = 9\ \text{ft}^2$ $C_DA = 6\ \text{ft}^2$ $C_DA = 2.5\ \text{ft}^2$
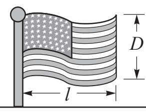 Fluttering flag	$A = \ell D$	ℓ/D : C_D 1 : 0.07 2 : 0.12 3 : 0.15
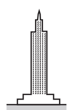 Empire State Building	Frontal area	1.4
 Six-car passenger train	Frontal area	1.8
Bikes		
 Upright commuter	$A = 5.5\ \text{ft}^2$	1.1
 Racing	$A = 3.9\ \text{ft}^2$	0.88
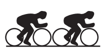 Drafting	$A = 3.9\ \text{ft}^2$	0.50
 Streamlined	$A = 5.0\ \text{ft}^2$	0.12
Tractor-trailer trucks		
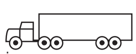 Standard	Frontal area	0.96
Fairing 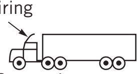 With fairing	Frontal area	0.76
Gap seal 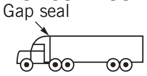 With fairing and gap seal	Frontal area	0.70
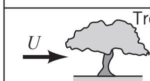 Tree U = 10 m/s U = 20 m/s U = 30 m/s	Frontal area	0.43 0.26 0.20
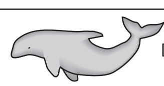 Dolphin	Wetted area	0.0036 at Re = 6×10^6 (flat plate has $C_{Df} = 0.0031$)
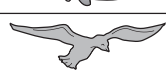 Large birds	Frontal area	0.40

■ **FIGURE 9.30** **Typical drag coefficients for objects of interest (Refs. 5, 6, 15, 20).**

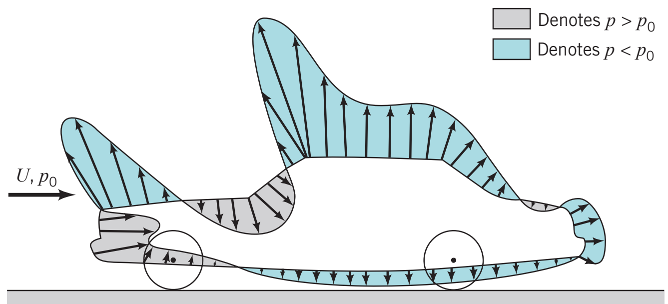

■ FIGURE 9.31 **Pressure distribution on the surface of an automobile.**

EXAMPLE 9.14 Lift from Pressure and Shear Stress Distributions

GIVEN When a uniform wind of velocity U blows past the semicircular building shown in Fig. E9.14*a,b*, the wall shear stress and pressure distributions on the outside of the building are as given previously in Figs. E9.8*b* and E9.9*a*, respectively.

FIND If the pressure in the building is atmospheric (i.e., the value, p_0, far from the building), determine the lift coefficient and the lift on the roof.

SOLUTION

From Eq. 9.2 we obtain the lift as

$$\mathscr{L} = -\int p \sin\theta \, dA + \int \tau_w \cos\theta \, dA \qquad (1)$$

As is indicated in Fig. E9.14*b*, we assume that on the inside of the building the pressure is uniform, $p = p_0$, and that there is no shear stress. Thus, Eq. 1 can be written as

$$\mathscr{L} = -\int_0^\pi (p - p_0)\sin\theta \, b\left(\frac{D}{2}\right) d\theta + \int_0^\pi \tau_w \cos\theta \, b\left(\frac{D}{2}\right) d\theta$$

or

$$\mathscr{L} = \frac{bD}{2}\left[-\int_0^\pi (p - p_0)\sin\theta \, d\theta + \int_0^\pi \tau_w \cos\theta \, d\theta\right] \qquad (2)$$

where b and D are the length and diameter of the building, respectively, and $dA = b(D/2)d\theta$. Equation 2 can be put into dimensionless form by using the dynamic pressure, $\rho U^2/2$, planform area, $A = bD$, and dimensionless shear stress

$$F(\theta) = \tau_w(\mathrm{Re})^{1/2}/(\rho U^2/2)$$

to give

$$\mathscr{L} = \frac{1}{2}\rho U^2 A\left[-\frac{1}{2}\int_0^\pi \frac{(p - p_0)}{\frac{1}{2}\rho U^2}\sin\theta \, d\theta + \frac{1}{2\sqrt{\mathrm{Re}}}\int_0^\pi F(\theta)\cos\theta \, d\theta\right] \qquad (3)$$

From the data in Figs. E9.8b and E9.9a, the values of the two integrals in Eq. 3 can be obtained by determining the area under the curves of $[(p - p_0)/(\rho U^2/2)] \sin\theta$ versus θ and $F(\theta)\cos\theta$ versus θ plotted in Figs. E9.14*c* and E9.14*d*. The results are

$$\int_0^\pi \frac{(p - p_0)}{\frac{1}{2}\rho U^2}\sin\theta \, d\theta = -1.76$$

and

$$\int_0^\pi F(\theta)\cos\theta \, d\theta = 3.92$$

Thus, the lift is

$$\mathscr{L} = \frac{1}{2}\rho U^2 A\left[\left(-\frac{1}{2}\right)(-1.76) + \frac{1}{2\sqrt{\mathrm{Re}}}(3.92)\right]$$

or

$$\mathscr{L} = \left(0.88 + \frac{1.96}{\sqrt{\mathrm{Re}}}\right)\left(\frac{1}{2}\rho U^2 A\right) \qquad \textbf{(Ans)}$$

and

$$C_L = \frac{\mathscr{L}}{\frac{1}{2}\rho U^2 A} = 0.88 + \frac{1.96}{\sqrt{\mathrm{Re}}} \qquad (4) \quad \textbf{(Ans)}$$

COMMENTS Consider a typical situation with $D = 20$ ft, $U = 30$ ft/s, $b = 50$ ft, and standard atmospheric conditions ($\rho = 2.38 \times 10^{-3}$ slugs/ft^3 and $\nu = 1.57 \times 10^{-4}$ ft^2/s), which gives a Reynolds number of

$$\mathrm{Re} = \frac{UD}{\nu} = \frac{(30 \text{ ft/s})(20 \text{ ft})}{1.57 \times 10^{-4} \text{ ft}^2/\text{s}} = 3.82 \times 10^6$$

Hence, the lift coefficient is

$$C_L = 0.88 + \frac{1.96}{(3.82 \times 10^6)^{1/2}} = 0.88 + 0.001 = 0.881$$

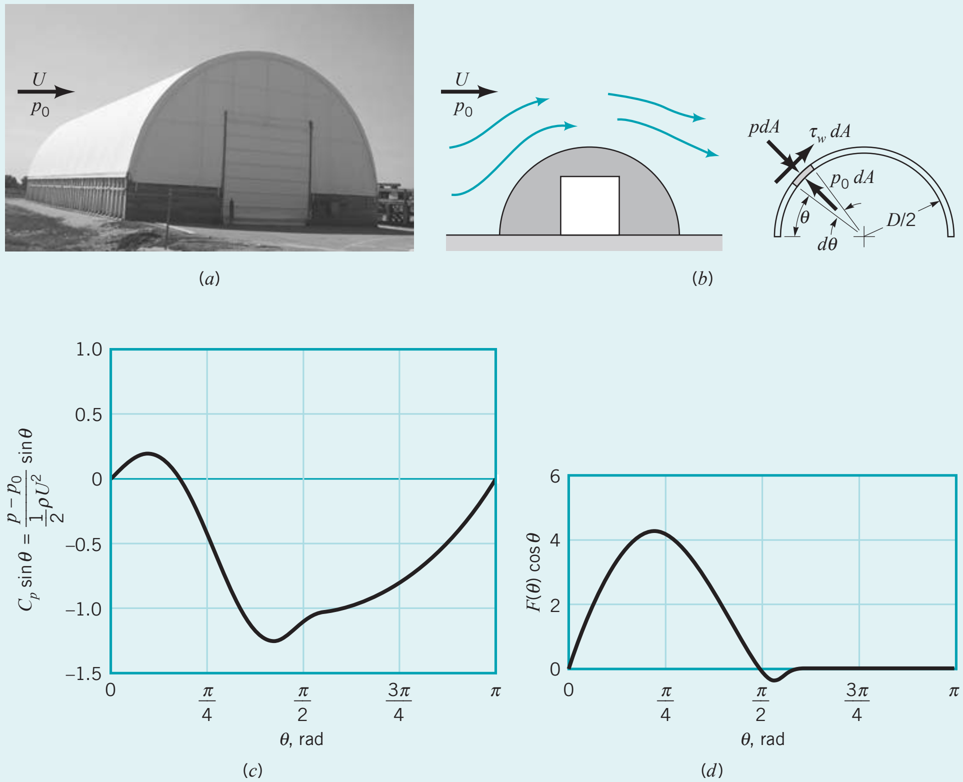

■ FIGURE E9.14

Note that the pressure contribution to the lift coefficient is 0.88 whereas that due to the wall shear stress is only $1.96/(\text{Re}^{1/2}) = 0.001$. The Reynolds number dependency of C_L is quite minor. The lift is pressure dominated. Recall from Example 9.9 that this is also true for the drag on a similar shape.

From Eq. 4 with $A = 20 \text{ ft} \times 50 \text{ ft} = 1000 \text{ ft}^2$, we obtain the lift for the assumed conditions as

$$\mathcal{L} = \tfrac{1}{2}\rho U^2 A C_L = \tfrac{1}{2}(0.00238 \text{ slugs/ft}^3)(30 \text{ ft/s})^2(1000 \text{ ft}^2)(0.881)$$

or

$$\mathcal{L} = 944 \text{ lb}$$

There is a considerable tendency for the building to lift off the ground. Clearly this is due to the object being nonsymmetrical. The lift force on a complete circular cylinder is zero, although the fluid forces do tend to pull the upper and lower halves apart.

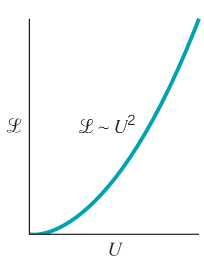

A typical device designed to produce lift does so by generating a pressure distribution that is different on the top and bottom surfaces. For large Reynolds number flows these pressure distributions are usually directly proportional to the dynamic pressure, $\rho U^2/2$, with viscous effects being of secondary importance. Hence, as indicated by the figure in the margin, for a given airfoil the lift is proportional to the square of the airspeed. Two airfoils used to produce lift are indicated in Fig. 9.32. Clearly the symmetrical one cannot produce lift unless the angle of attack, α, is nonzero. Because of the asymmetry of the nonsymmetric airfoil, the pressure distributions on the upper and lower surfaces are different, and a lift is produced even with $\alpha = 0$. Of course, there will be a certain value of α (less than zero for this case) for which the lift is zero. For this situation, the pressure distributions on the upper and lower surfaces are different, but their resultant (integrated) pressure forces will be equal and opposite.

Since most airfoils are thin, it is customary to use the planform area, $A = bc$, in the definition of the lift coefficient. Here b is the length of the airfoil and c is the *chord length*—the length from the leading edge to the trailing edge as indicated in Fig. 9.32. Typical lift coefficients so defined are on the order of unity. That is, the lift force is on the order of the dynamic pressure times the planform area of the wing, $\mathcal{L} \approx (\rho U^2/2)A$. The *wing loading*, defined as the average lift per unit area of the wing, $\mathcal{L}/A$, therefore, increases with speed. For example, the wing loading of the

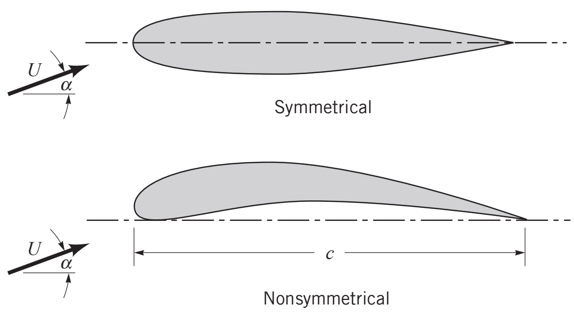

■ FIGURE 9.32 Symmetrical and nonsymmetrical airfoils.

1903 Wright Flyer aircraft was 1.5 lb/ft^2, while for the present-day Boeing 747 aircraft it is 150 lb/ft^2. The wing loading for a bumble bee is approximately 1 lb/ft^2 (Ref. 15).

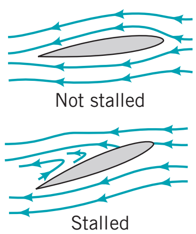

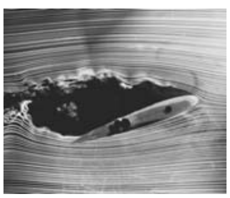

At large angles of attack the boundary layer separates and the wing stalls.

Typical lift and drag coefficient data as a function of angle of attack, α, and *aspect ratio*, $\mathscr{A}$, are indicated in Figs. 9.33*a* and 9.33*b*. The aspect ratio is defined as the ratio of the square of the wing length to the planform area, $\mathscr{A} = b^2/A$. If the chord length, c, is constant along the length of the wing (a rectangular planform wing), this reduces to $\mathscr{A} = b/c$.

In general, the lift coefficient increases and the drag coefficient decreases with an increase in aspect ratio. Long wings are more efficient because their wing tip losses are relatively more minor than for short wings. The increase in drag due to the finite length ($\mathscr{A} < \infty$) of the wing is often termed induced drag. It is due to the interaction of the complex swirling flow structure near the wing tips (see Fig. 9.37) and the free stream (Ref. 13). High-performance soaring airplanes and highly efficient soaring birds (i.e., the albatross and sea gull) have long, narrow wings. Such wings, however, have considerable inertia that inhibits rapid maneuvers. Thus, highly maneuverable fighter or acrobatic airplanes and birds (i.e., the falcon) have small-aspect-ratio wings.

Although viscous effects and the wall shear stress contribute little to the direct generation of lift, they play an extremely important role in the design and use of lifting devices. This is because of the viscosity-induced boundary layer separation that can occur on nonstreamlined bodies such as airfoils that have too large an angle of attack (see Fig. 9.18). As is indicated in Fig. 9.33, up to a certain point, the lift coefficient increases rather steadily with the angle of attack. If α is too large, the boundary layer on the upper surface separates, the flow over the wing develops a wide, turbulent wake region, the lift decreases, and the drag increases. This condition, as indicated by the figures in the margin, is termed ***stall***. Such conditions are extremely dangerous if they occur while the airplane is flying at a low altitude where there is not sufficient time and altitude to recover from the stall.

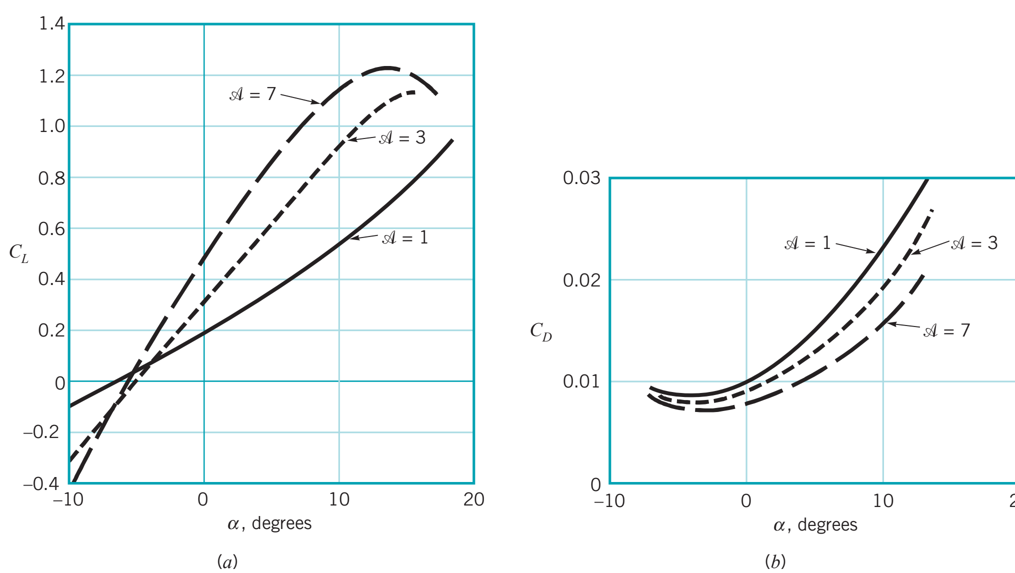

■ FIGURE 9.33 Typical lift and drag coefficient data as a function of angle of attack and the aspect ratio of the airfoil: (*a*) lift coefficient, (*b*) drag coefficient.

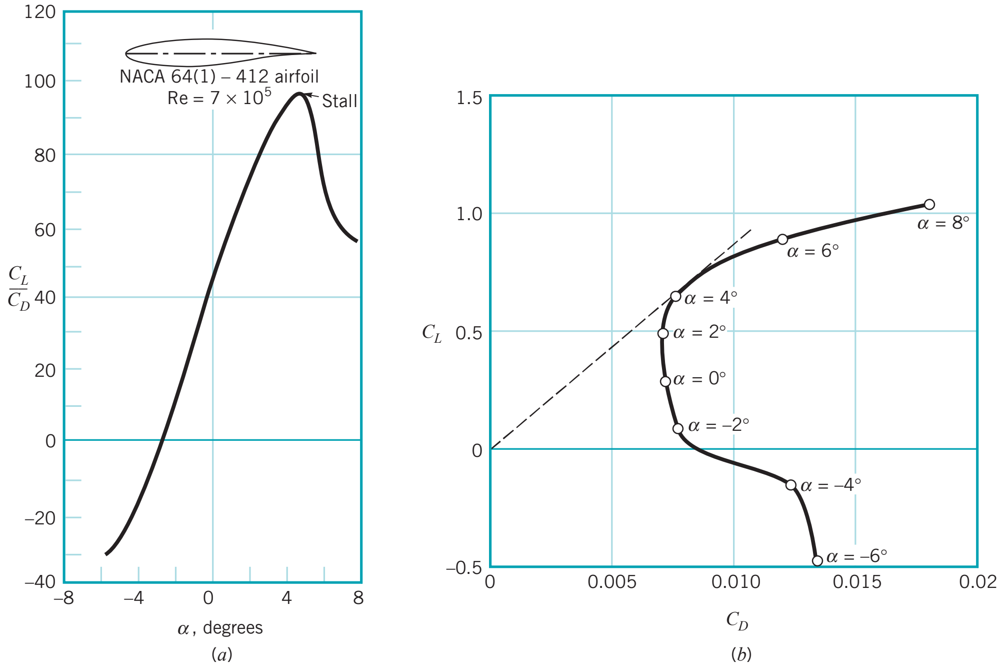

■ **FIGURE 9.34** **Two representations of the same lift and drag data for a typical airfoil: (*a*) lift-to-drag ratio as a function of angle of attack, with the onset of boundary layer separation on the upper surface indicated by the occurrence of stall, (*b*) the lift and drag polar diagram with the angle of attack indicated (Ref. 27).**

V9.15 Stalled airfoil

V9.16 Bat flying

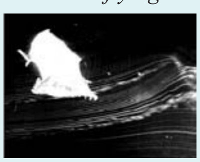

In many lift-generating devices the important quantity is the ratio of the lift to drag developed, $\mathscr{L}/\mathscr{D} = C_L/C_D$. Such information is often presented in terms of C_L/C_D versus α, as is shown in Fig. 9.34*a*, or in a *lift-drag polar* of C_L versus C_D with α as a parameter, as is shown in Fig. 9.34*b*. The most efficient angle of attack (i.e., largest C_L/C_D) can be found by drawing a line tangent to the $C_L - C_D$ curve from the origin, as is shown in Fig. 9.34*b*. High-performance airfoils generate lift that is perhaps 100 or more times greater than their drag. This translates into the fact that in still air they can glide a horizontal distance of 100 m for each 1 m drop in altitude.

Fluids in the News

Bats feel turbulence Researchers have discovered that at certain locations on the wings of bats, there are special touch-sensing cells with a tiny hair poking out of the center of the cell. These cells, which are very sensitive to air flowing across the wing surface, can apparently detect turbulence in the flow over the wing. If these hairs are removed the bats fly well in a straight line, but when maneuvering to avoid obstacles, their elevation control is erratic. When the hairs grow back, the bats regain their complete flying skills. It is proposed that these touch-sensing cells are used to detect turbulence on the wing surface and thereby tell bats when to adjust the angle of attack and curvature of their wings in order to avoid stalling out in midair.

V9.17 Trailing edge flap

As is indicated above, the lift and drag on an airfoil can be altered by changing the angle of attack. This actually represents a change in the shape of the object. Other shape changes can be used to alter the lift and drag when desirable. In modern airplanes it is common to utilize leading edge and trailing edge flaps as is shown in Fig. 9.35. To generate the necessary lift during the relatively low-speed landing and takeoff procedures, the airfoil shape is altered by extending special flaps on the front and/or rear portions of the wing. Use of the flaps considerably enhances the lift, although it is at the expense of an increase in the drag (the airfoil is in a "dirty" configuration). This increase in drag is not of much concern during landing and takeoff operations—the decrease in landing or takeoff speed is more important than is a temporary increase in drag. During normal flight with the flaps retracted (the "clean" configuration), the drag is relatively small, and the needed lift force is achieved with the smaller lift coefficient and the larger dynamic pressure (higher speed).

V9.18 Leading edge flap

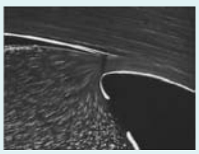

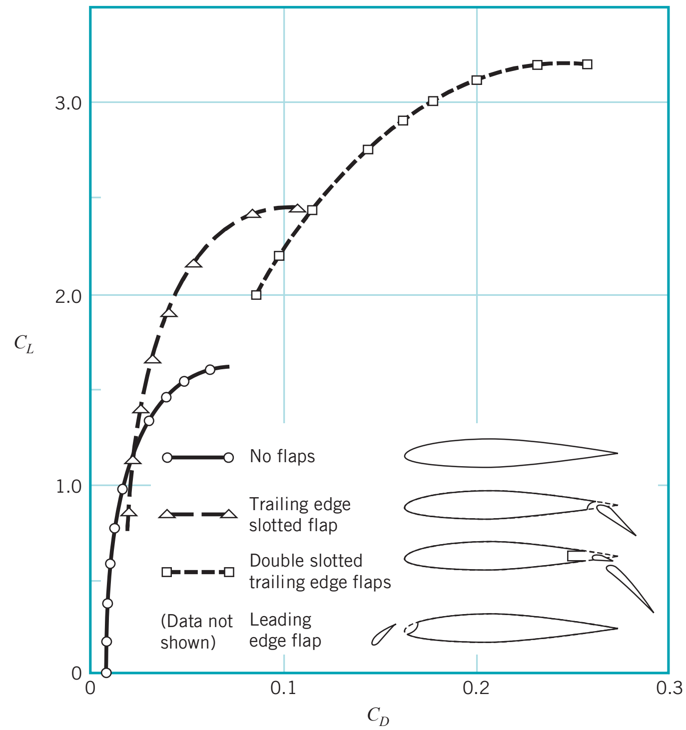

FIGURE 9.35 Typical lift and drag alterations possible with the use of various types of flap designs (Ref. 21).

Fluids in the News

Learning from nature For hundreds of years humans looked toward nature, particularly birds, for insight about flying. However, all early airplanes that closely mimicked birds proved to be unsuccessful. Only after much experimenting with rigid (or at least nonflapping) wings did human flight become possible. Recently, however, engineers have been turning to living systems—birds, insects, and other biological models—in an attempt to produce breakthroughs in aircraft design. Perhaps it is possible that nature's basic design concepts can be applied to airplane systems. For example, by morphing and rotating their wings in three dimensions, birds have remarkable maneuverability that to date has no technological parallel. Birds can control the airflow over their wings by moving the feathers on their wingtips and the leading edges of their wings, providing designs that are more efficient than the flaps and rigid, pivoting tail surfaces of current aircraft (Ref. 15). On a smaller scale, understanding the mechanism by which insects dynamically manage unstable flow to generate lift may provide insight into the development of microscale air vehicles. With new hi-tech materials, computers, and automatic controls, aircraft of the future may mimic nature more than was once thought possible. (See Problem 9.110.)

A wide variety of lift and drag information for airfoils can be found in standard aerodynamics books (Ref. 13, 14, 29).

EXAMPLE 9.15 Lift and Power for Human Powered Flight

GIVEN In 1977 the *Gossamer Condor*, shown in Fig. E9.15*a*, won the Kremer prize by being the first human-powered aircraft to complete a prescribed figure-of-eight course around two turning points 0.5 mi apart (Ref. 22). The following data pertain to this aircraft:

flight speed $= U = 15$ ft/s

wing size $= b = 96$ ft, $c = 7.5$ ft (average)

weight (including pilot) $= \mathscr{W} = 210$ lb

drag coefficient $= C_D = 0.046$ (based on planform area)

power train efficiency $= \eta$

$=$ power to overcome drag/pilot power $= 0.8$

FIND Determine

(a) the lift coefficient, C_L, and

(b) the power, $\mathscr{P}$, required by the pilot.

FIGURE E9.15a (Photograph copyright © Don Monroe.)

SOLUTION

(a) For steady flight conditions the lift must be exactly balanced by the weight, or

$$\mathcal{W} = \mathcal{L} = \tfrac{1}{2}\rho U^2 A C_L$$

Thus,

$$C_L = \frac{2\mathcal{W}}{\rho U^2 A}$$

where $A = bc = 96 \text{ ft} \times 7.5 \text{ ft} = 720 \text{ ft}^2$, $\mathcal{W} = 210$ lb, and $\rho = 2.38 \times 10^{-3} \text{ slugs/ft}^3$ for standard air. This gives

$$C_L = \frac{2(210 \text{ lb})}{(2.38 \times 10^{-3} \text{ slugs/ft}^3)(15 \text{ ft/s})^2(720 \text{ ft}^2)} = 1.09 \qquad \textbf{(Ans)}$$

a reasonable number. The overall lift-to-drag ratio for the aircraft is $C_L/C_D = 1.09/0.046 = 23.7$.

(b) The product of the power that the pilot supplies and the power train efficiency equals the useful power needed to overcome the drag, $\mathcal{D}$. That is,

$$\eta\mathcal{P} = \mathcal{D}U$$

where

$$\mathcal{D} = \tfrac{1}{2}\rho U^2 A C_D$$

Thus,

$$\mathcal{P} = \frac{\mathcal{D}U}{\eta} = \frac{\tfrac{1}{2}\rho U^2 A C_D U}{\eta} = \frac{\rho A C_D U^3}{2\eta} \qquad (1)$$

or

$$\mathcal{P} = \frac{(2.38 \times 10^{-3} \text{ slugs/ft}^3)(720 \text{ ft}^2)(0.046)(15 \text{ ft/s})^3}{2(0.8)}$$

$$\mathcal{P} = 166 \text{ ft} \cdot \text{lb/s}\left(\frac{1 \text{ hp}}{550 \text{ ft} \cdot \text{lb/s}}\right) = 0.302 \text{ hp} \qquad \textbf{(Ans)}$$

COMMENT This power level is obtainable by a well-conditioned athlete (as is indicated by the fact that the flight was successfully completed). Note that only 80% of the pilot's power (i.e., $0.8 \times 0.302 = 0.242$ hp, which corresponds to a drag of $\mathcal{D} = 8.86$ lb) is needed to force the aircraft through the air. The other 20% is lost because of the power train inefficiency.

By repeating the calculations for various flight speeds, the results shown in Fig. E9.15*b* are obtained. Note from Eq. 1 that for a constant drag coefficient, the power required increases as U^3—a doubling of the speed to 30 ft/s would require an eightfold increase in power (i.e., 2.42 hp, well beyond the range of any human).

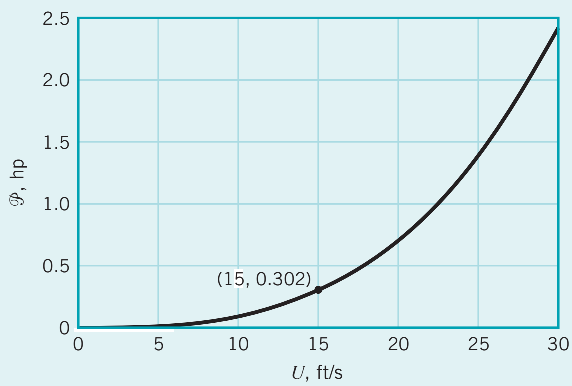

■ FIGURE E9.15*b*

9.4.2 Circulation

Inviscid flow analysis can be used to obtain ideal flow past airfoils.

Since viscous effects are of minor importance in the generation of lift, it should be possible to calculate the lift force on an airfoil by integrating the pressure distribution obtained from the equations governing inviscid flow past the airfoil. That is, the potential flow theory discussed in Chapter 6 should provide a method to determine the lift. Although the details are beyond the scope of this book, the following is found from such calculations (Ref. 4).

The calculation of the inviscid flow past a two-dimensional airfoil gives a flow field as indicated in Fig. 9.36. The predicted flow field past an airfoil with no lift (i.e., a symmetrical airfoil at zero angle of attack, Fig. 9.36*a*) appears to be quite accurate (except for the absence of thin boundary layer regions). However, as is indicated in Fig. 9.36*b*, the calculated flow past the same airfoil at a nonzero angle of attack (but one small enough so that boundary layer separation would not occur) is not proper near the trailing edge. In addition, the calculated lift for a nonzero angle of attack is zero—in conflict with the known fact that such airfoils produce lift.

In reality, the flow should pass smoothly over the top surface as is indicated in Fig. 9.36*c*, without the strange behavior indicated near the trailing edge in Fig. 9.36*b*. As is shown in Fig. 9.36*d*, the unrealistic flow situation can be corrected by adding an appropriate clockwise swirling flow around the airfoil. The results are twofold: (1) The unrealistic behavior near the trailing edge is eliminated (i.e.,

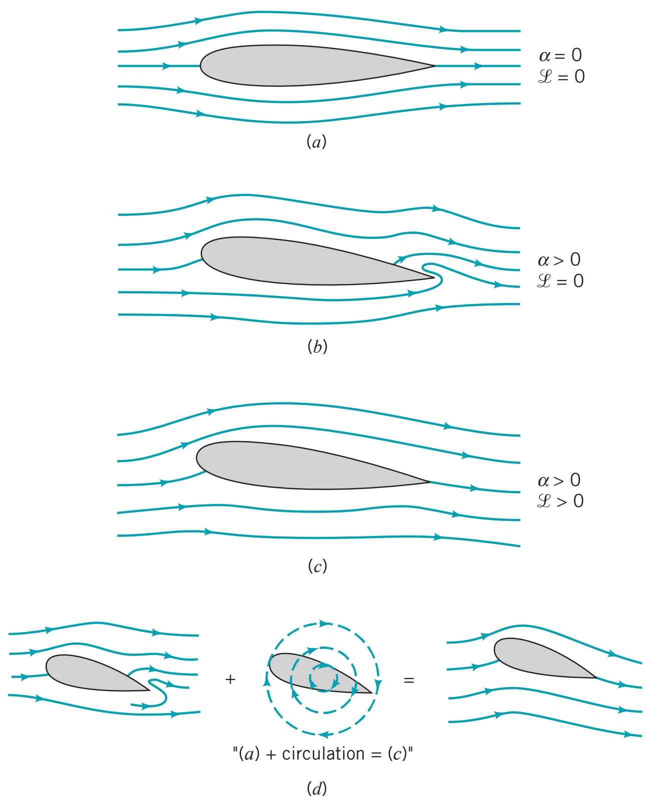

■ **FIGURE 9.36 Inviscid flow past an airfoil: (*a*) symmetrical flow past the symmetrical airfoil at a zero angle of attack; (*b*) same airfoil at a nonzero angle of attack—no lift, flow near trailing edge not realistic; (*c*) same conditions as for (*b*) except circulation has been added to the flow—nonzero lift, realistic flow; (*d*) superposition of flows to produce the final flow past the airfoil.**

the flow pattern of Fig. 9.36*b* is changed to that of Fig. 9.36*c*), and (2) the average velocity on the upper surface of the airfoil is increased while that on the lower surface is decreased. From the Bernoulli equation concepts (i.e., $p/\gamma + V^2/2g + z =$ constant), the average pressure on the upper surface is decreased and that on the lower surface is increased. The net effect is to change the original zero lift condition to that of a lift-producing airfoil.

The addition of the clockwise swirl is termed the addition of ***circulation***. The amount of swirl (circulation) needed to have the flow leave the trailing edge smoothly is a function of the airfoil size and shape and can be calculated from potential flow (inviscid) theory (see Section 6.6.3 and Ref. 29). Although the addition of circulation to make the flow field physically realistic may seem artificial, it has well-founded mathematical and physical grounds. For example, consider the flow past a finite length airfoil, as is indicated in Fig. 9.37. For lift-generating conditions the average pressure on the lower surface is greater than that on the upper surface. Near the tips of the wing this pressure difference will cause some of the fluid to attempt to migrate from the lower to the upper surface, as is indicated in Fig. 9.37*b*. At the same time, this fluid is swept downstream, forming a *trailing vortex* (swirl) from each wing tip (see Fig. 4.3). It is speculated that the reason some birds migrate in vee-formation is to take advantage of the updraft produced by the trailing vortex of the preceding bird. [It is calculated that for a given expenditure of energy, a flock of 25 birds flying in vee-formation could travel 70% farther than if each bird were to fly separately (Ref. 15).]

V9.19 Wing tip vortices

The trailing vortices from the right and left wing tips are connected by the *bound vortex* along the length of the wing. It is this vortex that generates the circulation that produces the lift. The combined vortex system (the bound vortex and the trailing vortices) is termed a horseshoe vortex. The strength of the trailing vortices (which is equal to the strength of the bound vortex) is proportional to the lift generated. Large aircraft (for example, a Boeing 747) can generate very strong trailing vortices that persist for a long time before viscous effects and instability mechanisms finally cause them to die out. Such vortices are strong enough to flip smaller aircraft out of control if they follow too closely behind the large aircraft. The figure in the margin clearly shows a trailing vortex produced during a wake vortex study in which an airplane flew through a column of smoke.

(Photograph courtesy of NASA.)

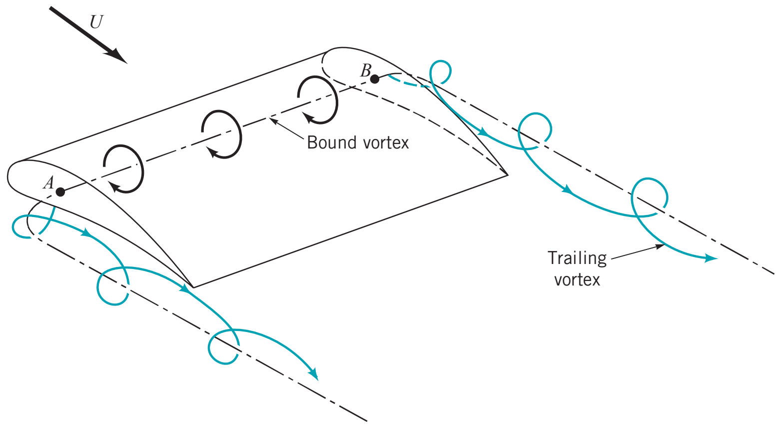

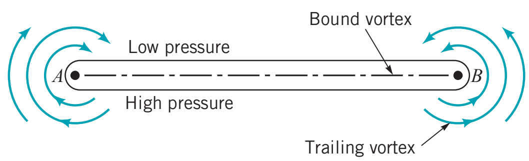

■ **FIGURE 9.37** **Flow past a finite length wing: (*a*) the horseshoe vortex system produced by the bound vortex and the trailing vortices; (*b*) the leakage of air around the wing tips produces the trailing vortices.**

Fluids in the News

Why winglets? Winglets, those upward turning ends of airplane wings, boost the performance by reducing drag. This is accomplished by reducing the strength of the *wingtip vortices* formed by the difference between the high pressure on the lower surface of the wing and the low pressure on the upper surface of the wing. These vortices represent an energy loss and an increase in drag. In essence, the winglet provides an effective increase in the aspect ratio of the wing without extending the wingspan. Winglets come in a variety of styles—the Airbus A320 has a very small upper and lower winglet; the Boeing 747-400 has a conventional, vertical upper winglet; and the Boeing Business Jet (a derivative of the Boeing 737) has an eight-foot winglet with a curving transition from wing to winglet. Since the airflow around the winglet is quite complicated, the winglets must be carefully designed and tested for each aircraft. In the past, winglets were more likely to be retrofitted to existing wings, but new airplanes are being designed with winglets from the start. Unlike tailfins on cars, winglets really do work. (See Problem 9.111.)

As is indicated above, the generation of lift is directly related to the production of a swirl or vortex flow around the object. A nonsymmetric airfoil, by design, generates its own prescribed amount of swirl and lift. A symmetric object like a circular cylinder or sphere, which normally provides no lift, can generate swirl and lift if it rotates.

As is discussed in Section 6.6.3, the inviscid flow past a circular cylinder has the symmetrical flow pattern indicated in Fig. 9.38*a*. By symmetry the lift and drag are zero. However, if the cylinder is rotated about its axis in a stationary real ($\mu \neq 0$) fluid, the rotation will drag some of the fluid around, producing circulation about the cylinder as in Fig. 9.38*b*. When this circulation is combined with an ideal, uniform upstream flow, the flow pattern indicated in Fig. 9.38*c* is obtained. The flow is no longer symmetrical about the horizontal plane through the center of the cylinder; the average pressure is greater on the lower half of the cylinder than on the upper half, and a lift is generated. This effect is called the ***Magnus effect,*** after Heinrich Magnus (1802–1870), a German chemist and physicist who first investigated this phenomenon. A similar lift is generated on a rotating sphere. It accounts for the various types of pitches in baseball (i.e., curve ball, floater, sinker, etc.), the ability of a soccer player to hook the ball, and the hook or slice of a golf ball.

A spinning sphere or cylinder can generate lift.

Typical lift and drag coefficients for a smooth, spinning sphere are shown in Fig. 9.39. Although the drag coefficient is fairly independent of the rate of rotation, the lift coefficient is strongly

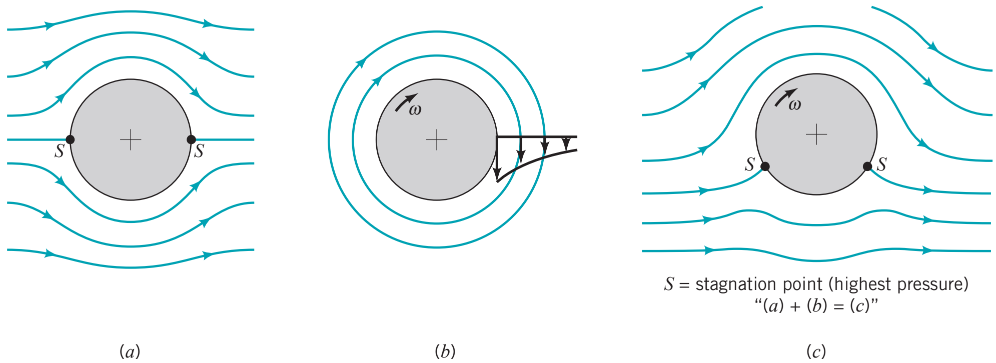

■ FIGURE 9.38 Inviscid flow past a circular cylinder: (*a*) uniform upstream flow without circulation, (*b*) free vortex at the center of the cylinder, (*c*) combination of free vortex and uniform flow past a circular cylinder giving nonsymmetric flow and a lift.

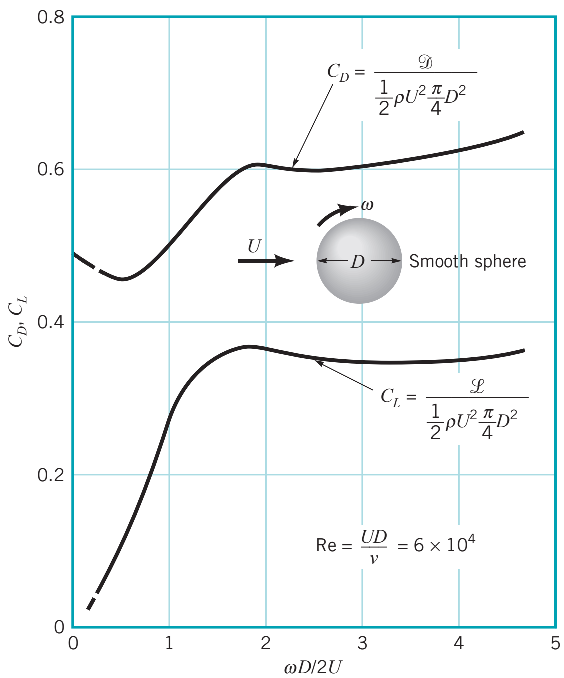

■ FIGURE 9.39 Lift and drag coefficients for a spinning smooth sphere (Ref. 23).

A dimpled golf ball has less drag and more lift than a smooth one.

dependent on it. In addition (although not indicated in the figure), both C_L and C_D are dependent on the roughness of the surface. As was discussed in Section 9.3, in a certain Reynolds number range an increase in surface roughness actually decreases the drag coefficient. Similarly, an increase in surface roughness can increase the lift coefficient because the roughness helps drag more fluid around the sphere increasing the circulation for a given angular velocity. Thus, a rotating, rough golf ball travels farther than a smooth one because the drag is less and the lift is greater. However, do not expect a severely roughed up (cut) ball to work better—extensive testing has gone into obtaining the optimum surface roughness for golf balls.

EXAMPLE 9.16 Lift on a Rotating Sphere

GIVEN A table tennis ball weighing 2.45×10^{-2} N with diameter $D = 3.8 \times 10^{-2}$ m is hit at a velocity of $U = 12$ m/s with a back spin of angular velocity ω as is shown in Fig. E9.16.

FIND What is the value of ω if the ball is to travel on a horizontal path, not dropping due to the acceleration of gravity?

SOLUTION

For horizontal flight, the lift generated by the spinning of the ball must exactly balance the weight, $\mathscr{W}$, of the ball so that

$$\mathscr{W} = \mathscr{L} = \tfrac{1}{2}\rho U^2 A C_L$$

or

$$C_L = \frac{2\mathscr{W}}{\rho U^2(\pi/4)D^2}$$

where the lift coefficient, C_L, can be obtained from Fig. 9.39. For standard atmospheric conditions with $\rho = 1.23 \text{ kg/m}^3$ we obtain

$$C_L = \frac{2(2.45 \times 10^{-2}\text{ N})}{(1.23 \text{ kg/m}^3)(12 \text{ m/s})^2(\pi/4)(3.8 \times 10^{-2}\text{ m})^2} = 0.244$$

which, according to Fig. 9.39, can be achieved if

$$\frac{\omega D}{2U} = 0.9$$

or

$$\omega = \frac{2U(0.9)}{D} = \frac{2(12 \text{ m/s})(0.9)}{3.8 \times 10^{-2}\text{ m}} = 568 \text{ rad/s}$$

Thus,

$$\omega = (568 \text{ rad/s})(60 \text{ s/min})(1 \text{ rev}/2\pi \text{ rad}) = 5420 \text{ rpm} \qquad \textbf{(Ans)}$$

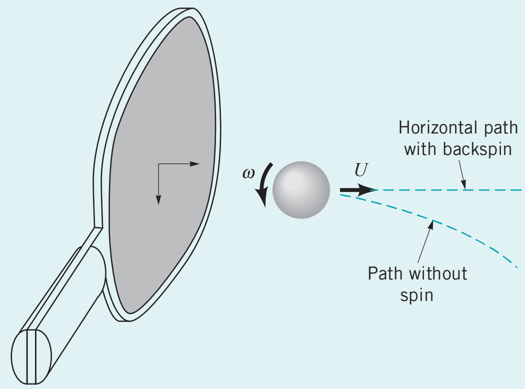

■ FIGURE E9.16

COMMENT Is it possible to impart this angular velocity to the ball? With larger angular velocities the ball will rise and follow an upward curved path. Similar trajectories can be produced by a well-hit golf ball—rather than falling like a rock, the golf ball trajectory is actually curved up and the spinning ball travels a greater distance than one without spin. However, if topspin is imparted to the ball (as in an improper tee shot) the ball will curve downward more quickly than under the action of gravity alone—the ball is "topped" and a negative lift is generated. Similarly, rotation about a vertical axis will cause the ball to hook or slice to one side or the other.

9.5 Chapter Summary and Study Guide

drag
lift
lift coefficient
drag coefficient
wake region
boundary layer
laminar boundary layer
turbulent boundary layer
boundary layer thickness
transition
free-stream velocity
favorable pressure gradient
adverse pressure gradient
boundary layer separation
friction drag
pressure drag
stall
circulation
Magnus effect

In this chapter the flow past objects is discussed. It is shown how the pressure and shear stress distributions on the surface of an object produce the net lift and drag forces on the object.

The character of flow past an object is a function of the Reynolds number. For large Reynolds number flows a thin boundary layer forms on the surface. Properties of this boundary layer flow are discussed. These include the boundary layer thickness, whether the flow is laminar or turbulent, and the wall shear stress exerted on the object. In addition, boundary layer separation and its relationship to the pressure gradient are considered.

The drag, which contains portions due to friction (viscous) effects and pressure effects, is written in terms of the dimensionless drag coefficient. It is shown how the drag coefficient is a function of shape, with objects ranging from very blunt to very streamlined. Other parameters affecting the drag coefficient include the Reynolds number, Froude number, Mach number, and surface roughness.

The lift is written in terms of the dimensionless lift coefficient, which is strongly dependent on the shape of the object. Variation of the lift coefficient with shape is illustrated by the variation of an airfoil's lift coefficient with angle of attack.

The following checklist provides a study guide for this chapter. When your study of the entire chapter and end-of-chapter exercises has been completed you should be able to

- write out meanings of the terms listed here in the margin and understand each of the related concepts. These terms are particularly important and are set in ***italic, bold, and color*** type in the text.

- determine the lift and drag on an object from the given pressure and shear stress distributions on the object.
- for flow past a flat plate, calculate the boundary layer thickness, the wall shear stress, the friction drag, and determine whether the flow is laminar or turbulent.
- explain the concept of the pressure gradient and its relationship to boundary layer separation.
- for a given object, obtain the drag coefficient from appropriate tables, figures, or equations and calculate the drag on the object.
- explain why golf balls have dimples.
- for a given object, obtain the lift coefficient from appropriate figures and calculate the lift on the object.

Some of the important equations in this chapter are:

Lift coefficient and drag coefficient
$$C_L = \frac{\mathscr{L}}{\frac{1}{2}\rho U^2 A}, \quad C_D = \frac{\mathscr{D}}{\frac{1}{2}\rho U^2 A} \qquad \textbf{(9.39), (9.36)}$$

Boundary layer displacement thickness
$$\delta^* = \int_0^\infty \left(1 - \frac{u}{U}\right) dy \qquad \textbf{(9.3)}$$

Boundary layer momentum thickness
$$\Theta = \int_0^\infty \frac{u}{U}\left(1 - \frac{u}{U}\right) dy \qquad \textbf{(9.4)}$$

Blasius boundary layer thickness, displacement thickness, and momentum thickness for flat plate
$$\frac{\delta}{x} = \frac{5}{\sqrt{\mathrm{Re}_x}}, \quad \frac{\delta^*}{x} = \frac{1.721}{\sqrt{\mathrm{Re}_x}}, \quad \frac{\Theta}{x} = \frac{0.664}{\sqrt{\mathrm{Re}_x}} \qquad \textbf{(9.15), (9.16), (9.17)}$$

Blasius wall shear stress for flat plate
$$\tau_w = 0.332 U^{3/2} \sqrt{\frac{\rho\mu}{x}} \qquad \textbf{(9.18)}$$

Drag on flat plate
$$\mathscr{D} = \rho b U^2 \, \Theta \qquad \textbf{(9.23)}$$

Blasius wall friction coefficient and friction drag coefficient for flat plate
$$c_f = \frac{0.664}{\sqrt{\mathrm{Re}_x}}, \quad C_{Df} = \frac{1.328}{\sqrt{\mathrm{Re}_\ell}} \qquad \textbf{(9.32)}$$

References

1. Schlichting, H., *Boundary Layer Theory*, 8th Ed., McGraw-Hill, New York, 2000.
2. Rosenhead, L., *Laminar Boundary Layers*, Oxford University Press, London, 1963.
3. White, F. M., *Viscous Fluid Flow*, 3rd Ed., McGraw-Hill, New York, 2005.
4. Currie, I. G., *Fundamental Mechanics of Fluids*, McGraw-Hill, New York, 1974.
5. Blevins, R. D., *Applied Fluid Dynamics Handbook*, Van Nostrand Reinhold, New York, 1984.
6. Hoerner, S. F., *Fluid-Dynamic Drag*, published by the author, Library of Congress No. 64,19666, 1965.
7. Happel, J., *Low Reynolds Number Hydrodynamics*, Prentice-Hall, Englewood Cliffs, NJ, 1965.
8. Van Dyke, M., *An Album of Fluid Motion*, Parabolic Press, Stanford, Calif., 1982.
9. Thompson, P. A., *Compressible-Fluid Dynamics*, McGraw-Hill, New York, 1972.
10. Zucrow, M. J., and Hoffman, J. D., *Gas Dynamics*, *Vol. I*, Wiley, New York, 1976.
11. Clayton, B. R., and Bishop, R. E. D., *Mechanics of Marine Vehicles*, Gulf Publishing Co., Houston, 1982.
12. *CRC Handbook of Tables for Applied Engineering Science*, 2nd Ed., CRC Press, Boca Raton, Florida, 1973.
13. Shevell, R. S., *Fundamentals of Flight*, 2nd Ed., Prentice-Hall, Englewood Cliffs, NJ, 1989.
14. Kuethe, A. M., and Chow, C. Y., *Foundations of Aerodynamics*, *Bases of Aerodynamics Design*, 4th Ed., Wiley, New York, 1986.

15. Vogel, J., *Life in Moving Fluids*, 2nd Ed., Willard Grant Press, Boston, 1994.
16. Kreider, J. F., *Principles of Fluid Mechanics*, Allyn and Bacon, Newton, Mass., 1985.
17. Dobrodzicki, G. A., Flow Visualization in the National Aeronautical Establishment's Water Tunnel, National Research Council of Canada, Aeronautical Report LR-557, 1972.
18. White, F. M., *Fluid Mechanics*, 6th Ed., McGraw-Hill, New York, 2008.
19. Vennard, J. K., and Street, R. L., *Elementary Fluid Mechanics*, 7th Ed., Wiley, New York, 1995.
20. Gross, A. C., Kyle, C. R., and Malewicki, D. J., The Aerodynamics of Human Powered Land Vehicles, *Scientific American*, Vol. 249, No. 6, 1983.
21. Abbott, I. H., and Von Doenhoff, A. E., *Theory of Wing Sections*, Dover Publications, New York, 1959.
22. MacReady, P. B., "Flight on 0.33 Horsepower: The Gossamer Condor," *Proc. AIAA 14th Annual Meeting* (Paper No. 78-308), Washington, DC, 1978.
23. Goldstein, S., *Modern Developments in Fluid Dynamics*, Oxford Press, London, 1938.
24. Achenbach, E., Distribution of Local Pressure and Skin Friction around a Circular Cylinder in Cross-Flow up to Re $= 5 \times 10^6$, *Journal of Fluid Mechanics*, Vol. 34, Pt. 4, 1968.
25. Inui, T., Wave-Making Resistance of Ships, *Transactions of the Society of Naval Architects and Marine Engineers*, Vol. 70, 1962.
26. Sovran, G., et al. (ed.), *Aerodynamic Drag Mechanisms of Bluff Bodies and Road Vehicles*, Plenum Press, New York, 1978.
27. Abbott, I. H., von Doenhoff, A. E., and Stivers, L. S., Summary of Airfoil Data, NACA Report No. 824, Langley Field, Va., 1945.
28. Society of Automotive Engineers Report HSJ1566, "Aerodynamic Flow Visualization Techniques and Procedures," 1986.
29. Anderson, J. D., *Fundamentals of Aerodynamics*, 4th Ed., McGraw-Hill, New York, 2007.
30. Hucho, W. H., *Aerodynamics of Road Vehicles*, Butterworth–Heinemann, 1987.
31. Homsy, G. M., et al., *Multimedia Fluid Mechanics*, 2nd Ed., CD-ROM, Cambridge University Press, New York, 2008.

Review Problems

Go to Appendix G for a set of review problems with answers. Detailed solutions can be found in *Student Solution Manual and Study Guide for Fundamentals of Fluid Mechanics*, by Munson et al. (© 2009 John Wiley and Sons, Inc.).

Problems

Note: Unless otherwise indicated use the values of fluid properties found in the tables on the inside of the front cover. Problems designated with an (*) are intended to be solved with the aid of a programmable calculator or a computer. Problems designated with a (†) are "open ended" problems and require critical thinking in that to work them one must make various assumptions and provide the necessary data. There is not a unique answer to these problems.

Answers to the even-numbered problems are listed at the end of the book. Access to the videos that accompany problems can be obtained through the book's web site, www.wiley.com/college/munson. The lab-type problems and FlowLab problems can also be accessed on this web site.

Section 9.1 General External Flow Characteristics

9.1 Obtain photographs/images of external flow objects that are exposed to both a low Reynolds number and high Reynolds number. Print these photos and write a brief paragraph that describes the situations involved.

9.2 A thin square is oriented perpendicular to the upstream velocity in a uniform flow. The average pressure on the front side of the square is 0.7 times the stagnation pressure and the average pressure on the back side is a vacuum (i.e., less than the free stream pressure) with a magnitude 0.4 times the stagnation pressure. Determine the drag coefficient for this square.

9.3 A small 15-mm-long fish swims with a speed of 20 mm/s. Would a boundary layer type flow be developed along the sides of the fish? Explain.

9.4 The average pressure and shear stress acting on the surface of the 1-m-square flat plate are as indicated in Fig. P9.4. Determine the lift and drag generated. Determine the lift and drag if the shear stress is neglected. Compare these two sets of results.

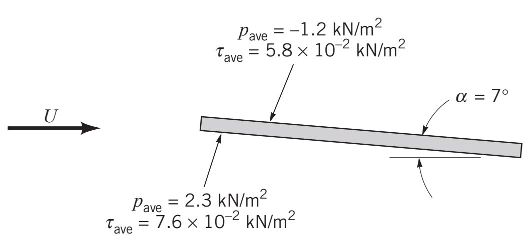

■ FIGURE P9.4

*9.5 The pressure distribution on the 1-m-diameter circular disk in Fig. P9.5 is given in the table. Determine the drag on the disk.

r (m)	p (kN/m^2)
0	4.34
0.05	4.28
0.10	4.06
0.15	3.72
0.20	3.10
0.25	2.78
0.30	2.37
0.35	1.89
0.40	1.41
0.45	0.74
0.50	0.0

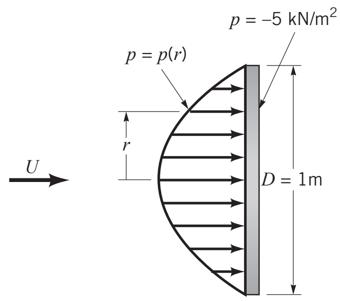

■ FIGURE P9.5

9.6 When you walk through still air at a rate of 1 m/s, would you expect the character of the air flow around you to be most like that depicted in Fig. 9.6a, b, or c? Explain.

9.7 A 0.10 m-diameter circular cylinder moves through air with a speed U. The pressure distribution on the cylinder's surface is approximated by the three straight line segments shown in Fig. P9.7. Determine the drag coefficient on the cylinder. Neglect shear forces.

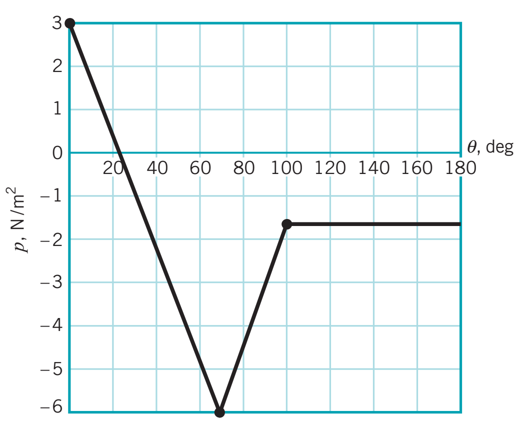

■ FIGURE P9.4

9.8 Typical values of the Reynolds number for various animals moving through air or water are listed below. For which cases is inertia of the fluid important? For which cases do viscous effects dominate? For which cases would the flow be laminar; turbulent? Explain.

Animal	Speed	Re
(a) large whale	10m /s	300,000,000
(b) flying duck	20m /s	300,000
(c) large dragonfly	7m /s	30,000
(d) invertebrate larva	1m m/s	0.3
(e) bacterium	0.01mm /s	0.00003

†9.9 Estimate the Reynolds numbers associated with the following objects moving through water: **(a)** a kayak, **(b)** a minnow, **(c)** a submarine, **(d)** a grain of sand settling to the bottom, **(e)** you swimming.

Section 9.2 Boundary Layer Characteristics (Also see Lab Problems 9.112 and 9.113.)

9.10 Obtain a photograph/image of an object that can be approximated as flow past a flat plate, in which you could use equations from Section 9.2 to approximate the boundary layer characteristics. Print this photo and write a brief paragraph that describes the situation involved.

9.11 Discuss any differences in boundary layers between internal flows (e.g., pipe flow) and external flows.

9.12 Water flows past a flat plate that is oriented parallel to the flow with an upstream velocity of 0.5 m/s. Determine the approximate location downstream from the leading edge where the boundary layer becomes turbulent. What is the boundary layer thickness at this location?

9.13 A viscous fluid flows past a flat plate such that the boundary layer thickness at a distance 1.3 m from the leading edge is 12 mm. Determine the boundary layer thickness at distances of 0.20, 2.0, and 20 m from the leading edge. Assume laminar flow.

9.14 If the upstream velocity of the flow in Problem 9.13 is $U = 1.5$ m/s, determine the kinematic viscosity of the fluid.

9.15 Water flows past a flat plate with an upstream velocity of $U = 0.02$ m/s. Determine the water velocity a distance of 10 mm from the plate at distances of $x = 1.5$ m and $x = 15$ m from the leading edge.

9.16 Approximately how fast can the wind blow past a 0.25-in.-diameter twig if viscous effects are to be of importance throughout the entire flow field (i.e., Re < 1)? Explain. Repeat for a 0.004-in.-diameter hair and a 6-ft-diameter smokestack.

9.17 As is indicated in Table 9.2, the laminar boundary layer results obtained from the momentum integral equation are relatively insensitive to the shape of the assumed velocity profile. Consider the profile given by $u = U$ for $y > \delta$, and $u = U\{1 - [(y - \delta)/\delta]^2\}^{1/2}$ for $y \leq \delta$ as shown in Fig. P9.17. Note that this satisfies the conditions $u = 0$ at $y = 0$ and $u = U$ at $y = \delta$. However, show that such a profile produces meaningless results when used with the momentum integral equation. Explain.

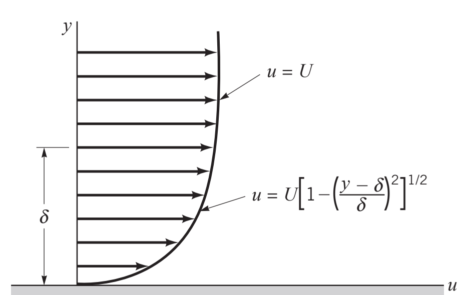

■ FIGURE P9.17

9.18 If a high-school student who has completed a first course in physics asked you to explain the idea of a boundary layer, what would you tell the student?

9.19 Because of the velocity deficit, $U - u$, in the boundary layer, the streamlines for flow past a flat plate are not exactly parallel to the plate. This deviation can be determined by use of the displacement thickness, δ^*. For air blowing past the flat plate shown in Fig. P9.19, plot the streamline A–B that passes through the edge of the boundary layer ($y = \delta_B$ at $x = \ell$) at point B. That is, plot $y = y(x)$ for streamline A–B. Assume laminar boundary layer flow.

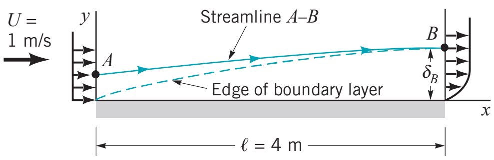

■ FIGURE P9.19

9.20 Air enters a square duct through a 1-ft opening as is shown in Fig. P9.20. Because the boundary layer displacement thickness increases in the direction of flow, it is necessary to increase the cross-sectional size of the duct if a constant $U = 2$ ft/s velocity is to be maintained outside the boundary layer. Plot a graph of the duct size, d, as a function of x for $0 \le x \le 10$ ft if U is to remain constant. Assume laminar flow.

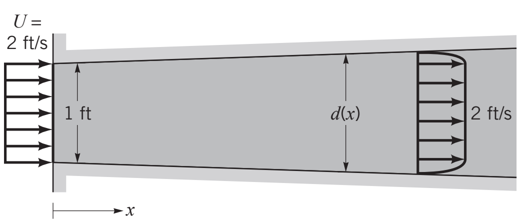

■ FIGURE P9.20

9.21 A smooth, flat plate of length $\ell = 6$ m and width $b = 4$ m is placed in water with an upstream velocity of $U = 0.5$ m/s. Determine the boundary layer thickness and the wall shear stress at the center and the trailing edge of the plate. Assume a laminar boundary layer.

9.22 An atmospheric boundary layer is formed when the wind blows over the earth's surface. Typically, such velocity profiles can be written as a power law: $u = ay^n$, where the constants a and n depend on the roughness of the terrain. As is indicated in Fig. P9.22, typical values are $n = 0.40$ for urban areas, $n = 0.28$ for woodland or suburban areas, and $n = 0.16$ for flat open country (Ref. 23). **(a)** If the velocity is 20 ft/s at the bottom of the sail on your boat ($y = 4$ ft), what is the velocity at the top of the mast ($y = 30$ ft)? **(b)** If the average velocity is 10 mph on the tenth floor of an urban building, what is the average velocity on the sixtieth floor?

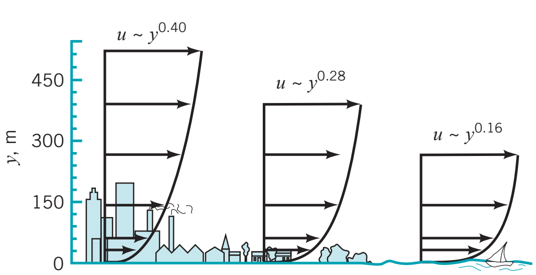

■ FIGURE P9.22

9.23 It is relatively easy to design an efficient nozzle to accelerate a fluid. Conversely, it is very difficult to build an efficient diffuser to decelerate a fluid without boundary layer separation and its subsequent inefficient flow behavior. Use the ideas of favorable and adverse pressure gradients to explain these facts.

9.24 A 30-story office building (each story is 12 ft tall) is built in a suburban industrial park. Plot the dynamic pressure, $\rho u^2/2$, as a function of elevation if the wind blows at hurricane strength (75 mph) at the top of the building. Use the atmospheric boundary layer information of Problem 9.22.

9.25 Show that for any function $f = f(\eta)$ the velocity components u and v determined by Eqs. 9.12 and 9.13 satisfy the incompressible continuity equation, Eq. 9.8.

***9.26** Integrate the Blasius equation (Eq. 9.14) numerically to determine the boundary layer profile for laminar flow past a flat plate. Compare your results with those of Table 9.1.

9.27 An airplane flies at a speed of 400 mph at an altitude of 10,000 ft. If the boundary layers on the wing surfaces behave as those on a flat plate, estimate the extent of laminar boundary layer flow along the wing. Assume a transitional Reynolds number of $\text{Re}_{xcr} = 5 \times 10^5$. If the airplane maintains its 400-mph speed but descends to sea-level elevation, will the portion of the wing covered by a laminar boundary layer increase or decrease compared with its value at 10,000 ft? Explain.

†9.28 If the boundary layer on the hood of your car behaves as one on a flat plate, estimate how far from the front edge of the hood the boundary layer becomes turbulent. How thick is the boundary layer at this location?

9.29 A laminar boundary layer velocity profile is approximated by $u/U = [2 - (y/\delta)](y/\delta)$ for $y \le \delta$, and $u = U$ for $y > \delta$. **(a)** Show that this profile satisfies the appropriate boundary conditions. **(b)** Use the momentum integral equation to determine the boundary layer thickness, $\delta = \delta(x)$.

9.30 A laminar boundary layer velocity profile is approximated by the two straight-line segments indicated in Fig. P9.30. Use the momentum integral equation to determine the boundary layer thickness, $\delta = \delta(x)$, and wall shear stress, $\tau_w = \tau_w(x)$. Compare these results with those in Table 9.2.

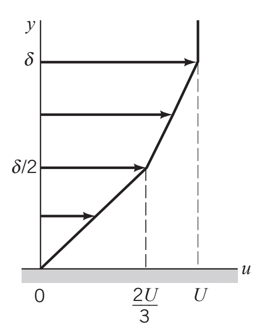

■ FIGURE P9.30

***9.31** For a fluid of specific gravity $SG = 0.86$ flowing past a flat plate with an upstream velocity of $U = 5$ m/s, the wall shear stress on a flat plate was determined to be as indicated in the table below. Use the momentum integral equation to determine the boundary layer momentum thickness, $\Theta = \Theta(x)$. Assume $\Theta = 0$ at the leading edge, $x = 0$.

x (m)	τ_w (N/m^2)
0	—
0.2	13.4
0.4	9.25
0.6	7.68
0.8	6.51
1.0	5.89
1.2	6.57
1.4	6.75
1.6	6.23
1.8	5.92
2.0	5.26

Section 9.3 Drag

9.32 Obtain a photograph/image of an everyday item in which drag plays a key role. Print this photo and write a brief paragraph that describes the situation involved.

9.33 Should a canoe paddle be made rough to get a "better grip on the water" for paddling purposes? Explain.

9.34 Define the purpose of "streamlining" a body.

9.35 Water flows over two flat plates with the same laminar free-stream velocity. Both plates have the same width, but Plate #2 is twice as long as Plate #1. What is the relationship between the drag force for these two plates?

9.36 Fluid flows past a flat plate with a drag force $\mathscr{D}_1$. If the free-stream velocity is doubled, will the new drag force, $\mathscr{D}_2$, be larger or smaller than $\mathscr{D}_1$ and by what amount?

9.37 A model is placed in an air flow with a given velocity and then placed in water flow with the same velocity. If the drag coefficients are the same between these two cases, how do the drag forces compare between the two fluids?

9.38 The drag coefficient for a newly designed hybrid car is predicted to be 0.21. The cross-sectional area of the car is 30 ft^2. Determine the aerodynamic drag on the car when it is driven through still air at 55 mph.

9.39 A 5-m-diameter parachute of a new design is to be used to transport a load from flight altitude to the ground with an average vertical speed of 3 m/s. The total weight of the load and parachute is 200 N. Determine the approximate drag coefficient for the parachute.

9.40 A 50-mph wind blows against an outdoor movie screen that is 70 ft wide and 20 ft tall. Estimate the wind force on the screen.

9.41 The aerodynamic drag on a car depends on the "shape" of the car. For example, the car shown in Fig. P9.41 has a drag coefficient of 0.36 with the windows and roof closed. With the windows and roof open, the drag coefficient increases to 0.45.

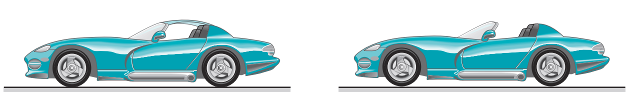

Windows and roof closed: $C_D = 0.35$ — Windows open; roof open: $C_D = 0.45$

■ **FIGURE P9.41**

With the windows and roof open, at what speed is the amount of power needed to overcome aerodynamic drag the same as it is at 65 mph with the windows and roof closed? Assume the frontal area remains the same. Recall that power is force times velocity.

9.42 A rider on a bike with the combined mass of 100 kg attains a terminal speed of 15 m/s on a 12% slope. Assuming that the only forces affecting the speed are the weight and the drag, calculate the drag coefficient. The frontal area is 0.9 m^2. Speculate whether the rider is in the upright or racing position.

9.43 A baseball is thrown by a pitcher at 95 mph through standard air. The diameter of the baseball is 2.82 in. Estimate the drag force on the baseball.

9.44 A logging boat is towing a log that is 2 m in diameter and 8 m long at 4 m/s through water. Estimate the power required if the axis of the log is parallel to the tow direction.

9.45 A sphere of diameter D and density ρ_s falls at a steady rate through a liquid of density ρ and viscosity μ. If the Reynolds number, Re $= \rho DU/\mu$, is less than 1, show that the viscosity can be determined from $\mu = gD^2(\rho_s - \rho)/18\,U$.

9.46 The square, flat plate shown in Fig. P9.46*a* is cut into four equal-sized pieces and arranged as shown in Fig. P9.46*b*. Determine the ratio of the drag on the original plate [case **(a)**] to the drag on the plates in the configuration shown in **(b)**. Assume laminar boundary flow. Explain your answer physically.

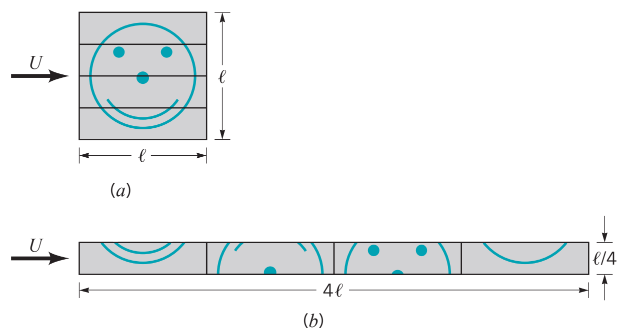

■ **FIGURE P9.46**

9.47 If the drag on one side of a flat plate parallel to the upstream flow is $\mathscr{D}$ when the upstream velocity is U, what will the drag be when the upstream velocity is $2U$; or $U/2$? Assume laminar flow.

9.48 Water flows past a triangular flat plate oriented parallel to the free stream as shown in Fig. P9.48. Integrate the wall shear stress over the plate to determine the friction drag on one side of the plate. Assume laminar boundary layer flow.

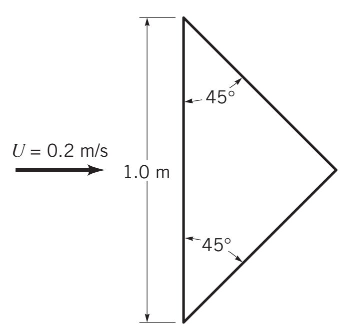

■ **FIGURE P9.48**

9.49 For small Reynolds number flows the drag coefficient of an object is given by a constant divided by the Reynolds number (see Table 9.4). Thus, as the Reynolds number tends to zero, the drag coefficient becomes infinitely large. Does this mean that for small velocities (hence, small Reynolds numbers) the drag is very large? Explain.

9.50 A rectangular car-top carrier of 1.6-ft height, 5.0-ft length (front to back), and 4.2-ft width is attached to the top of a car. Estimate the additional power required to drive the car with the carrier at 60 mph through still air compared with the power required to driving only the car at 60 mph.

9.51 As shown in **Video V9.2** and Fig. P9.51*a*, a kayak is a relatively streamlined object. As a first approximation in calculating the drag on a kayak, assume that the kayak acts as if it were a smooth, flat plate 17 ft long and 2 ft wide. Determine the drag as a function of speed and compare your results with the measured values given in Fig. P9.51*b*. Comment on reasons why the two sets of values may differ.

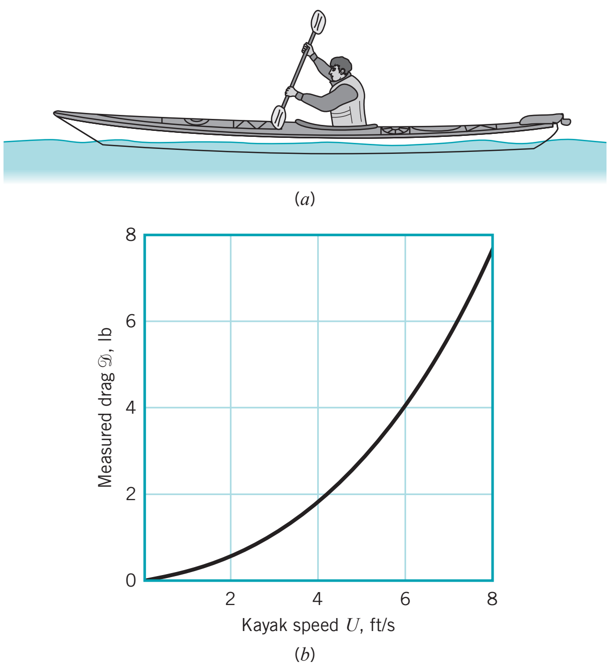

■ FIGURE P9.51

9.52 A 38.1-mm-diameter, 0.0245-N table tennis ball is released from the bottom of a swimming pool. With what velocity does it rise to the surface? Assume it has reached its terminal velocity.

9.53 To reduce aerodynamic drag on a bicycle, it is proposed that the cross-sectional shape of the handlebar tubes be made "teardrop" shape rather than circular. Make a rough estimate of the reduction in aerodynamic drag for a bike with this type of handlebars compared with the standard handlebars. List all assumptions.

9.54 A hot air balloon roughly spherical in shape has a volume of 70,000 ft^3 and a weight of 500 lb (including passengers, basket, ballon fabric, etc.). If the outside air temperature is 80 ºF and the temperature within the balloon is 165 ºF, estimate the rate at which it will rise under steady state conditions if the atmospheric pressure is 14.7 psi.

9.55 It is often assumed that "sharp objects can cut through the air better than blunt ones." Based on this assumption, the drag on the object shown in Fig. P9.55 should be less when the wind blows from right to left than when it blows from left to right. Experiments show that the opposite is true. Explain.

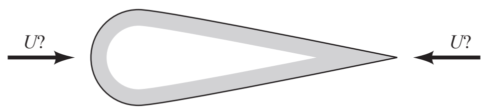

■ FIGURE P9.55

***9.56** The device shown in Fig. P9.56 is to be designed to measure the wall shear stress as air flows over the smooth surface with an upstream velocity U. It is proposed that τ_w can be obtained by measuring the bending moment, M, at the base [point (1)] of the support that holds the small surface element which is free from contact with the surrounding surface. Plot a graph of M as a function of U for $5 \leq U \leq 50$ m/s, with $\ell = 2, 3, 4,$ and 5 m.

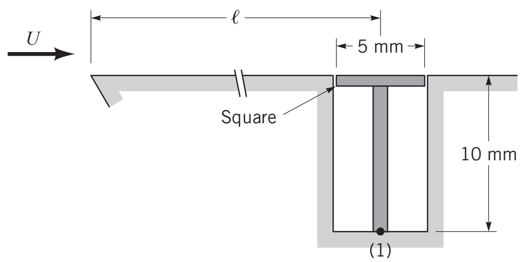

■ FIGURE P9.56

9.57 A 12-mm-diameter cable is strung between a series of poles that are 50 m apart. Determine the horizontal force this cable puts on each pole if the wind velocity is 30 m/s.

9.58 How fast do small water droplets of 0.06 μm (6×10^{-8} m) diameter fall through the air under standard sea-level conditions? Assume the drops do not evaporate. Repeat the problem for standard conditions at 5000-m altitude.

9.59 A strong wind can blow a golf ball off the tee by pivoting it about point 1 as shown in Fig. P9.59. Determine the wind speed necessary to do this.

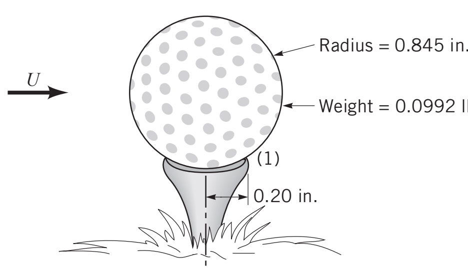

■ FIGURE P9.59

9.60 A 22 in. by 34 in. speed limit sign is supported on a 3-in. wide, 5-ft-long pole. Estimate the bending moment in the pole at ground level when a 30-mph wind blows against the sign. (See **Video V9.9.**) List any assumptions used in your calculations.

9.61 Determine the moment needed at the base of 20-m-tall, 0.12-m-diameter flag pole to keep it in place in a 20 m/s wind.

9.62 Repeat Problem 9.61 if a 2-m by 2.5-m flag is attached to the top of the pole. See Fig. 9.30 for drag coefficient data for flags.

†9.63 During a flash flood, water rushes over a road as shown in Fig. P9.63 with a speed of 12 mph. Estimate the maximum water depth, h, that would allow a car to pass without being swept away. List all assumptions and show all calculations.

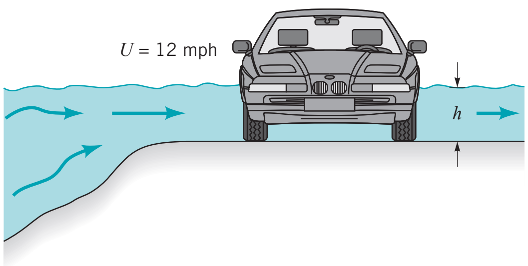

■ FIGURE P9.63

9.64 How much more power is required to pedal a bicycle at 15 mph into a 20-mph head-wind than at 15 mph through still air? Assume a frontal area of 3.9 ft^2 and a drag coefficient of $C_D = 0.88$.

†9.65 Estimate the wind velocity necessary to knock over a 10-lb garbage can that is 3 ft tall and 2 ft in diameter. List your assumptions.

9.66 On a day without any wind, your car consumes x gallons of gasoline when you drive at a constant speed, U, from point A to point B and back to point A. Assume that you repeat the journey, driving at the same speed, on another day when there is a steady wind blowing from B to A. Would you expect your fuel consumption to be less than, equal to, or greater than x gallons for this windy round-trip? Support your answer with appropriate analysis.

9.67 The structure shown in Fig. P9.67 consists of three cylindrical support posts to which an elliptical flat-plate sign is attached. Estimate the drag on the structure when a 50-mph wind blows against it.

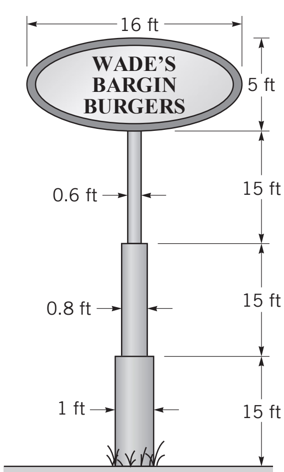

■ FIGURE P9.67

9.68 As shown in **Video V9.13** and Fig. P9.68, the aerodynamic drag on a truck can be reduced by the use of appropriate air deflectors. A reduction in drag coefficient from $C_D = 0.96$ to $C_D = 0.70$ corresponds to a reduction of how many horsepower needed at a highway speed of 65 mph?

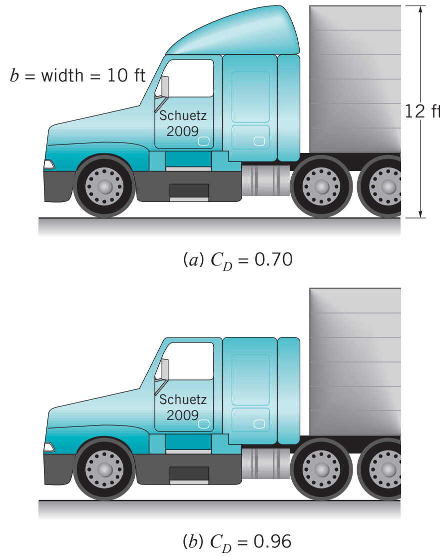

■ FIGURE P9.68

9.69 As shown in **Video V9.7** and Fig. P9.69, a vertical wind tunnel can be used for skydiving practice. Estimate the vertical wind speed needed if a 150-lb person is to be able to "float" motionless when the person **(a)** curls up as in a crouching position or **(b)** lies flat. See Fig. 9.30 for appropriate drag coefficient data.

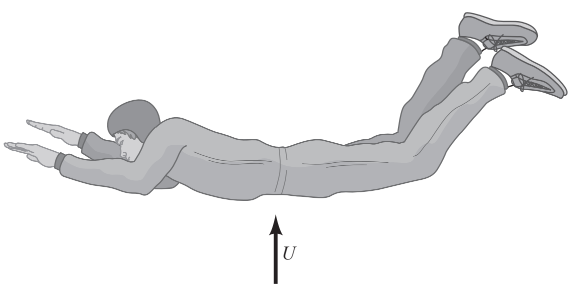

■ FIGURE P9.69

*9.70 The helium-filled balloon shown in Fig. P9.70 is to be used as a wind speed indicator. The specific weight of the helium is $\gamma = 0.011$ lb/ft^3, the weight of the balloon material is 0.20 lb, and the weight of the anchoring cable is negligible. Plot a graph of θ as a function of U for $1 \leq U \leq 50$ mph. Would this be an effective device over the range of U indicated? Explain.

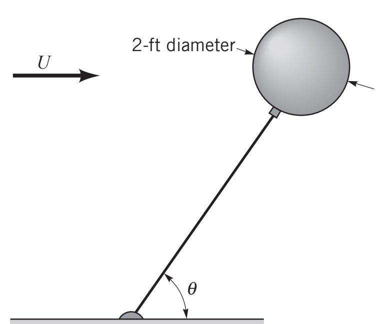

■ FIGURE P9.70

9.71 A 0.30-m-diameter cork ball ($SG = 0.21$) is tied to an object on the bottom of a river as is shown in Fig. P9.71. Estimate the speed of the river current. Neglect the weight of the cable and the drag on it.

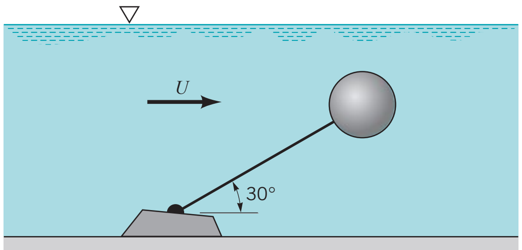

■ FIGURE P9.71

9.72 A shortwave radio antenna is constructed from circular tubing, as is illustrated in Fig. P9.72. Estimate the wind force on the antenna in a 100 km/hr wind.

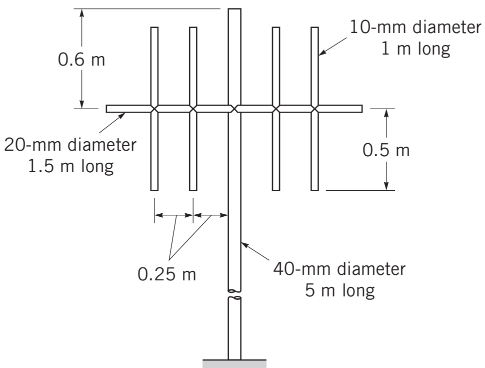

■ FIGURE P9.72

9.73 The large, newly planted tree shown in Fig. P9.73 is kept from tipping over in a wind by use of a rope as shown. It is assumed that the sandy soil cannot support any moment about the center of the soil ball, point A. Estimate the tension in the rope if the wind is 80 km/hr. See Fig. 9.30 for drag coefficient data.

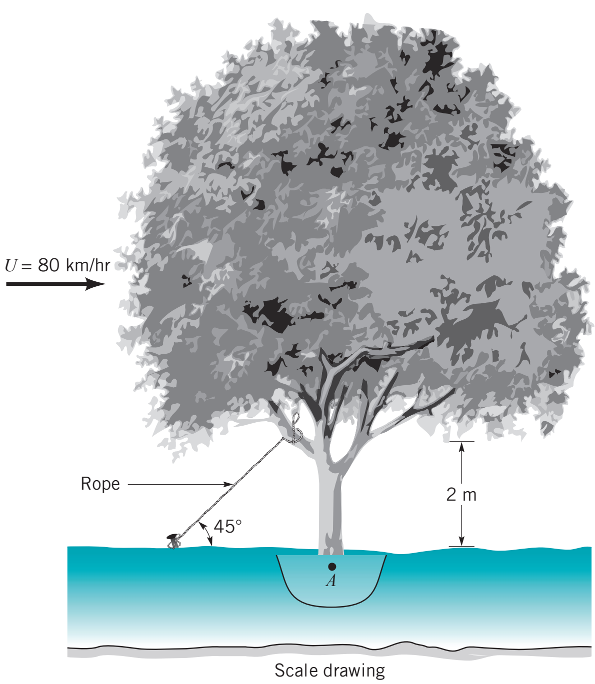

■ FIGURE P9.73

9.74 Estimate the wind force on your hand when you hold it out of your car window while driving 55 mph. Repeat your calculations if you were to hold your hand out of the window of an airplane flying 550 mph.

†9.75 Estimate the energy that a runner expends to overcome aerodynamic drag while running a complete marathon race. This expenditure of energy is equivalent to climbing a hill of what height? List all assumptions and show all calculations.

9.76 A 2-mm-diameter meteor of specific gravity 2.9 has a speed of 6 km/s at an altitude of 50,000 m where the air density is 1.03×10^{-3} kg/m^3. If the drag coefficient at this large Mach number condition is 1.5, determine the deceleration of the meteor.

9.77 Air flows past two equal sized spheres (one rough, one smooth) that are attached to the arm of a balance as is indicated in Fig. P9.77. With $U = 0$ the beam is balanced. What is the minimum air velocity for which the balance arm will rotate clockwise?

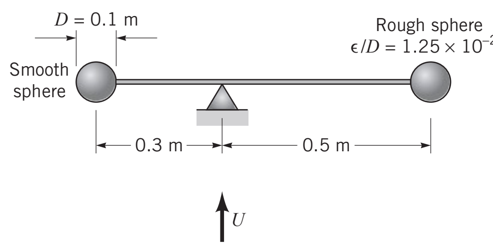

■ FIGURE P9.77

9.78 A 2-in.-diameter sphere weighing 0.14 lb is suspended by the jet of air shown in Fig. P9.78 and **Video V3.2.** The drag coefficient for the sphere is 0.5. Determine the reading on the pressure gage if friction and gravity effects can be neglected for the flow between the pressure gage and the nozzle exit.

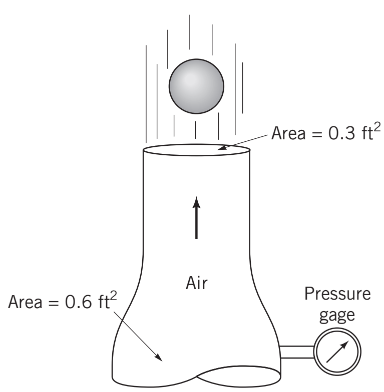

■ FIGURE P9.78

9.79 The United Nations Building in New York is approximately 87.5-m wide and 154-m tall. **(a)** Determine the drag on this building if the drag coefficient is 1.3 and the wind speed is a uniform 20 m/s. **(b)** Repeat your calculations if the velocity profile against the building is a typical profile for an urban area (see Problem 9.22) and the wind speed halfway up the building is 20 m/s.

9.80 A regulation football is 6.78 in. in diameter and weighs 0.91 lb. If its drag coefficient is $C_D = 0.2$, determine its deceleration if it has a speed of 20 ft/s at the top of its trajectory.

9.81 An airplane tows a banner that is $b = 0.8$ m tall and $\ell = 25$ m long at a speed of 150 km/hr. If the drag coefficient based on the area $b\ell$ is $C_D = 0.06$, estimate the power required to tow the banner. Compare the drag force on the banner with that on a rigid flat plate of the same size. Which has the larger drag force and why?

†9.82 Skydivers often join together to form patterns during the free-fall portion of their jump. The current *Guiness Book of World Records* record is 297 skydivers joined hand-to-hand. Given that they can't all jump from the same airplane at the same time, describe how they manage to get together (see **Video V9.7**). Use appropriate fluid mechanics equations and principles in your answer.

9.83 The paint stirrer shown in Fig. P9.83 consists of two circular disks attached to the end of a thin rod that rotates at 80 rpm. The specific gravity of the paint is $SG = 1.1$ and its viscosity is $\mu = 2 \times 10^{-2}$ lb · s/ft^2. Estimate the power required to drive the mixer if the induced motion of the liquid is neglected.

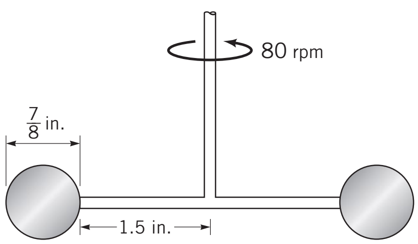

■ FIGURE P9.83

†9.84 If the wind becomes strong enough, it is "impossible" to paddle a canoe into the wind. Estimate the wind speed at which this will happen. List all assumptions and show all calculations.

9.85 A fishnet consists of 0.10-in.-diameter strings tied into squares 4 in. per side. Estimate the force needed to tow a 15-ft by 30-ft section of this net through seawater at 5 ft/s.

9.86 As indicated in Fig. P9.86, the orientation of leaves on a tree is a function of the wind speed, with the tree becoming "more streamlined" as the wind increases. The resulting drag coefficient for the tree (based on the frontal area of the tree, HW) as a function of Reynolds number (based on the leaf length, L) is approximated as shown. Consider a tree with leaves of length $L = 0.3$ ft. What wind speed will produce a drag on the tree that is 6 times greater than the drag on the tree in a 15 ft/s wind?

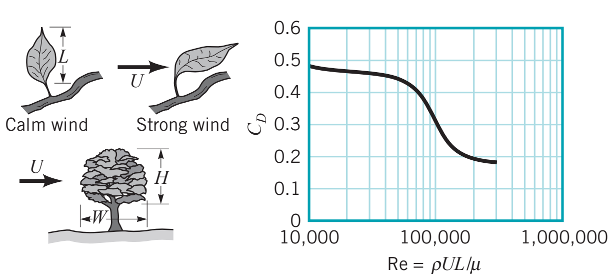

■ FIGURE P9.86

9.87 The blimp shown in Fig. P9.87 is used at various athletic events. It is 128 ft long and has a maximum diameter of 33 ft. If its drag coefficient (based on the frontal area) is 0.060, estimate the power required to propel it **(a)** at its 35-mph cruising speed, or **(b)** at its maximum 55-mph speed.

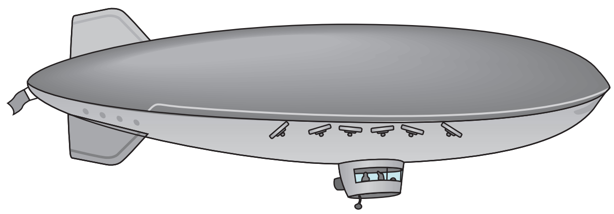

■ FIGURE P9.87

9.88 Show that for level flight at a given speed, the power required to overcome aerodynamic drag decreases as the altitude increases. Assume that the drag coefficient remains constant. This is one reason why airlines fly at high altitudes.

9.89 (See Fluids in the News article "Dimpled baseball bats," Section 9.3.3.) How fast must a 3.5-in.-diameter, dimpled baseball bat move through the air in order to take advantage of drag reduction produced by the dimples on the bat. Although there are differences, assume the bat (a cylinder) acts the same as a golf ball in terms of how the dimples affect the transition from a laminar to a turbulent boundary layer.

9.90 (See Fluids in the News article "At 10,240 mpg it doesn't cost much to 'fill 'er up,'" Section 9.3.3.) **(a)** Determine the power it takes to overcome aerodynamic drag on a small (6 ft^2 cross section), streamlined ($C_D = 0.12$) vehicle traveling 15 mph. **(b)** Compare the power calculated in part **(a)** with that for a large (36 ft^2 cross-sectional area), nonstreamlined ($C_D = 0.48$) SUV traveling 65 mph on the interstate.

Section 9.4 Lift

9.91 Obtain a photograph/image of a device, other than an aircraft wing, that creates lift. Print this photo and write a brief paragraph that describes the situation involved.

9.92 A rectangular wing with an aspect ratio of 6 is to generate 1000 lb of lift when it flies at a speed of 200 ft/s. Determine the length of the wing if its lift coefficient is 1.0.

9.93 Explain why aircraft and birds take off and land into the wind.

9.94 A Piper Cub airplane has a gross weight of 1750 lb, a cruising speed of 115 mph, and a wing area of 179 ft^2. Determine the lift coefficient of this airplane for these conditions.

9.95 A light aircraft with a wing area of 200 ft^2 and a weight of 2000 lb has a lift coefficient of 0.40 and a drag coefficient of 0.05. Determine the power required to maintain level flight.

9.96 As shown in **Video V9.19** and Fig. P9.96, a spoiler is used on race cars to produce a negative lift, thereby giving a better tractive force. The lift coefficient for the airfoil shown is $C_L = 1.1$, and the coefficient of friction between the wheels and the pavement is 0.6. At a speed of 200 mph, by how much would use of the spoiler increase the maximum tractive force that could be generated between the wheels and ground? Assume the air speed past the spoiler equals the car speed and that the airfoil acts directly over the drive wheels.

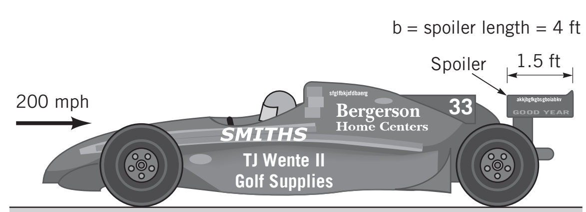

■ FIGURE P9.96

9.97 The wings of old airplanes are often strengthened by the use of wires that provided cross-bracing as shown in Fig. P9.97. If the drag coefficient for the wings was 0.020 (based on the planform area), determine the ratio of the drag from the wire bracing to that from the wings.

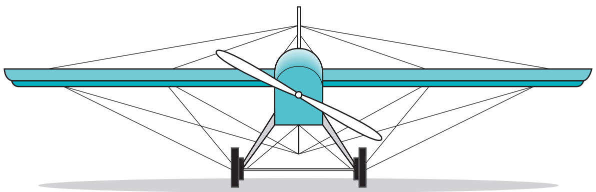

■ FIGURE P9.97

9.98 A wing generates a lift $\mathscr{L}$ when moving through sea-level air with a velocity U. How fast must the wing move through the air at an altitude of 10,000 m with the same lift coefficient if it is to generate the same lift?

9.99 Air blows over the flat-bottomed, two-dimensional object shown in Fig. P9.99. The shape of the object, $y = y(x)$, and the fluid speed along the surface, $u = u(x)$, are given in the table. Determine the lift coefficient for this object.

x(% c)	y(% c)	u/U
0	0	0
2.5	3.72	0.971
5.0	5.30	1.232
7.5	6.48	1.273
10	7.43	1.271
20	9.92	1.276
30	11.14	1.295
40	11.49	1.307
50	10.45	1.308
60	9.11	1.195
70	6.46	1.065
80	3.62	0.945
90	1.26	0.856
100	0	0.807

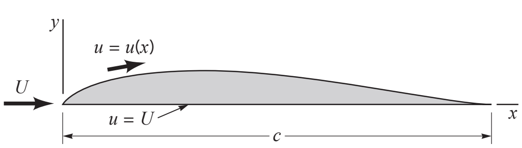

■ FIGURE P9.99

9.100 To help ensure safe flights, air-traffic controllers enforce a minimum time interval between takeoffs. During busy times this can result in a long queue of aircraft waiting for takeoff clearance. Based on the flow shown in Fig. 9.37 and Videos V4.6, V9.1, and V9.19, explain why the interval between takeoffs can be shortened if the wind has a cross-runway component (as opposed to blowing directly down the runway).

9.101 A Boeing 747 aircraft weighing 580,000 lb when loaded with fuel and 100 passengers takes off with an airspeed of 140 mph. With the same configuration (i.e., angle of attack, flap settings, etc.), what is its takeoff speed if it is loaded with 372 passengers? Assume each passenger with luggage weighs 200 lb.

9.102 Show that for unpowered flight (for which the lift, drag, and weight forces are in equilibrium) the glide slope angle, θ, is given by $\tan\theta = C_D/C_L$.

9.103 If the lift coefficient for a Boeing 777 aircraft is 15 times greater than its drag coefficient, can it glide from an altitude of 30,000 ft to an airport 80 mi away if it loses power from its engines? Explain. (See Problem 9.102.)

9.104 On its final approach to the airport, an airplane flies on a flight path that is 3.0° relative to the horizontal. What lift-to-drag ratio is needed if the airplane is to land with its engines idled back to zero power? (See Problem 9.102.)

9.105 Over the years there has been a dramatic increase in the flight speed (U) and altitude (h), weight ($\mathscr{W}$), and wing loading ($\mathscr{W}/A$ = weight divided by wing area) of aircraft. Use the data given in the table below to determine the lift coefficient for each of the aircraft listed.

Aircraft	Year	$\mathscr{W}$, lb	U, mph	$\mathscr{W}/A$, lb/ft²	h, ft
Wright Flyer	1903	750	35	1.5	0
Douglas DC-3	1935	25,000	180	25.0	10,000
Douglas DC-6	1947	105,000	315	72.0	15,000
Boeing 747	1970	800,000	570	150.0	30,000

9.106 The landing speed of an airplane such as the Space Shuttle is dependent on the air density. (See Video V9.1.) By what percent must the landing speed be increased on a day when the temperature is 110 °F compared to a day when it is 50 °F? Assume that the atmospheric pressure remains constant.

9.107 Commercial airliners normally cruise at relatively high altitudes (30,000 to 35,000 ft). Discuss how flying at this high altitude (rather than 10,000 ft, for example) can save fuel costs.

9.108 A pitcher can pitch a "curve ball" by putting sufficient spin on the ball when it is thrown. A ball that has absolutely no spin will follow a "straight" path. A ball that is pitched with a very small amount of spin (on the order of one revolution during its flight between the pitcher's mound and home plate) is termed a knuckle ball. A ball pitched this way tends to "jump around" and "zig-zag" back and forth. Explain this phenomenon. Note: A baseball has seams.

9.109 For many years, hitters have claimed that some baseball pitchers have the ability to actually throw a rising fastball. Assuming that a top major leaguer pitcher can throw a 95-mph pitch and impart an 1800-rpm spin to the ball, is it possible for the ball to actually rise? Assume the baseball diameter is 2.9 in. and its weight is 5.25 oz.

9.110 (See Fluids in the News article "Learning from nature," Section 9.4.1.) As indicated in Fig. P9.110, birds can significantly

■ FIGURE P9.110

alter their body shape and increase their planform area, A, by spreading their wing and tail feathers, thereby reducing their flight speed. If during landing the planform area is increased by 50% and the lift coefficient increased by 30% while all other parameters are held constant, by what percent is the flight speed reduced?

9.111 (See Fluids in the News article "Why winglets?," Section 9.4.2.) It is estimated that by installing appropriately designed winglets on a certain airplane the drag coefficient will be reduced by 5%. For the same engine thrust, by what percent will the aircraft speed be increased by use of the winglets?

Lab Problems

9.112 This problem involves measuring the boundary layer profile on a flat plate. To proceed with this problem, go to Appendix H which is located on the book's web site, www.wiley.com/college/munson.

9.113 This problem involves measuring the pressure distribution on a circular cylinder. To proceed with this problem, go to Appendix H which is located on the book's web site, www.wiley.com/college/munson.

Life Long Learning Problems

9.114 One of the "Fluids in the News" articles in this chapter discusses pressure-sensitive paint—a new technique of measuring surface pressure. There have been other advances in fluid measurement techniques, particularly in velocity measurements. One such technique is particle image velocimetry, or PIV. Obtain information about PIV and its advantages. Summarize your findings in a brief report.

9.115 For typical aircraft flying at cruise conditions, it is advantageous to have as much laminar flow over the wing as possible since there is an increase in friction drag once the flow becomes turbulent. Various techniques have been developed to help promote laminar flow over the wing, both in airfoil geometry configurations as well as active flow control mechanisms. Obtain information on one of these techniques. Summarize your findings in a brief report.

9.116 We have seen in this chapter that streamlining an automobile can help to reduce the drag coefficient. One of the methods of reducing the drag has been to reduce the projected area. However, it is difficult for some road vehicles, such as a tractor-trailer, to reduce this projected area due to the storage volume needed to haul the required load. Over the years, work has been done to help minimize some of the drag on this type of vehicle. Obtain information on a method that has been developed to reduce drag on a tractor-trailer. Summarize your findings in a brief report.

FlowLab Problems

***9.117** This FlowLab problem involves simulation of flow past an airfoil and investigation of the surface pressure distribution as a function of angle of attack. To proceed with this problem, go to the book's web site, www.wiley.com/college/munson.

***9.118** This FlowLab problem involves investigation of the effects of angle-of-attack on lift and drag for flow past an airfoil. To proceed with this problem, go to the book's web site, www.wiley.com/college/munson.

***9.119** This FlowLab problem involves simulating the effects of altitude on the lift and drag of an airfoil. To proceed with this problem, go to the book's web site, www.wiley.com/college/munson.

***9.120** This FlowLab problem involves comparison between inviscid and viscous flows past an airfoil. To proceed with this problem, go to the book's web site, www.wiley.com/college/munson.

***9.121** This FlowLab problem involves simulating the pressure distribution for flow past a cylinder and investigating the differences between inviscid and viscous flows. To proceed with this problem, go to the book's web site, www.wiley.com/college/munson.

***9.122** This FlowLab problem involves comparing CFD predictions and theoretical values of the drag coefficient of flow past a cylinder. To proceed with this problem, go to the book's web site, www.wiley.com/college/munson.

***9.123** This FlowLab problem involves simulating the unsteady flow past a cylinder. To proceed with this problem, go to the book's web site, www.wiley.com/college/munson.

FE Exam Problems

Sample FE (Fundamentals of Engineering) exam questions for fluid mechanics are provided on the book's web site, www.wiley.com/college/munson.